

DEVELOPMENT OF A PULSED FIBER LASER FOR LADAR SYSTEM

A THESIS SUBMITTED TO
THE GRADUATE SCHOOL OF NATURAL AND APPLIED SCIENCES
OF
MIDDLE EAST TECHNICAL UNIVERSITY

BY

EBRU DÜLGERGİL

IN PARTIAL FULFILLMENT OF THE REQUIREMENTS
FOR
THE DEGREE OF MASTER OF SCIENCE
IN
PHYSICS

AUGUST 2012

Approval of the thesis:

DEVELOPMENT OF A PULSED FIBER LASER FOR LADAR SYSTEM

submitted by **EBRU DÜLGERGİL** in partial fulfillment of the requirements for the degree of **Master of Science in Physics Department, Middle East Technical University** by,

Prof. Dr. Canan Özgen
Dean, Graduate School of **Natural and Applied Sciences**

Prof. Dr. Mehmet T. Zeyrek
Head of Department, **Physics**

Assoc. Prof. Dr. Hakan Altan
Supervisor, **Physics Dept., METU**

Examining Committee Members:

Assoc. Prof. Dr. Serhat Çakır
Physics Dept., METU

Assoc. Prof. Dr. Hakan Altan
Physics Dept., METU

Assist. Prof. Dr. F. Ömer İlday
Physics Dept., Bilkent University

Assist. Prof. Dr. Alpan Bek
Physics Dept., METU

Assist. Prof. Dr. A. Behzat Şahin
Electr. and Comm. Eng., YBU

Date: 31 August 2012

I hereby declare that all information in this document has been obtained and presented in accordance with academic rules and ethical conduct. I also declare that, as required by these rules and conduct, I have fully cited and referenced all material and results that are not original to this work.

Name, Last name :

Signature :

ABSTRACT

DEVELOPMENT OF A PULSED FIBER LASER FOR LADAR SYSTEM

Ebru Dülgergil

Master, Physics Department

Supervisor : Assoc. Prof. Dr. Hakan Altan

August 2012, 94 pages

In recent years laser technology has increasingly developed with the use of fiber lasers and this has provided the possibility to implement different techniques in the defense industry. LADAR is at the forefront of these techniques. Fiber lasers constitute a perfect source for LADAR systems due to their excellent robustness, compact size and high-power generation capability. In this study we will explore the development of a pulsed fiber laser source for a LADAR system that can obtain high resolution 3D images in eye-safe region.

A high power, all fiber integrated erbium system with strictly single mode operation in eye-safe region based on MOPA (master oscillator power amplifier) configuration with seed source and amplifier part was developed. Both the use of an actively mode locked laser with erbium doped fiber and fiber coupled modulated distributed feedback diode laser were investigated as seed sources for the amplifier part. Both erbium doped single clad fiber and erbium-ytterbium doped double clad gain fiber were used in this amplifier system. After amplification of the actively mode locked laser, 12 W of average optical power was obtained through single mode fiber with 1ns pulse duration at 10 MHz which corresponds to 1.2 kW peak power. For the fiber coupled DFB diode laser, 9.5W average power was obtained with around 8 ns duration pulses at 100 kHz and about 9.2 W average power was also obtained with around 700 ps duration pulses at 1 MHz through strictly single mode fiber at the output of the same amplifier system as was used in the actively mode locked seed source. In both cases calculated peak power was around 10 kW

which is estimated as the highest peak power for an all fiber integrated system with single mode operation.

The development of such a fiber system with high power capability, compact size and free of misalignment is expected to be useful for LADAR application as well as other areas such as eye surgery, 3D silicon processing or any other material processing applications.

Keywords: LADAR, fiber laser, erbium doped fiber laser system, pulsed laser operation, high power laser.

ÖZ

LADAR SİSTEMİ İÇİN ATIMLI FİBER LAZER GELİŞTİRİLMESİ

Ebru Dülgergil

Yüksek lisans, Fizik Bölümü

Tez Yöneticisi : Doç. Dr. Hakan Altan

Ağustos 2012, 94 sayfa

Lazer teknolojisi fiber lazerlerin gündeme gelmesiyle son yıllarda giderek gelişmiş ve savunma sanayinde değişik teknikleri hayata geçirmeyi mümkün kılmıştır. Bu tekniklerin başında LADAR sistemi gelmektedir. Fiber lazerlerin yüksek kararlılık ve küçük ebatlarıyla yüksek güçlere ulaşabilme özelliği LADAR sistemi için mükemmel bir kaynak oluşturmaktadır. Bu çalışmada da yüksek çözünürlüklü üç boyutlu görüntüleme özelliği sağlayan, LADAR sistemi için göze zararlı olmayan dalgaboyunda çalışan fiber lazer kaynağı geliştirilmesi esas alınacaktır.

Yüksek güçlü, fibere tümleşik ve tek kipli çıkış sağlayan, göze zararlı olmayan dalgaboyu aralığında çalışan, kaynak ve yükseltici kısımlarından oluşan MOPA konfigürasyonu temeline dayanan bir sistem geliştirilmiştir. Hem Erbiyum katkılı kazanç fiberi içeren aktif kip kilitli lazer salıngacı, hem de fibere tümleşik modüle edilebilir geri beslemeli lazer diyot (DFB; distributed feedback laser), yükseltici kısmı için kullanılan kaynaklar olarak incelenmiştir. Yükseltici kısımda hem tek kılıflı Erbiyum katkılı kazanç fiberi hem de çift kılıflı Erbiyum ve Ytterbiyum katkılı kazanç fiberi kullanılmıştır. Aktif kip kilitli lazer salıngacının yükseltme işleminden sonra 1 ns atım uzunluğuna sahip ve 10 MHz tekrar frekansında 12 W ortalama optik güç, tek kipli fiber çıkışında elde edilmiştir ki bu değer 1.2 kW tepe gücüne denk gelmektedir. DFB lazer sinyalinin yükseltilmesi ile, sistemin tek kipli fiber çıkışında 100 kHz tekrar frekansında 8 ns lik atımlar 9.5 W ortalama optik güçle elde edilmiş, aynı sistemin 1 MHz tekrar frekansında yaklaşık

700 ps atım uzunluęu oluřturan versiyonu ise 9.2 W ortalama optik gce ykseltilmiřtir. DFB lazer sonrası elde edilen bu iki durum iin de hesaplanan tepe gc yaklařık 10 kW'tır ki bu deęer tek kipli ıkıřı olan fibere tmleřik yapılar da tahmin edilen en yksek tepe gc deęeridir.

Geliřtirilen yksek g kapasitesine sahip, kompakt ve hizalama sorunu olmayan bu fiber sisteminin LADAR uygulamaları kadar gz ameliyatları,  boyutlu silikon iřleme ya da dięer malzeme iřleme uygulamaları iin de kullanıřlı olması beklenmektedir.

Anahtar kelimeler: LADAR, fiber lazer, Erbiyum katkılı fiber lazer sistemi, atımlı lazer operasyonu, yksek gl lazer.

To my parents

ACKNOWLEDGEMENTS

In the first place, I would like to thank my advisor Hakan Altan for his valuable support and guidance during my study. And I want to express my special thanks to F. Ömer İlday for his enthusiastic support of my thesis. I would also like to thank him for the excellence working environment and laboratory facilities that he provided during this study.

I am grateful to Ihor Pavlov for his support in both experimental study and numerical simulation part of the thesis. His collaboration and our theoretical discussion were very fruitful.

I would like to express my special thanks to Alper Bayrı for all his support during this study.

I am grateful to Seydi Yavaş and Levent Budunoğlu for their friendship and support. Thanks to our discussions during every step of this study, I could improve my works.

I am grateful to Çağrı Şenel, Önder Akçaalan, Mutlu Erdoğan, Kutan Gürel, Emrah İlbey, Sinem Yılmaz, Bülent Öktem, Hamit Kalaycıoğlu, Parviz Elahi, Kıvanç Özgören, Gizem Erkilet, Uğur Teğın and the rest of the members of Ultrafast Optics & Lasers Group for their support and friendship.

Kaan Akar, Şaban Bilek and Murat Vural from Meteksa Savunma. A. Ş. made important contributions especially on the development of the desired LADAR source in terms of industrial aspects.

Finally I would like to thank and acknowledge my thesis examination committee: Assoc. Prof. Dr. Hakan Altan, Asst. Prof. Dr. F. Ömer İlday, Assoc. Prof. Dr. Serhat Çakır, Asst. Prof. Dr. Alpan Bek and Asst. Prof. Dr. A. Behzat Şahin.

This work was supported by SAN-TEZ under grant 510.STZ.2009-2. and SSM Fiber Laser Project.

TABLE OF CONTENTS

ABSTRACT	iv
ÖZ	vi
ACKNOWLEDGEMENTS	ix
LIST OF TABLES	xi
LIST OF FIGURES	xii
CHAPTERS	
1.INTRODUCTION.....	1
1.1- Overview of LADAR/LIDAR systems	1
1.2- Fiber lasers as a LADAR/LIDAR source.....	5
1.3- Overview of fiber lasers	6
2.MODE LOCKING THEORY	9
2.1- Passive mode locking	13
2.2- Active mode locking	15
3.AMPLIFICATION IN RARE-EARTH DOPED FIBERS.....	22
3.1- Gain medium.....	23
3.2- Erbium doped fiber amplifiers	26
3.3- Main limitations	34
4.EXPERIMENTAL DEVELOPMENT OF FIBER LASER SOURCE FOR LADAR/LIDAR SYSTEMS	41
4.1- Seed sources	41
4.1.1- Actively mode locked laser	42
4.1.2- Fiber coupled modulated distributed feedback semiconductor laser	50
4.1.3- Discussion	55
4.2- Amplifier system.....	56
4.2.1- Actively mode locked laser amplification.....	56
4.2.2- Fiber coupled modulated DFB laser amplification	63
5.CONCLUSION	78
REFERENCES.....	81
APPENDICES	
A. Impulse generator specifications	86
B. C++ code for preamplifier simulation	88

LIST OF TABLES

TABLES

Table 1: Common laser-active ions with host glasses and important emission wavelengths [43].	23
Table 2: Parameters used in preamplifier simulation.	57

LIST OF FIGURES

FIGURES

Figure 1.1: The basic block diagram of LADAR systems.	2
Figure 1.2: Dependency of optical losses in silica fiber with respect to wavelength [adapted from Ref. 24].	7
Figure 2.1: Temporal evolution of optical power and losses in a passively mode-locked laser with a fast saturable absorber [36].	13
Figure 2.2: Temporal evolution of optical power and losses in a passively mode-locked laser with a slow saturable absorber [36].	14
Figure 2.3: Temporal evolution of optical power and losses in an actively mode-locked laser [38].	16
Figure 2.4: Schematic setup of an acousto optic modulator [40].	18
Figure 2.5: Schematic setup for fiber coupled phase modulator [adapted from Ref. 41].	20
Figure 2.6: Schematic setup for fiber coupled intensity modulator [adapted from Ref. 41].	21
Figure 3.1: Illustration of three and four level lasing schemes [adapted from Ref. 44].	24
Figure 3.2: Energy levels of the triply ionized erbium ion, Er ³⁺ [adapted from Ref. 46].	27
Figure 3.3: Schematic of EDFA configurations utilizing (a) forward pumping (b) backward pumping (c) co-pumping.	28
Figure 3.4: Absorption bands of Er ³⁺ (solid lines) and the pump efficiency (vertical bars) [46].	29
Figure 3.5: Emission cross section for erbium ion [adapted from Ref. 49].	30
Figure 3.6: Double-clad fiber consists of a rare-earth-doped core surrounded by a much larger and higher-NA inner cladding [52].	31
Figure 3.7: Various designs of double-clad fibers. The fiber core is shown in blue, the inner cladding in light gray, and the outer cladding in dark gray [54].	31
Figure 3.8: Energy level diagram of erbium-ytterbium co-doped silica [adapted from Ref. 56].	32
Figure 3.9: Raman gain spectrum of standard single mode fiber around 1.5 μm pump wavelength [adapted from Ref. 67].	36
Figure 3.10: SPM-broadened spectra for an un-chirped Gaussian pulse [66].	37
Figure 3.11: Photomicrographs of catastrophic damage to the fiber core [69].	38
Figure 3.12: Photomicrographs of damage to a fiber end face [69].	39
Figure 3.13: Photomicrograph of optically induced damage at the glass-polymer interface [69].	39
Figure 4.1: First constructed actively mode locked laser scheme for this study.	42
Figure 4.2: Pulse train of constructed actively mode locked fiber laser.	44

Figure 4.3: RF spectrum of constructed cavity; a) 200MHz span, b) 8GHz span	44
Figure 4.4: Optical spectrum of constructed cavity.....	45
Figure 4.5: Experimental results which show the relation between τ_a vs. ω_M	46
Figure 4.6: Revised actively mode locked laser cavity.	46
Figure 4.7: Pulse train of revised actively mode locked cavity.....	47
Figure 4.8: RF spectrum of revised cavity; a) 50MHz span, b) 3GHz span	47
Figure 4.9: Optical spectrum of revised cavity.	48
Figure 4.10: RF spectrum near 10 MHz with high resolution and low span.....	49
Figure 4.11: Recent photo of actively mode locked fiber laser built for this study. .	49
Figure 4.12: Impulse generator output voltage with respect to repetition frequency.	51
Figure 4.13: Output power of DFB laser with respect to repetition frequency.	52
Figure 4.14: Impulse generator pulse duration at 7 MHz.....	52
Figure 4.15: DFB laser pulse duration at 7 MHz.	53
Figure 4.16: Optical spectrum for DFB laser with 1551nm central wavelength (inset; logarithmic scale).	53
Figure 4.17: Optical spectrum for DFB laser with 1555nm central wavelength (inset; logarithmic scale).	54
Figure 4.18: DFB lasers pulse train with nanosecond modulation.....	55
Figure 4.19: Simulation result for ASE creation in both direction in time (left) and along fiber (right).	58
Figure 4.20: Simulation results for 1.2 m erbium fiber with 300 mW pump power and 4 mW seed signal from actively mode locked laser.	59
Figure 4.21: Pre-amplifier scheme.....	59
Figure 4.22: Output spectrum of pre-amplifier for actively mode locked laser (inset; logarithmic scale).	60
Figure 4.23: Amplifier system scheme for actively mode locked laser.	60
Figure 4.24: Pump power vs. output power from actively mode locked laser amplifier system.	61
Figure 4.25: Output spectrum of actively mode locked laser amplification system at 12 W (inset; logarithmic scale).....	62
Figure 4.26: Pulse train of actively mode locked laser amplification system at 12 W.	62
Figure 4.27: Amplifier scheme for modulated DFB laser included pulse picking process (inset; cooling system for splice point).	64
Figure 4.28: Spectrum after AOM (inset; logarithmic scale).....	65
Figure 4.29: Pulse train after AOM.....	65
Figure 4.30: Pre-amplifier output after pulse picking process for picosecond amplifier system (inset; logarithmic scale).	66
Figure 4.31: Middle stage output for picosecond amplifier system (inset; logarithmic scale).....	67
Figure 4.32: Spectrum of 6 W average power at the output of picosecond amplifier system (inset; logarithmic scale).	68

Figure 4.33: Pulse train of 6 W average power at the output of picosecond amplifier system.	68
Figure 4.34: Simulation results of preamplifier for nanosecond and picosecond regime showing the ASE creation with nanosecond seed.	70
Figure 4.35: Two-stage preamplifier configuration for nanosecond pulse amplification.	70
Figure 4.36: preamplifier stages output spectrum for nanosecond seed (inset; logarithmic scale).	71
Figure 4.37: Spectrum after AOM for nanosecond seed (inset; logarithmic scale). .	72
Figure 4.38: Pulse train after AOM for nanosecond seed.	72
Figure 4.39: Amplifier system scheme for nanosecond seed.	73
Figure 4.40: Output pulse with 9.5 W average power at the output of nanosecond seed amplifier system (inset; spectrum for same condition in logarithmic scale)....	74
Figure 4.41: Power under the pulse measurement set-up.	75
Figure 4.42: Amplifier system output in time domain at 9.2 W for picosecond seed (inset; spectrum for same condition in logarithmic scale).....	76
Figure 4.43: Recent photo of amplifier system during operation.	77

CHAPTER 1

INTRODUCTION

In recent years, with the improvement of laser technologies, the application areas of lasers have become wider. Previously known as an impractical implementation of lasers like LADAR's (Laser Detection And Ranging), use of lasers as directed energy weapons, coherent sensor applications, THz imaging, etc. are now starting to proliferate thanks to variety of developed laser systems. Nowadays, for the aforementioned applications, one of the most attractive and intensely studied research areas in lasers are fiber lasers due to their excellent robustness, compact size and high-power generation capability. In light of these recent developments in technology, this study demonstrates development of a fiber laser source for one of the forefront application areas of lasers which is LADAR system. Special emphasis is placed on developing an eye-safe fiber laser system that uses two different pulsed seed sources. In one embodiment, the system is started with an actively mode locked Erbium doped fiber laser oscillator and subsequently amplified. In another embodiment, the system uses a pulsed laser diode operating in the eye-safe region. Subsequently the laser diode pulses are fed into a fiber amplifier system to be used in eye-safe LADAR applications. Advantages and disadvantages of both systems are compared and discussed.

1.1- Overview of LADAR/LIDAR systems

LADAR which is known as 'Laser Radar' in defense industry describes an optical detection and ranging system with a laser source. Although the name comes from the acronym of **L**Aser **D**etection **A**nd **R**anging (LADAR) as mentioned before, the first proposed idea was to use light for detection, this is known also as **L**Ight **D**etection **A**nd **R**anging (LIDAR). In 1930, E. H. Synge suggested to measure the atmospheric density by observing the scattered light from the sky[1]. They used searchlights to illuminate sky and received scattered light with a detector located some distance away from the point where light was transmitted to the atmosphere.

By applying simple geometry, they obtained a height profile of scattered light intensity. With the improvement of technology, the receiver and transmitter parts of LADAR/LIDAR systems were combined together and that provided the opportunity to use a pulsed source to detect the distance from time of flight of light. First pulsed system was used in 1938 to determine cloud base heights [2]. After the invention of laser in 1960 by Theodore H. Maiman [3], LADAR/LIDAR studies gained momentum. In 1962, F.J. McClung and R.W. Hellworth developed giant pulsed laser from ruby [4]. In this way, the previous pulsed source approach was also implemented for LADAR/LIDAR with modern laser technology. Smullins and Fiocco applied this technology by using a pulsed ruby laser to detect light scattered from the surface of the moon and from the lower atmosphere [5], [6].

Though the starting point of LADAR/LIDAR systems are mostly related to atmospheric measurements, nowadays there are several other application areas such as agriculture, geology and archeology. The latter is used for obtaining the topographical or high resolution digital elevation maps of a desired field. Recently, the systems have been used in transportation for automobiles' adaptive cruise control systems and in the military for the purpose of detection of targets. Regardless of application area and usage profile, there are common basic concepts related to these systems. In general, the main components of all LADAR systems are transmitter, receiver and detector shown in the following block diagram in Figure 1.1.

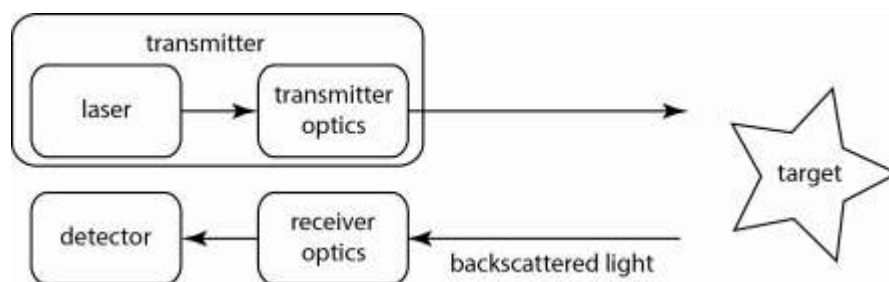


Figure 1.1: The basic block diagram of LADAR systems.

Transmitter part consists of a laser, which produces the beam with desired parameters and transmitter optics that send the beam to the target. With respect to

the application, laser sources can vary from generating pulsed or continuous signal beams at a variety of wavelengths ranging from infrared to the ultraviolet [7]. Pulsed or continuous regime for laser source indicates which information can be collected from the target. With a pulsed system it is easy to make ranging from the time of flight of scattered light, while continuous source with some modulation techniques can also give information based on phase differences. In pulsed regime the important parameters are pulse duration that characterizes the resolution of the LADAR system and pulse repetition rate that characterizes the range. Pulse duration should be short enough to detect the separation between two different targets with respect to desired application. And, pulse repetition rate should be low enough that one pulse has time to reach the target inside the range of system and return before the next pulse is fired. On the other hand in continuous regime, characteristics of modulation and the line width of the laser source decide the resolution and range. Although such systems require different and complex detection methods compared to the pulsed one, they have few advantages like carrying more information related to the target such as velocity. In addition, continuous laser has more average power that makes the detection easy. One disadvantage is that they have limited range due to the coherency of the source. Moreover, modulation requires complex electronics that also make the system complex. Both laser operational modes have some advantages and disadvantages, even though they are preferred for different application areas. It is possible to improve LADAR systems by combining pulsed and continuous beams, and increase the application area of the same system.

Also, lasers became a suitable source for LADAR systems due to the variety of wavelengths with narrow spectral width and low beam divergence. As mentioned in [8] some measurements require specific wavelengths, like atmospheric measurements. For example, the infrared region is preferred mostly due to the high absorption band of several gases and atmospheric particles. The wavelength is also important in terms of eye-safety, since some measurements require people to perform [9]. Wavelengths longer than $1.4\mu\text{m}$ don't reach the retina of eye. So, it is safe to work at these longer wavelengths. According to Harris et al. there are three realistic laser wavelength bands centered at $1.5\mu\text{m}$, $2\mu\text{m}$ and $10\mu\text{m}$ under the consideration of available technology [10]. Between these three, $1.5\mu\text{m}$ is more advantageous due to the intense study of this wavelength range in the recent past compared to the others and the low cost, widely available fiber-optic components

tailored for this range [11]. After deciding the suitable wavelength for the application, the spectral width is taken into consideration. The bandwidth of the laser source is important for filtering the detected signal to decrease the background noise. In other words, the narrower the spectral width means the larger signal to noise ratio due to the capability of wide filtering. Another parameter that decreases background noise is beam divergence. For operating in a long range application like atmospheric studies, the laser source should have low beam divergence with good collimation that allows the possibility to use a receiver with a low field of view, preventing a huge amount of background noise. In order to construct a good collimated beam with low divergence from the transmitter, a beam expander can be used as a transmitter optic, since the minimum beam divergence angle decreases with increasing beam waist radius. In addition, expanding beam diameter is useful for increasing the scanning area on target while decreasing the measurement time. It also helps to reduce the transmitted power per unit area. Even though laser operational wavelength is chosen in the eye safe region, there is a limit in terms of optical power that eyes can handle without any damage. So, it is important to reduce transmitted power per unit area to achieve eye safety while keeping the total power constant.

The second main component of LADAR systems is the receiver which collects the backscattered light from the target under examination and sends it to the detector. For this purpose, a telescopic system is used in the receiver. A significant parameter which affects the performance of the system is the size of the telescope. By increasing the diameter, photon number collected by receiver increases, and similarly the strength of the electrical signal obtained in detector becomes higher. The usual diameter range for such LADAR telescope systems are from 10cm to a few meters. The small diameter has advantages in the near field while the bigger sizes are more suitable to collect enough data from the large distance middle and upper regions of the atmosphere [12]. In many LADAR systems, after collecting enough signal with primary receiver optics, filtering is applied based on wavelength, polarization and/or range with respect to the needs of the application [7]. The simplest case is to use spectral filtering around the operational wavelength of the transmitter so that unwanted background noise with large spectrum bandwidth is diminished. Although spectral filtering is commonly used in almost every LADAR system, polarization and range filtering are also quite common. Former one has ben

applied during atmospheric aerosol studies while the latter one is mostly used for preventing detector damage due to the high level backscattered signal from near-field obstacles [13].

The last component for LADAR is the detector. Receiver part collects photons and sends to the detector and the detector records information about the signal by either using photon counting methods, analog signal detection or coherent detection methods [7]. Photon counting method and analog signal detection are commonly used for pulsed systems to convert optical signal into electronic current for analyzing the information from a target. The only difference between these two techniques is that, the former counts every photon individually by creating an electronic signal that corresponds to each photon, however in latter method, the average current due to the pulses is recorded. Although these detection types have different advantages and they are preferred for different purposes in LADAR systems, they cannot be used for velocity measurements. In order to get the phase data and calculate the velocity from the Doppler shift, coherent detection is used by mixing the backscattered laser light with emitted light from the laser source of the transmitter to obtain beat frequency. This type of system is widely used for wind velocity measurement, but it has also some disadvantages like the requirement of good coherence of the laser source in order to work in long ranges.

1.2- Fiber lasers as a LADAR/LIDAR source

The rapid development of laser technology is followed by the improvements of LADAR transmitter systems. Until this time, LADAR systems have used CO₂, HeNe, Ruby, and other solid state gain media such as ND:YAG [14]. Although the laser power levels have scaled very rapidly and now reach kilowatt levels, these LADAR systems are not suitable for commercial purposes that may require transport due to the large size laser source. For atmospheric studies high power levels of the transmitter is more desirable than a transportable system, however current and emerging LADAR applications require high efficiency and reliability with minimum size and power consumption. Fiber laser technology is used to meet these requirements.

Fiber laser research is one of the most intensely studied areas in laser research, with very rapid progress being reported [15]. There are several main

reasons such as robust and free alignment operation, high average power, which has exceeded multi-kW level for cw operation [see reference 15 for review]. With also the development of low-cost, high brightness, fiber coupled pump diodes; quick progress is obtained in this branch of laser physics. All these advancements make the fiber laser a promising candidate for the transmitter of LADAR systems. Although semiconductor based LADAR's have improved their emission efficiency, electronic compatibility, and reduce the system size and cost, their divergent, elliptical beam profile make them unsuitable sources for long-range applications [16]. Compared to the semiconductor laser, fiber based systems have diffraction limited beam profile that render fiber lasers superior. Moreover, in [17], authors mentioned the advantage of fiber architecture is that it is not only easy to adjust and be mechanically reliable in a vibrating environment, but also can be split up into subsystems spatially far apart and linked together. If power levels are taken under consideration, large-mode-area (LMA) fibers give an opportunity to reach high peak power without nonlinear effects, while maintaining a good spatial mode and polarization state. In addition, master oscillator power amplifier (MOPA) architecture in fiber systems provides a scheme to reach desired power levels with flexible pulse duration and repetition rate. It means LADAR systems with fiber laser transmitter source can fulfill a significant part of requirements either with high spatial resolution or long range.

1.3- Overview of fiber lasers

The origin of fiber technology is based on the communication needs of people. With the invention of telephone and radio, the requirement for fast and reliable communication links had emerged. Although the idea, using the waveguide for light (information) propagation by total internal reflection, was clear to solve the problem, applying the idea properly took longer time. First optical fibers were fabricated in 1920 [18], but these fibers had no cladding which affected the performance dramatically. After the invention of cladded fibers in 1950s [19, 20], studies in this area had accelerated again. In 1961, Elias Snitzer measured the strongest emitter that fluoresced in the IR as neodymium and demonstrated the first neodymium glass laser, called the first fiber laser, in a millimeter-scale rod with the neodymium high index core [21]. By making thicker rods of glass higher power lasers could be reached, however, this was a divergence from the nowadays fibers. In 1964, Charles Koaster and Snitzer demonstrated the first fiber amplifier, using a

spring-shaped coil of fiber slipped around a linear flash lamp [22]. Although these developments improved the usage of fibers, there was a basic difficulty that conventional glass couldn't transfer the light well enough in long distances due to the impurities. In 1966, Kao and Hockamm published a paper about studies to construct better fiber waveguides, made pure enough to carry signals for miles [23]. After they showed that glass could do much better, people continued the research and found that dealing with impurity alone is not enough. Another important parameter to send the information in a long distance was choosing the signal wavelength. Studies showed that there are two fundamental loss limits for silica-based glass fibers called Rayleigh scattering at short wavelengths and the material absorption (the infrared absorption) at long wavelengths. Theoretically, minimum loss level could be predicted at a wavelength of 1550nm where the two curves cross as shown in Figure 1.2. This fact also explains the main reason why the modern telecommunication is based on this wavelength.

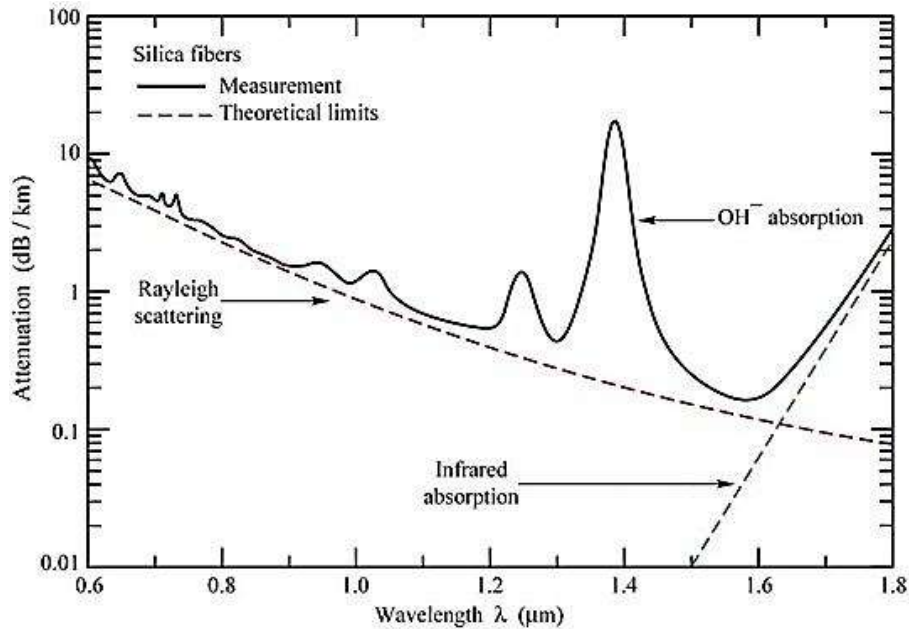


Figure 1.2: Dependency of optical losses in silica fiber with respect to wavelength [adapted from Ref. 24].

In 1970, Corning Glass researchers Robert Maurer, Donald Keck, and Peter Schultz succeeded in developing a glass fiber that exhibited attenuation less than 20 dB/km, the threshold for making fiber optics a viable technology [25]. At about the same time, researchers also paid a lot of attention to develop a light source mostly based on semiconductor lasers for fiber optical communications. After fabricating a series of optical fibers and studies on semiconductor lasers as a pump for fiber optics, in 1985, David Payne from Southampton University decided to try doping fiber cores with rare-earth elements to make fiber laser and he published a paper related to neodymium doped fiber laser pumped with a GaAs laser [26]. This can be accepted as a starting point for fiber laser systems of today. After this work, he and his team from the same university continued to work on this issue and rapidly obtained very good results. First they developed tunable single mode fiber lasers [27], then Payne reported 26dB gain at 1536nm by pumping an erbium-doped fiber [28]. With this study, the focus shifted from semiconductor amplifiers to fiber amplifiers in order to improve telecommunication and also fiber optic systems for other purposes. In early fiber amplifier systems, power level was restricted with the limited brightness of the solid state laser that typically exhibited inefficient coupling to the core of the fiber. By the invention of double clad gain fiber design [29], the problem was solved by sending the pump light through the clad which increased the coupling ratio. Nowadays, power level of fiber lasers can reach kW levels and every year this level has improved. Not only the power levels, but also beam quality robustness and efficiency are the main reasons why fiber lasers are replacing other types of free-space lasers in many areas.

After this brief introduction related to LADAR systems and fiber lasers, next chapter will summarize mode locking theory which is a pulse creation method in fiber laser cavity, divided into two parts as passive and active mode locking. Chapter three will explain the amplification process of signal in fiber configuration after seed source and its limitations while chapter four will demonstrate all experimental studies during the development of fiber laser source for LADAR system. Chapter 5 will conclude all study and mention future plans.

CHAPTER 2

MODE LOCKING THEORY

This study proposes a pulsed fiber laser source for LADAR applications and mode locking technique is generally used to provide pulsed operation in fiber laser configuration, although there are less frequent techniques like gain switching or cavity damping. Generation of pulses is important for LADAR application, since specifications of system are determined with respect to pulse parameters of source as mentioned in the previous chapter. In order to get a deeper understanding about the pulse creation and the condition of created pulses, this chapter will cover mode locking theory which is divided into two sections namely passive and active mode locking.

Mode locking is a technique used to generate pulses that can be many orders of magnitude shorter than the laser cavity round trip time. In other words, it means simultaneous lasing of multiple longitudinal modes where all modes have a fixed mode spacing and fixed phase relationship with each other. Eventually, interference between these modes forms a stationary waveform in time and spectral domain which is called the point that mode lock is achieved. Although the first studies on theory of mode locking was done in frequency domain [30]-[32], Hermann Haus showed that it was easy to understand the stability and stationary pulse formation in time domain [33]. Haus's approach is based on the changes in pulse shape during several round-trips due to each optical component, and he assumed that the effect of one round-trip over the pulse shape is small. He started to form his physical model with complex amplitude in time domain which described single pulse circulation in laser cavity. Then he calculated the changes of the amplitude within a single round trip due to laser gain, optical losses or other effects inside the cavity. Finally he introduced combined changes of the amplitude per round trip with respect to round trip time as an equation of motion describing the mode-locked laser dynamics which is called the master equation of mode locking. It is given as,

$$T_R \frac{\partial A(T,t)}{\partial T} = -l A(T,t) + i \sum_{n=2}^{\infty} D_n i \frac{\partial^n}{\partial t^n} A(T,t) \quad (2.1)$$

$$+ g T \left[1 + \frac{1}{\Omega_g^2} \frac{\partial^2}{\partial t^2} \right] A(T,t) - q(T,t) A(T,t) - i \delta A(T,t)^2 A(T,t).$$

where $T_R = \frac{2L}{v_{g0}}$ is resonator round trip time (v_{g0} is the group velocity at the central wavenumber of the pulse), l is the amplitude loss per round trip, A is normalized wave amplitude, D_n is the dispersion coefficients, $g(T)$ is the gain, Ω_g is the half width at half maximum gain bandwidth, q is saturable absorption coefficient and δ is the self-phase modulation coefficient which is coefficient of nonlinear phase modulation caused by the intensity of signal itself (see ref. [34] for detailed derivation). Briefly, the left hand side shows the amplitude changes per round trip in time domain while right hand side demonstrates the linear optical losses, higher order dispersion (frequency dependency of refractive index) terms, optical gain profile, time dependent nonlinear loss (saturable absorber loss) and third order nonlinearity inside the cavity, respectively. This equation describes the pulse dynamics on two timescales. One of them, t , is the timescale that resolves the shape of the pulse and other one, T , is the order of multiple round trip time ($T = nT_R$) in the resonator on which the pulse shape develops.

Master equation demonstrates the equation of motion of single pulse and in order to get many pulses with a pulse train from laser cavity, a phase relation between the many longitudinal modes which can exist in the cavity should be found. Interference between these modes generates pulses.

$$n\lambda_n = L \quad (2.2)$$

Equation 2.2 shows the possible modes in the laser cavity, where L is the length of the cavity, n is the mode number and λ_n is the corresponding wavelength. Then the total electric field in the cavity with respect to separate modes is,

$$E(z,t) = \sum_n E_n(z,t) = \sum_n E_{n,0} e^{ik_n z - i\omega_n t} = \sum_n E_{n,0} e^{i\phi_n} e^{ik_n z - i\omega_n t} \quad (2.3)$$

where $E_{n,0}$ is the complex amplitude of the n^{th} mode and ϕ_n is the phase. In order to simplify the equation, it can be assumed the square shaped spectrum that all modes have the same amplitude equal to E_0 . With this assumption, intensity can be written as,

$$I(z, t) \propto E(z, t) E^*(z, t) = E_0^2 \prod_{n=1}^N \prod_{m=1}^N e^{i(\phi_n - \phi_m)(m-n)\Omega(\frac{z}{c} - t)} \quad (2.4)$$

where,

$$\Omega = \omega_{n+1} - \omega_n = \frac{2\pi c}{L} \quad (2.5)$$

defines the frequency difference between two constructive modes. Then the intensity can be written as,

$$I(z, t) = E_0^2 e^{i\delta\phi} \prod_{n=1}^N \prod_{m=1}^N e^{i(m-n)\Omega(\frac{z}{c} - t)} \quad (2.6)$$

by assuming all modes have a fixed phase relation to achieve mode locking condition. The summation in the above equation will be equal to unity, if the following condition is valid,

$$\Omega \left(\frac{z}{c} - t \right) = 2\pi j \quad (2.7)$$

where j is an integer. With this way, the intensity will be maximum that indicate a pulse formation with,

$$I_{max} = N^2 E_0^2 \equiv N^2 I_0. \quad (2.8)$$

The spatial and temporal separation of neighboring pulses can be derived from the equation 2.7 as,

$$\Delta z = 2L, \quad \Delta t = \frac{2L}{c} \equiv T_R \quad (2.9)$$

It means that there is a maximum intensity inside the cavity at any one time which repeats with the round trip time T_R of the laser resonator. Due to a fixed phase relationship between the modes in the cavity, pulses with peak intensity I_{max} will grow with the square of the number of modes as shown in equation 2.8. The full width at half maximum (FWHM) of the pulses can be calculated by assuming similar interference between N planar waves at a fixed time $t = 0$. Using geometric series, equation 2.6 becomes,

$$I(t) = I_0 \frac{\sin^2(\frac{N\Omega}{2}t)}{\sin^2(\frac{\Omega}{2}t)} \quad (2.10)$$

Then, FWHM of the pulses can be derived as,

$$I \Delta T = \frac{1}{2} I_{max}, \quad \Delta T = \frac{1}{N} \frac{2L}{c} = \frac{1}{N} T_R \quad (2.11)$$

The relation in equation 2.11 shows that pulse width decreases with increasing the number of superposed modes and it is proportional with the round trip time of the cavity.

Mode locking can be achieved by creating a modulated gain (or loss) in the cavity with frequency Ω . Due to this modulation, electromagnetic field in the cavity gets additional time dependence,

$$\begin{aligned} E_n(z, t) &= E_{n,0} + E_{n,mod} \cos \Omega t e^{ik_n z - i\omega_n t} \\ &= E_{n,0} e^{-i\omega_n t} + E_{n,mod} \frac{1}{2} e^{-i\Omega t} + e^{i\Omega t} e^{-i\omega_n t} e^{ik_n z} \\ &= E_{n,0} e^{-i\omega_n t} + \frac{1}{2} E_{n,mod} e^{-i\omega_{n+1} t} + \frac{1}{2} E_{n,mod} e^{-i\omega_{n-1} t} e^{ik_n z} \end{aligned} \quad (2.12)$$

Equation 2.12 demonstrates that time dependence in every mode induces sidebands and the frequencies of these sidebands match with the one of the neighboring modes. This is valid for total frequency bandwidth and in this way phase synchronization, in other words mode lock between all longitudinal modes is achieved.

There are different ways in order to get mode locking condition by creating the desired gain or loss modulation. These are basically divided into two groups which are passive mode locking and active mode locking. For passive mode locking mostly saturable absorbers are used while active mode locking is achieved by using acousto-optic or electro-optic modulators. Although the next parts summarize both passive and active mode locking, this study utilizes active mode locking.

2.1- Passive mode locking

Passive mode locking can be described as a situation when the dynamics inside of the cavity promote the pulse formation from the noise without any external effect. Most of the time a saturable absorber is used to create time dependent loss inside the cavity and the basic principle for saturable absorber is a decrease in loss when faced with more intense powers. This effect naturally favors the pulse formation since continuous wave (cw) light encounters more loss than a pulse. Depending on the saturable absorber recovery time, there are two different mode-locking techniques, namely fast saturable absorber mode locking and slow saturable absorber mode locking. The main difference between these two methods is that; fast one neglects the gain saturation due to the low intracavity pulse energies compared to the saturation energy of the gain medium while the slow one has to take into account the change of gain in the passage of one pulse [35]. The following graphs demonstrate the behaviour of gain, loss and optical power in time domain during the fast and slow saturable absorber mode locking regimes respectively.

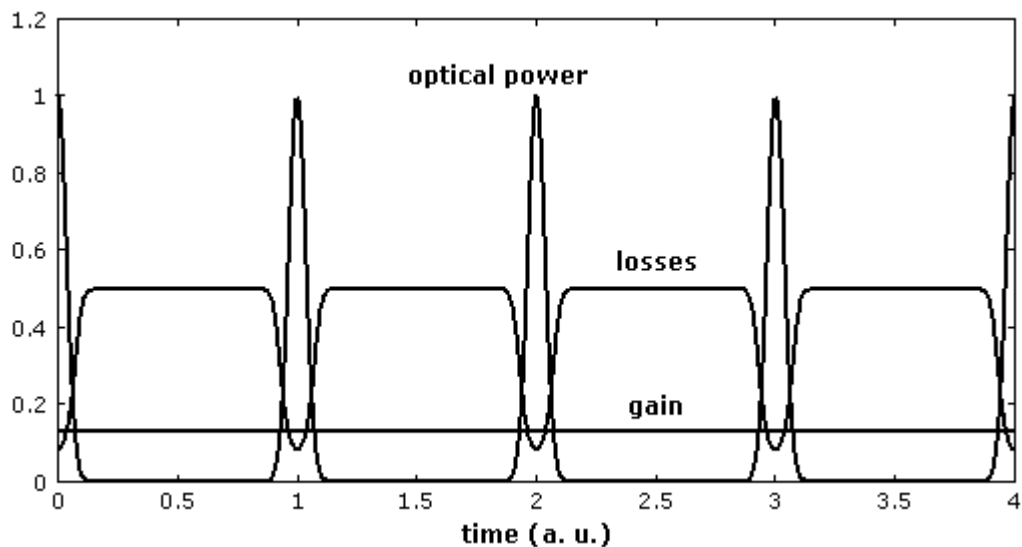


Figure 2.1: Temporal evolution of optical power and losses in a passively mode-locked laser with a fast saturable absorber [36].

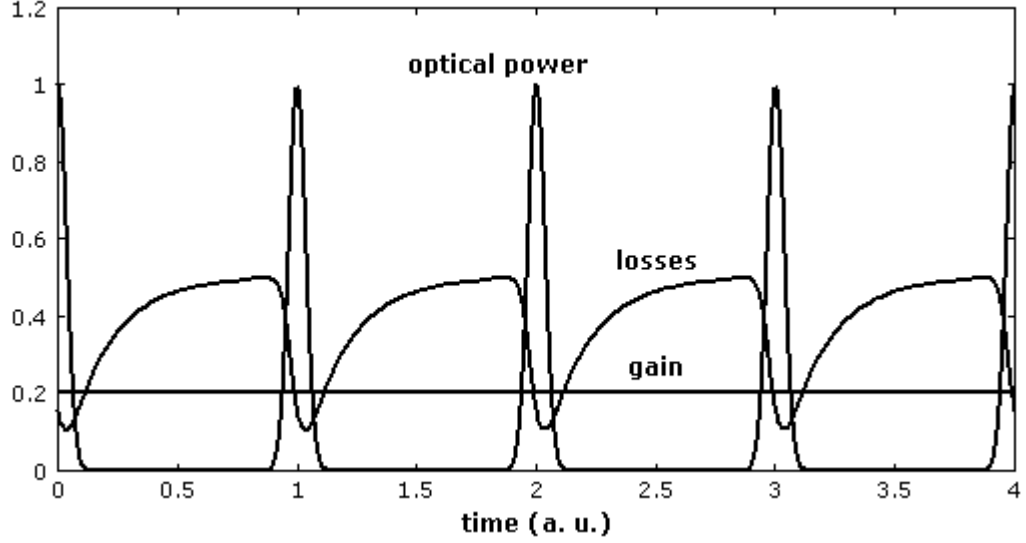


Figure 2.2: Temporal evolution of optical power and losses in a passively mode-locked laser with a slow saturable absorber [36].

For the master equation of fast saturable absorber mode locking, the losses q can be assumed to react instantly on the intensity or power $P(t) = A(t)^2$ of the field [33-34],

$$q A = \frac{q_0}{1 + \frac{A^2}{P_A}} \quad (2.13)$$

where P_A is the saturation power of the absorber and q_0 is the nonsaturated loss. There is no analytic solution of master equation with equation 2.13. So an expansion is used. If the absorber is not saturated, the response can be expanded for small intensities like,

$$q A = q_0 - \gamma A^2 \quad (2.14)$$

where $\gamma = q_0/P_A$ is the saturable absorber modulation coefficient. Then master equation (2.1) becomes,

$$T_R \frac{\partial A(T,t)}{\partial T} = (g(T) - l - q_0 + i \sum_{n=2}^{\infty} D_n i \frac{\partial^n}{\partial t^n} + \gamma A^2) A(T,t) + \frac{g(T)}{\Omega_g^2} \frac{\partial^2}{\partial t^2} A(T,t) - i\delta A(T,t) \quad (2.15)$$

For slow saturable absorber, the changing of gain for one passage of pulse is given as,

$$g(t) = g_i e^{-E(t)/E_L} \quad (2.16)$$

where g_i is the initial small signal gain, $E(t)$ is pulse energy and E_L is the saturation energy of the gain. Similar equation can be written for loss of saturable absorber like,

$$q(t) = q_0 e^{-E(t)/E_A} \quad (2.17)$$

where E_A is the saturation energy of saturable absorber. Then the master equation for slow saturable absorber becomes,

$$\begin{aligned} T_R \frac{\partial A(T, t)}{\partial T} = & \left((g_i e^{-\frac{E t}{E_L}}) - l - q_0 e^{-\frac{E t}{E_A}} + i \sum_{n=2}^{\infty} D_n i \frac{\partial^n}{\partial t^n} \right. \\ & \left. + \frac{1}{\Omega_g^2} \frac{\partial^2}{\partial t^2} - i \delta A(T, t) \right) A(T, t) . \end{aligned} \quad (2.18)$$

These master equations (2.15 and 2.18) for fast and slow saturable absorber have no analytic solution. In order to get the solution and obtain the pulse duration created inside the cavity, some approximation is needed with respect to the cavity conditions. Solutions and detailed derivations for pulse train with a certain balance of nonlinear and dispersive effects can be found in ref. [37].

2.2- Active mode locking

In active mode locking case, different than passive one, loss modulation is controlled by an active element inside of the cavity which can be acousto-optic modulator (AOM) or electro-optic modulator (EOM). The response is shown in Figure 2.3.

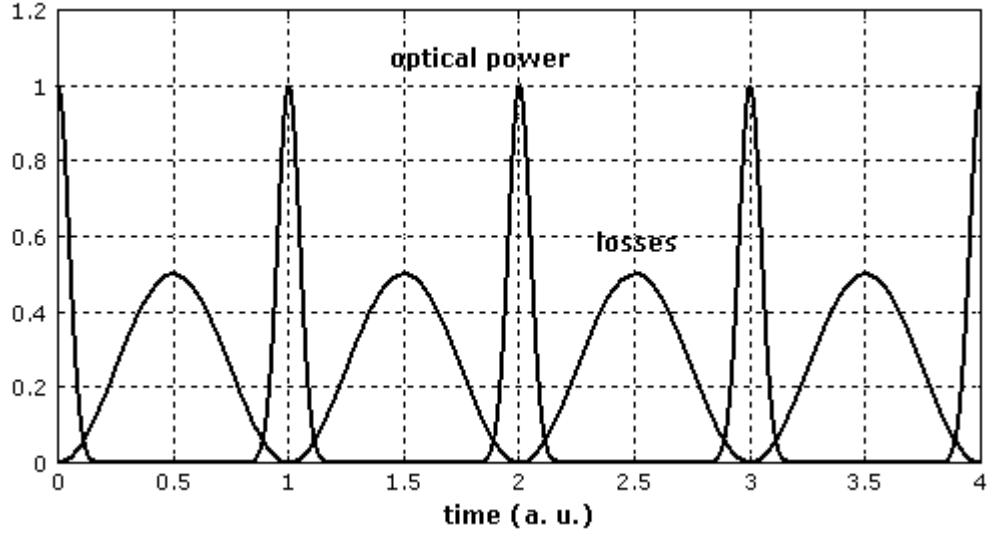


Figure 2.3: Temporal evolution of optical power and losses in an actively mode-locked laser [38].

Although both of them are used for intensity modulation, acousto-optic modulators use sound effect to create changes in refractive index of a crystal while electro-optic modulators are based on the linear electro-optic effect which means the modification of refractive index by an electric field proportional to the field strength. In both cases, periodically varying intracavity loss can be introduced as,

$$q(t) = M(1 - \cos \omega_M t) \quad (2.19)$$

where M is modulation and ω_M is modulation frequency. The most important requirement of active mode locking is that the modulation frequency has to very precisely match with resonator round trip time, $\omega_M = 2\pi/T_R$. If group delay dispersion (GDD) and self-phase modulation (SPM) are neglected which corresponds the second and third terms in equation 2.1, then active mode locking process is formulated with the following master equation,

$$T_R \frac{\partial A}{\partial T} = g(T) + D_g \frac{\partial^2}{\partial t^2} - l - M(1 - \cos \omega_M t) A \quad (2.20)$$

where $D_g = g(T)/\Omega_g^2$ is gain dispersion.

In 2.20, if we fix the gain at its stationary value, then the equation becomes a partial differential equation with separated variables in both sides. Here pulse width

is expected to be much shorter than the round trip time T_R and cosine function in modulation part can be approximated by a parabola, since pulses are created at the minimum loss points of modulation. After this approximation 2.20 becomes,

$$T_R \frac{\partial A}{\partial T} = g - l + D_g \frac{\partial^2}{\partial t^2} - M_s t^2 A \quad (2.21)$$

where M_s is the modulation strength which corresponds to the curvature of the loss modulation in time domain at the minimum loss point

$$M_s = \frac{M\omega_M^2}{2} \quad (2.22)$$

The differential operator on the right side of equation 2.21 is the Schrödinger Operator of harmonic oscillator problem whose eigen functions are Hermite-Gaussians,

$$A_n T, t = A_n t e^{\lambda_n T/T_R} \quad (2.23)$$

$$A_n t = \frac{\overline{W_n}}{2^n \frac{\pi n! \tau_a}{\tau_a}} H_n\left(\frac{t}{\tau_a}\right) e^{-\frac{t^2}{2\tau_a^2}} \quad (2.24)$$

where W_n is the energy of the corresponding solution, τ_a is the width of Gaussian. If this solution is placed into equation 2.21, then the relationship between pulse width and modulation is obtained as (see Ref. 37 for detailed derivation),

$$\tau_a = \sqrt[4]{D_g/M_s} \quad (2.25)$$

Equation 2.25 demonstrates that pulse width obtained by active mode locking decreases with increasing modulation strength which is increasing with the square of modulation frequency. It means that system is restricted with external modulation which is dependent on the electronic speed. Under the limitation of electronic speed, highest modulation can be obtained at the GHz level. Since such repetition rates require very short cavity length (for 10 GHz modulation, cavity length should be approximately 2cm, if speed of light is assumed as 2×10^8 m/s inside the fiber medium), harmonic active mode locking is used. In this technique, the only difference is the number of pulses that rotate inside the cavity. If the fundamental cavity length is adjusted as a modulation frequency, mode lock condition is achieved and just one pulse rotates inside the cavity. If modulation frequency is adjusted multiple integer (n) of the cavity length, then n pulses rotate inside the cavity. This

provides higher modulation frequency, so lower pulse duration without necessity to construct short cavity. However there is a trade off between the pulse energy subtracted from laser source and number of pulses inside the cavity. Since gain can be assumed as a constant value, higher number of pulses means less pulse energy at the output. With respect to the needs, laser parameters like pulse duration, repetition rate and pulse energy should be optimized. Usually minimum created pulse width is in picosecond regime (see Ref. [39] as example) with the help of harmonic mode locking method.

In order to understand active mode locking more deeply, modulators and the working principle of modulators can be examined. In the beginning of active mode locking topic, it was mentioned that loss modulation can be controlled with both AOM and EOM. Modulator types also affect pulse characteristics at the output of laser cavity due to their working bandwidth, rise time and fall time. Therefore it is important to choose suitable modulator with respect to desired condition of output signal. In AOM case, refractive index of a transparent medium or crystal changes periodically similar to the Bragg diffraction. This periodic index modulation is generated by sound waves which form a periodic density grating when propagating through the medium. Here the sound waves are created by a piezo electric transducer which is driven with radio frequency signal and absorber is used to prevent the sound wave from travelling back to the transducer like in Figure 2.4.

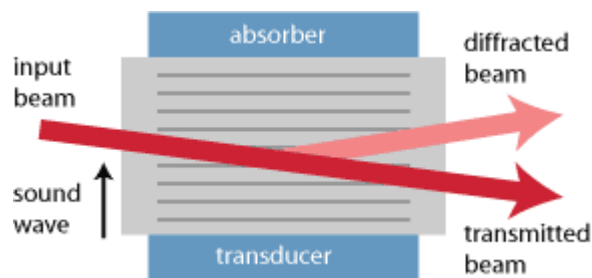


Figure 2.4: Schematic setup of an acousto optic modulator [40].

Due to the created Bragg diffraction, input beam changes its direction with the following equation,

$$\sin \theta = \frac{m\lambda}{n\Lambda} \quad (2.26)$$

where λ is the light wavelength, Λ is the sound wavelength, m is the order of diffraction and n is the refractive index of crystal. With respect to the device design, transmitted beam or diffracted beam is used as an output of AOM, so the efficiency of AOM depend on the fraction of the transmitted beam diffracted into the first order beam which is controlled with the intensity of the sound wave. For obtaining active mode locking, rf signal is used to control sound wave intensity to create loss modulation which is given in equation 2.19 by changing the efficiency of AOM. Modulation speed is limited with the time that sound wave needs to cross the beam diameter. So fast modulation is obtained with small beam diameter, but on the other hand, small beam diameter increases the risk to damage the modulator due to the high light intensity. Therefore, usually AOM is used for modulation up to a few hundred MHz level. For faster modulation EOM is preferred. This study also utilizes EOM as a mode locker inside of a laser cavity.

In EOM case, again refractive index of the crystal is changed but different from AOM, variation of index is generated by the influence of an external electric field. With this way, the phase of incoming light is controlled. Although there are three different types of electro optic modulators which are polarization modulator, phase modulator and intensity modulator, all of them use the same principle and just phase and intensity modulator are used for active mode locking. Polarization modulator is used to create phase shift between two different polarization states of input beam depending on the orientation and type of the crystal.

Phase modulator is the simplest type of an electro optic modulator whose schematic setup is shown in the following figure.

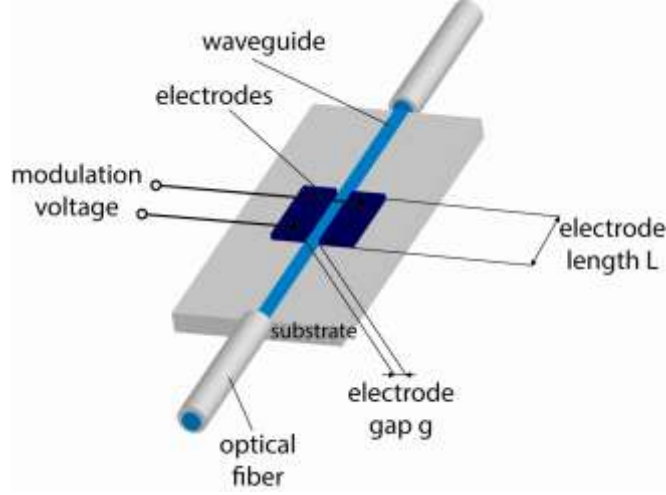


Figure 2.5: Schematic setup for fiber coupled phase modulator [adapted from Ref. 41].

With the help of electrodes, modulation voltage creates an electric field which affects the waveguide and shifts the phase of guided light. Here, there is no loss modulation inside the cavity, but if the case examined with respect to frequency domain, phase modulation with,

$$\Delta\phi = -M [1 - \cos(\omega_M t)] A \quad (2.27)$$

which can be accepted as imaginary part of intracavity loss $q t$, creates sidebands on each cavity mode as:

$$\begin{aligned} \Delta\phi &= -M [1 - \cos(\omega_M t)] \exp i\omega_{n_0} t \quad (2.28) \\ &= -M \exp(i\omega_{n_0} t) - \frac{1}{2} \exp(i(\omega_{n_0} t - \omega_M t)) - \frac{1}{2} \exp(i(\omega_{n_0} t + \omega_M t)) \\ &= M [-\exp(i\omega_{n_0} t) + \frac{1}{2} \exp(i\omega_{n_0-1} t) + \frac{1}{2} \exp(i\omega_{n_0+1} t)] \end{aligned}$$

where the modulation frequency is the same as the cavity round trip frequency. These sidebands promote the neighboring modes which end up being synchronized, in other words mode locked [34]. This type of modulators for active mode locking are limited with the high voltage driver electronics and due to the fast electro optic response, modulation rates can easily reach GHz levels.

Intensity modulator is another type of electro optic modulator which uses Mach-Zehnder interferometry between the arms with a phase modulator like in the following figure.

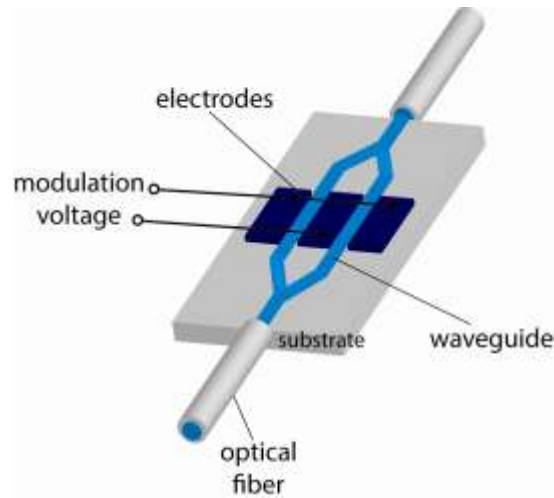


Figure 2.6: Schematic setup for fiber coupled intensity modulator [adapted from Ref. 41].

In this modulator, different than phase modulator, input light is divided into two arms and phase of these two arms are controlled again with the modulation voltage by using electrodes. Then the beams are recombined. If the phase difference between two arms is π , then light interfere destructively at the output of the modulator. This voltage value is defined as a half wave voltage (V_{π}) of the modulator. For zero delay or 2π , light interferes constructively and output will be its maximum value. By changing the modulation voltage it is easy to switch on and off state at the output and modulate the loss given equation 2.19 inside the cavity to get active mode locking. Like in phase modulator, rise and fall time of the intensity modulator is very fast due to the electronic speed, so it can be also used inside the active mode lock laser systems operated at GHz levels. This study also utilizes intensity modulator as a mode locker in experimental setup of the actively mode locked laser.

CHAPTER 3

AMPLIFICATION IN RARE-EARTH DOPED FIBERS

Previous chapter covered mode locking theory which explains the generation of pulses from a laser cavity. Although the cavity creates the desired pulses with suitable parameters, optical power level at the output generally does not exceed mW level for such configurations. Since LADAR applications require high powers, amplification process becomes important to complete the LADAR system transmitter part. This chapter will explain the amplification process in rare-earth doped fibers. First, gain medium will be covered then erbium doped systems will be introduced with a literature review. Finally, the main limitation for the amplification process will be examined.

Fiber amplifier studies also started with fiber laser development, since the laser requires a gain medium inside of the cavity. First results were obtained with neodymium doped glass in 1960s as was mentioned previously. Although the history of fiber amplifiers goes back quite a while, their usage became practical after the fabrication and characterization of low-loss, rare-earth doped fiber in 1980s. These dopants consist of 14 similar elements with atomic numbers in the range from 58 to 71 and when they are doped in silica, they become triply ionized [42]. This situation provides a lasing at desired wavelength with respect to selected doping elements. Table 1 demonstrates the common rare earth doped elements used as an active medium with common host glasses and important emission wavelengths.

Table 1: Common laser-active ions with host glasses and important emission wavelengths [43].

Element	Common host glasses	Important emission wavelengths
Neodymium (Nd)	Silicate and phosphate glasses	1.03–1.1 μm , 0.9–0.95 μm , 1.32–1.35 μm
Ytterbium (Yb)	Silicate glass	1.0–1.1 μm
Erbium (Er)	Silicate and phosphate glasses, fluoride glasses	1.5–1.6 μm , 2.7 μm , 0.55 μm
Thulium (Tm)	Silicate and germanate glasses, fluoride glasses	1.7–2.1 μm , 1.45–1.53 μm , 0.48 μm , 0.8 μm
Praseodymium (Pr)	Silicate and fluoride glasses	1.3 μm , 0.635 μm , 0.6 μm , 0.52 μm , 0.49 μm
Holmium (Ho)	Silicate and fluorozirconate glasses	2.1 μm , 2.9 μm

While erbium (1.5 μm), thulium (1.9 μm) and holmium (2.1 μm) are used for medicine, metrology including LADAR application etc. where the eye safe region is necessary, ytterbium (1.06 μm) is preferred if pure power is required such as in material processing.

3.1- Gain medium

Although there are several rare earth elements that can be used to create gain medium for fiber laser technology by doping into silica, a few of them like erbium and ytterbium stand out due to both their wavelength emission spectrum and availability of commercial pump sources and detectors to analyze the output beams. By improving the pump source technology and increasing the necessity for eye safe region emission in some specific application, thulium and holmium based doped fiber lasers have also gained some momentum. Despite possessing different emission, absorption wavelength and application areas, all these rare earth doped

fibers have similar gain dynamics which can be divided into two main groups as four level system and three level system.

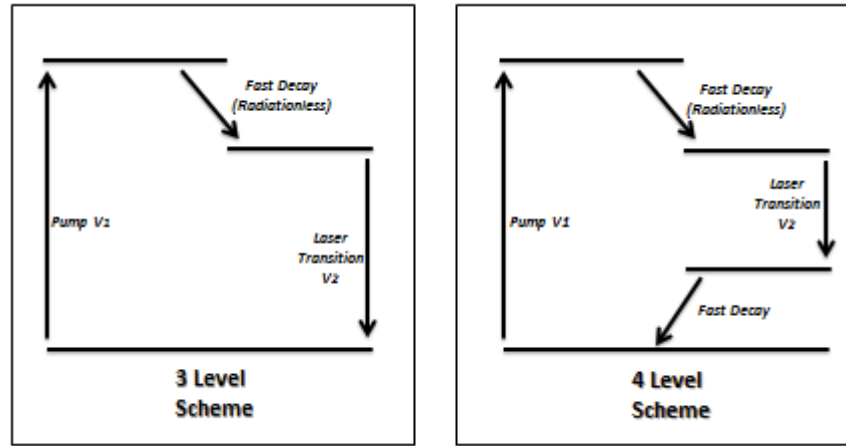


Figure 3.1: Illustration of three and four level lasing schemes [adapted from Ref. 44].

In both cases rare earth ions in fiber are excited to the higher energy levels with the absorption of pump photons. Then they rapidly experience fast decay to lower energy state without radiation. The storage energy is used for amplifying signal beam by stimulated emission. With this way pump energy transfers to the signal and amplification is achieved. The main difference between three and four level system is the energy state occupied by the dopant after the stimulated emission event. In the case of a three level scheme, the process ends up at the ground state, while it is an excited state in the four level scheme. In spite of this difference, in order to get desired gain and amplification from both systems, the most important thing is to get higher population inversion, meaning higher ion density in the upper state which depends on the pump power. In this study erbium doped fiber based system is under discussion where erbium has a three level lasing scheme. Therefore the focus will be on the gain dynamics of three level systems. To understand the behavior of such systems more deeply, the following rate equations should be examined.

For three level system, N_1 , N_2 and N_3 can be defined as a population for ground level, 1st and 2nd excited states respectively. Then, changes in this population

with time due to pump absorption, spontaneous and stimulated emission and also non-radiative transitions can be written respectively as [45],

$$\frac{dN_1}{dt} = W_{signal} N_2 - N_1 + W_{pump} N_3 - N_1 + \frac{N_2}{\tau_{21}} \quad (3.1)$$

$$\frac{dN_2}{dt} = W_{signal} N_1 - N_2 + \frac{N_3}{\tau_{32}} - \frac{N_2}{\tau_{21}} \quad (3.2)$$

$$\frac{dN_3}{dt} = W_{pump} N_1 - N_3 - \frac{N_3}{\tau_{32}} \quad (3.3)$$

where τ_{21} is the upper state life time for transition from 1th excited state to ground state (spontaneous emission), τ_{32} is the upper state life time for transition from 2nd excited state to 1th excited state (fast decay), W_{signal} is the signal absorption and emission probability and W_{pump} is the pump absorption and emission probability. W_{signal} and W_{pump} can be calculated from the following equations,

$$W_{signal} = \frac{P_{signal}}{S_{core} h\nu_{signal}} \sigma_{signal} \quad (3.4)$$

$$W_{pump} = \frac{P_{pump}}{S_{core} h\nu_{pump}} \sigma_{pump} \quad (3.5)$$

where P_{signal} and P_{pump} are signal and pump power, S_{core} is the core area of doped fiber, $h\nu_{signal}$ and $h\nu_{pump}$ are the signal and pump photon energy for single photon, σ_{signal} and σ_{pump} are signal absorption and emission cross section and pump absorption and emission cross section respectively. Here, signal absorption cross section and signal emission cross section are assumed to be equal. Same assumption is valid for also pump absorption cross section and pump emission cross section. In order to obtain gain from such a system, stimulated emission from first excited state to ground state should be much higher than the absorption through opposite direction. This situation requires more population in first excited states that is called as population inversion and the degree of population inversion is given with the following equation,

$$n = \frac{N_2}{N_2 - N_1} \quad (3.6)$$

Then, optical gain can be defined as,

$$g = \sigma(N_2 - N_1) \quad (3.7)$$

where σ is the transition cross section. This gain coefficient can be also written in terms of signal power (P), saturated signal power (P_s) and small signal gain (g_0) given in reference [45] as,

$$g = \frac{g_0}{1 + P/P_s} \quad (3.8)$$

where saturated signal power is defined as the power required for the gain to drop 3dB. It is clear in this equation that, the gain coefficient decreases when the signal power increases which is known as gain saturation in laser and amplifier systems. This is a result of depopulation of excited state due to an increasing number of signal photons.

3.2- Erbium doped fiber amplifiers

As mentioned in previous section, erbium is common rare earth element to construct fiber laser and amplifier system in an eye-safe region. It is also well developed due to interest in all optical communication systems. Since this study should include eye safety, erbium doped systems can meet all requirements for desired LADAR systems like cost, availability of suitable components and measurement tools. It is chosen as a best fit rare earth element for LADAR. This section will summarize erbium doped fiber amplifiers and their current situations in more detail.

Following figure shows the energy level of erbium ion.

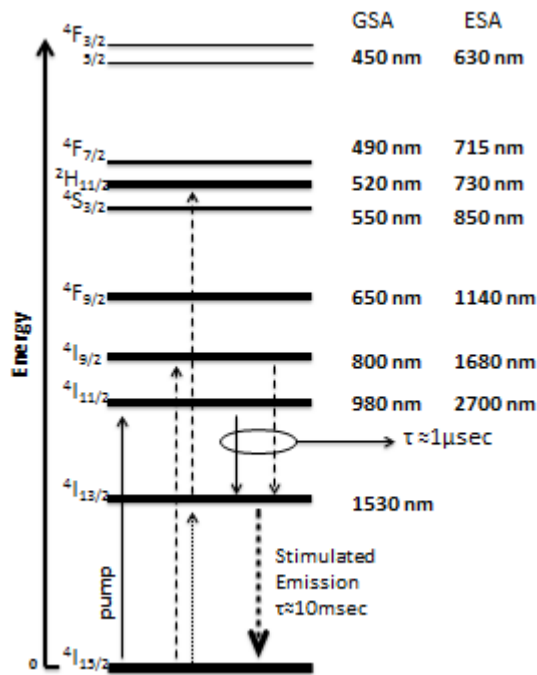


Figure 3.2: Energy levels of the triply ionized erbium ion, Er^{3+} [adapted from Ref. 46].

In energy level diagram, possible transitions with pump are shown. After obtaining population inversion, by sending signal photons it is possible to get stimulated emission at a signal wavelength. However there is a phenomenon to decrease the amplification efficiency called amplified spontaneous emission (ASE). There is an upper state lifetime for ions in excited state which is around 10 ms for erbium case. During this time if excited ions do not stimulate with signal, they fall down with spontaneous emission and this undesired photon or photons are also amplified like as in signal case. There are different methods to decrease ASE level in the system like adjusting signal power, pump power, pulse energy, repetition rate and gain fiber length properly to trigger stimulated emission of signal. Pumping direction also helps to decrease ASE creation by adjusting the pump power along the gain fiber. There are 3 main pumping configurations for fiber amplifier system which are shown in the following figure.

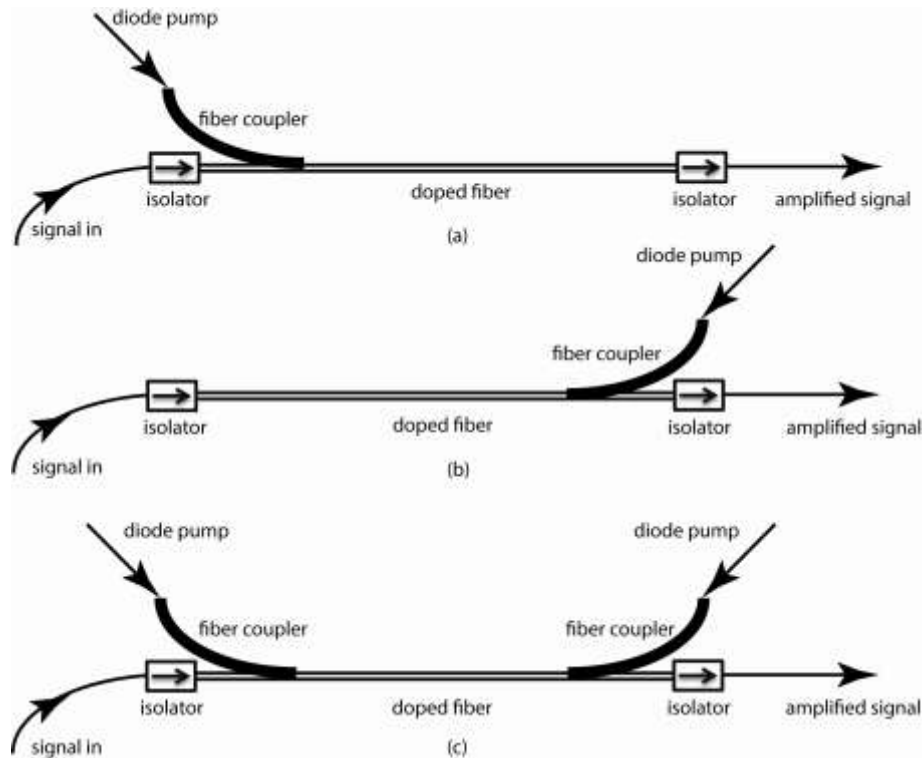


Figure 3.3: Schematic of EDFA configurations utilizing (a) forward pumping (b) backward pumping (c) co-pumping

In terms of the direction of pump and signal, they are called forward pumping, backward pumping and both forward and backward in other words co-pumping respectively. Although all of them are used practically in different systems, backward pumping has significant advantages. Signal beam and pump enter the gain fiber from different ends which means where the signal is weak also the pump and population inversion are weak. Therefore signal photons are enough to stimulate all excited ions in the upper states and this decreases the ASE creation. Moreover output of such system is pure signal even if there is an excess pump.

About the decision of pumping wavelengths, possible bands for erbium are shown in Figure 3.4.

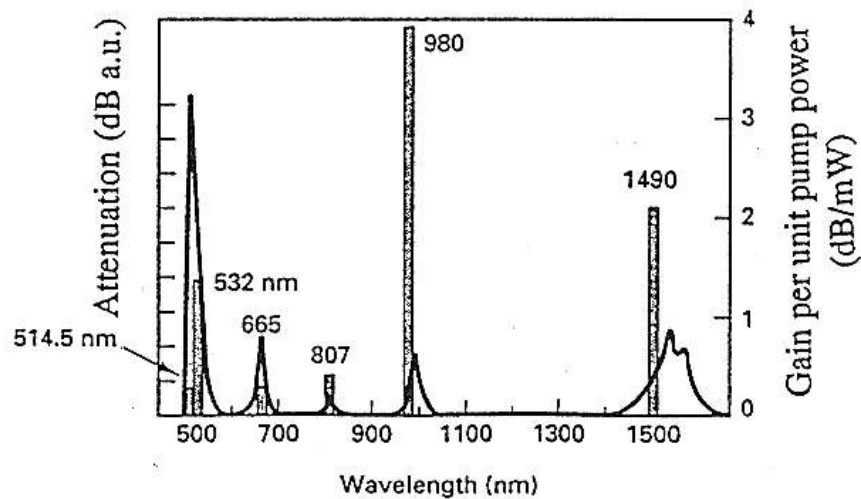


Figure 3.4: Absorption bands of Er^{3+} (solid lines) and the pump efficiency (vertical bars) [46].

Although there are 5 absorption bands for erbium, Payne's group found that 800 nm and other wavelengths lower than that are not suitable for pumping due to the excited state absorption which decreases the pump efficiency [48]. They proposed 980nm pumping as an efficient pump band. However, here a different problem arises which comes from the big difference between emission wavelength of erbium ions and absorbed pump wavelength. Since the emission of erbium doped fiber is around 1550nm which is shown in the following figure, signal photon energy is always less than pump photon energy even all pump photons are converted to the signal photons. This difference between signal and pump photon energy is called a quantum defect which effects the power efficiency of the system. For such systems with 980nm pumping, the maximum efficiency that can be achieved is around 64% theoretically.

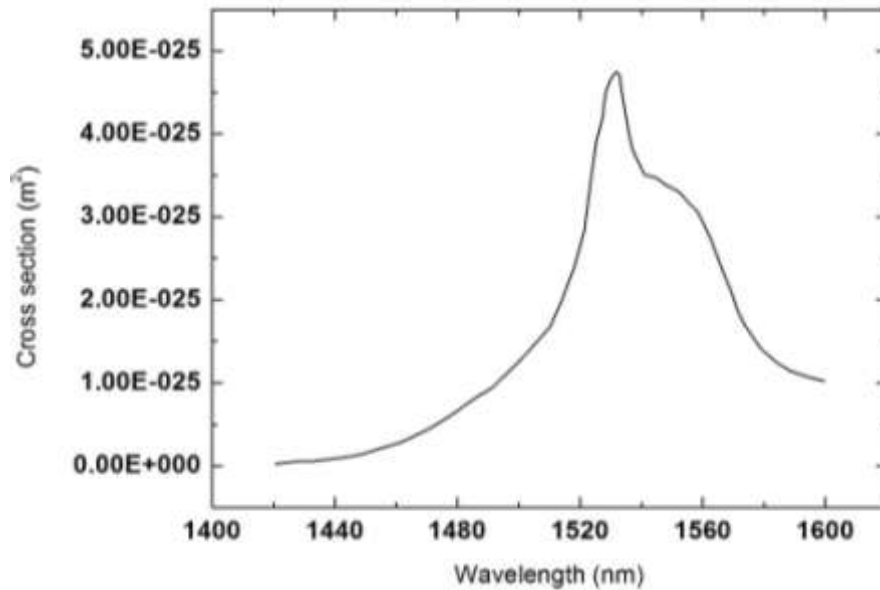


Figure 3.5: Emission cross section for erbium ion [adapted from Ref. 49].

For coping with this problem, further studies were made. In 1988, Snitzer found that 1480 nm would also be a good pump wavelength due to less quantum defect [50]. With the development of high quality and high power pump diodes, both pumping bands start to be widely used for different applications.

Although pump diode technology has increased rapidly affecting erbium laser amplification positively, the real jump at the output power was obtained with the invention of double clad fibers. Coupling of high pump power through single mode fiber is difficult. Even though single emitter pump diodes can give around ~50W output power, it is only possible to couple a few watts into a single mode fiber. With double clad fiber structure shown in Figure 3.6, pump from a broad stripe multimode diode can easily be coupled into an inner cladding which surrounds a single mode fiber core. If the geometry and size of the cladding are appropriate, the propagating pump can be efficiently absorbed inside the single mode core which is doped with active ions to produce optical gain [51]. The refractive index profile of double clad fibers is also shown in the figure. The highest value is inside of the core and it decreases towards the outer cladding.

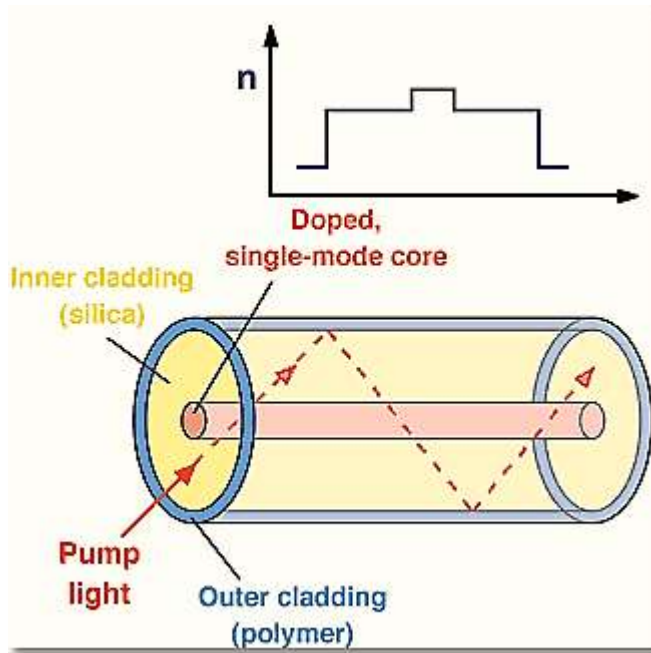


Figure 3.6: Double-clad fiber consists of a rare-earth-doped core surrounded by a much larger and higher-NA inner cladding [52].

Though this double clad configuration increases the pump power coupled to the gain fiber which can result in higher signal output, absorption efficiency of pump is limited with the interaction of pump and core. In order to increase the interaction, cladding is generally made asymmetric or at least non-circular, because if it is circular, there can be some guided modes due to the intensity distribution of pump light that could not be absorbed. Geometries, such as D-shaped or rectangular pump cores shown in the following figure, prevent the propagation of such undesired intensity distributions of the pump radiation by continuous mode mixing [53].



Figure 3.7: Various designs of double-clad fibers. The fiber core is shown in blue, the inner cladding in light gray, and the outer cladding in dark gray [54].

Amplification of pump absorption with such configuration of double clad fiber helps to improve output power from erbium amplifier systems. However, absorption is also limited due to the doping concentration of erbium ions in glass. Quenching through energy transfer between closely located neighboring ions results in a serious pump efficiency reduction in case of erbium [55]. Therefore doping concentration cannot be very high. As a result, high pump power systems require longer gain fiber that brings nonlinear effects into consideration. In order to handle this situation and increase in the absorption cross section by co-doping with ytterbium was thought of as a solution. Energy levels and transitions of erbium-ytterbium co-doped fiber are shown in the following figure.

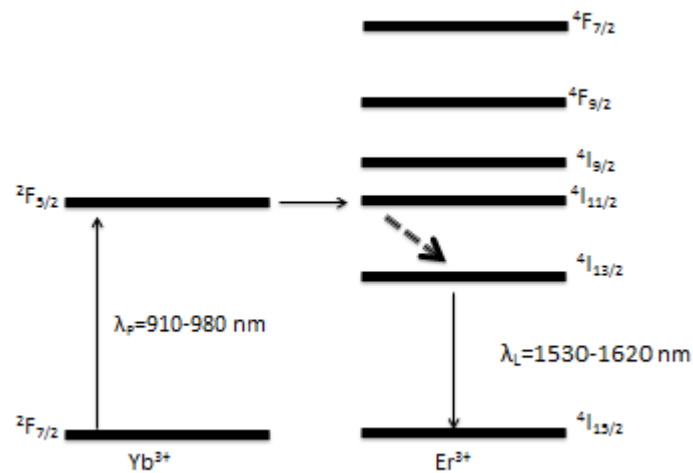


Figure 3.8: Energy level diagram of erbium-ytterbium co-doped silica [adapted from Ref. 56].

Pump light is absorbed by ytterbium ions and the energy is transferred non-radiatively to the erbium ions for stimulated emission inside of the erbium emission range. The main drawback of this approach is the possibility of amplified spontaneous emission (ASE) generation at 1030 nm at high pump powers, which sharply decreases efficiency at 1550 nm and limits the output power level. Despite this difficulty, with such configuration, absorption cross section is increased and that means that the required fiber length for the same value of pump is decreased. Until emerging of this technology, erbium systems were not considered as a big potential

of high power generation at telecommunication wavelengths, but co-doping improved the power levels rapidly. Nowadays co-doped double clad fibers serve the possibility both to pump harder and at the same time to cope with nonlinear effects via shorter fiber length. Of course, decreasing fiber length by increasing absorption cross section with ytterbium has limited effect on nonlinearity. It also increases with the intensity on the core which is necessary mostly for high output power. This situation has forced the scientists to use larger core to decrease the intensity that brings the laser into multimode operation regime. Although larger core diameter provides higher output power, such systems lose the main advantages of fiber lasers which are diffraction limited pulse quality. Fortunately there are some methods to suppress multimode operation in large mode area fiber like giving bending loss to maintain fundamental mode which is the least sensitive mode for bending [57], tapering fiber to pass the fundamental mode [58], and using special radial doping distribution to suppress multimode operation [59].

All these improvements in fiber technology explained up to this point provide development of high power, high quality fiber laser systems for different applications in the 1.5 μ m-1.6 μ m wavelength which is inside the eye-safe region. Reference [60] demonstrates 297 W output power achieved with erbium-ytterbium (Er-Yb) co-doped double clad large mode area fiber. In Ref. [61], the authors denote 100W class single mode linearly polarized all-fiber source again by using Er-Yb co-doped double clad large mode area fiber. Although highest power levels are achieved and reported with co-doped gain fiber in continuous wave (cw) regime, by improving the technology, Yb free erbium doped fiber amplifier systems and pulsed signal amplification has also gained acceleration. In Ref. [62], authors demonstrate 67W cw output power with erbium doped multimode fiber for 976 nm cladding pump. For pulsed regime, despite the difficulties that come from the high peak power that trigger nonlinearity, ~2.8 W average output power at 15 MHz repetition rate with beam quality (M^2) < 1.1 was reported in Ref. [63]. This system was pumped by Raman fiber lasers operating at 1480 nm and used large mode area Er-Yb co-doped fiber. Also high-energy amplification to the μ J-level has been demonstrated by several groups at low average powers and with amplifier configurations, which are not all-fiber-integrated [64, 65]. These systems included Er-Yb co-doped fiber with cladding pump at 980 nm and 1480 nm, typical slope efficiency (the ratio between system output power and pump power) reported up to

now is in the range ~40%–45% and ~58%–64% at best, respectively [56]. By considering these efficiencies, it seems that obtaining higher output power is possible with increasing the coupled pump power to the amplifier system. However, this is not the case every time due to some limitations which will be explained in the following section.

3.3- Main limitations

Fiber laser system provides several advantages like getting high beam quality, high power, compact, and robust source covering wide wavelength range with different repetition rate and pulse duration for a low cost. On the other hand, it has some limitations that come from the small mode size and large propagation length in nonlinear medium compared to the free-space solid state lasers. So it is understandable that the nonlinear effects are the main concern, coming before the material damage or thermal problems. This section will explain these difficulties that limit the laser from reaching higher power levels.

One of the most important nonlinear effects to limit output power and performance of the laser is Stimulated Brillouin Scattering (SBS) which is related to the third order susceptibility $\chi^{(3)}$. It can be created spontaneously even at low power levels with suitable conditions. The phenomenon occurs as a conversion of incident photon into a scattered photon with a slightly lower energy and an acoustic phonon. Due to the conservation of momentum, generally scattered photons are propagated opposite to the incident photon. These two counter-propagating waves create a traveling refractive index grating resulting in undesired backward optical signal. There can be also stimulated effects for higher optical powers where the phonon population depends on the optical fields. Here, the backscattered light has slightly shifted frequency due to the phase matching requirements. This shift is called a Brillouin frequency shift and it can be calculated as,

$$v_B = \frac{2nv_a}{\lambda} \quad (3.9)$$

where n is the effective refractive index of fiber v_a is the velocity of acoustic phonons and λ is the incident photon wavelength. For silica this shift is in the order of 10-20 GHz with a gain bandwidth of 10 MHz which is related to damping time of the acoustic waves determined by phonon lifetime. Since gain bandwidth is small,

SBS only affects systems with narrow bandwidth like single frequency lasers. For pulsed systems with pulse duration lower than 10 ns, SBS is negligible.

In fiber systems that have suitable conditions which allow them to suffer from SBS, it can be written that the Brillouin threshold occurs at a critical power of incident signal (P_{cr}) such that,

$$\frac{g_B P_{cr} L_{eff}}{A_{eff}} \approx 21 \quad (3.10)$$

where L_{eff} and A_{eff} are effective length and area of the fiber respectively, and g_B is the Brillouin gain with a peak value of $5 \times 10^{-11} \text{ m/W}$ [66]. Although this effect is the strongest limit for amplifiers, it can be possible to increase threshold and suppress SBS with non-uniform temperature distribution along the fiber. This helps to create variation in phonon phase velocity which decreases the Brillouin gain. If narrow bandwidth is not necessary for the application, increasing the signal bandwidth also helps to suppress SBS.

Another important nonlinear effect faced with during amplification process is Stimulated Raman Scattering (SRS). Different than Brillouin scattering, incident photon turns into a scattered photon with lower energy and an optical phonon. These lower energy photons construct Stokes wave with downshifted frequency. Incident photon can also interact with phonon which already exists inside the medium. Then energy of the incident photon increases and creates Anti-stokes wave with upshifted frequency. Since the possibility to absorb one phonon is low due to the limited population inside the medium, anti-stokes creation has lower probability compared to stokes wave. However, in both cases amplifier performance is affected negatively due to wavelength shift through outside of the gain bandwidth of the corresponding doping element. Intensity of shifted wavelength depends on Raman gain which is a function of the frequency difference between the incident wave and stokes or anti-stokes wave. Figure 17 demonstrates Raman gain spectrum of standard single mode fiber around $1.5 \mu\text{m}$.

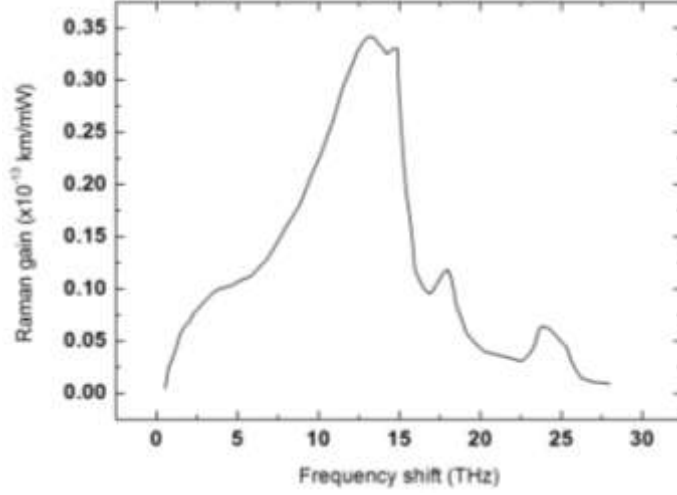


Figure 3.9: Raman gain spectrum of standard single mode fiber around 1.5 μm pump wavelength [adapted from Ref. 67].

The peak of Raman gain in silica fibers occurs about 13 THz from the incident photon wavelength. At 1550 nm this corresponds to a shift of about 100 nm. It means, after some threshold significant part of the signal energy will shift 100 nm right or left from the center of signal with respect to stokes or anti-stokes creation. This threshold optical power for signal input (P_{cr}) can be calculated from;

$$\frac{g_R P_{cr} L_{eff}}{A_{eff}} \approx 16 \quad (3.11)$$

where L_{eff} and A_{eff} are effective length and area of the fiber respectively, and g_R is the Raman gain [see detailed derivation of equation 3.11 in reference 66]. Although the threshold value is lower than SBS, with using special fiber designs (see e.g. [68]) it is possible to suppress this effect also.

Up to this point, the nonlinear effects that were explained are based on the interaction between photons and phonons inside the medium. Unlike photon-phonon interaction, another nonlinearity again caused by third order susceptibility ($\chi^{(3)}$), is four wave mixing (FWM) where two different frequency components of incident signal interact with each other and creates two new frequency comb lines with respect to the following equations;

$$\nu_3 = \nu_1 - \nu_2 - \nu_1, \nu_4 = \nu_2 + \nu_2 - \nu_1 \quad (3.12)$$

where ν_3 and ν_4 are created components, while ν_1 and ν_2 are incident beams. Similar to SRS, energy shifts towards the undesired frequency components and spectral broadening occurs. However, unlike SRS, the difference between created

frequency and signal is not so big to go outside gain range. Therefore amplification efficiency is not affected so much unless there is a spectrum bandwidth restriction and requirement of pulse compression for application. In any case, FWM is a phase sensitive process, so it can be suppressed if there is a strong mismatch.

Self-phase modulation (SPM) and cross phase modulation (XPM) are other refractive-index phenomena. In SPM, the peak intensity at the center increases the refractive index. And higher refractive index causes those wavelengths at the center of the pulse accumulate phase more quickly than wings. Following figure demonstrates typical progression of SPM on spectrum as a function of total nonlinear phase shift.

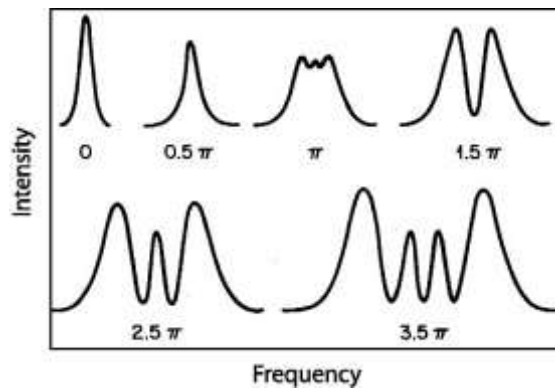


Figure 3.10: SPM-broadened spectra for an un-chirped Gaussian pulse [66].

Similar to FWM, SPM affects the performance of amplifier, if there is a spectral concern or pulse compression process. Increasing the effective area of fiber can decrease this effect due to the decreasing of intensity. On the other hand, in XPM, different than SPM, the effect of refractive index on a wavelength depends on not only the intensity of that wavelength, but also the intensity of other wavelengths propagating in the same medium. This interaction can occur also between the two orthogonal polarizations of the same wave. It can be suppressed again by decreasing the intensity with increasing the effective mode area of the fiber.

When building a high power amplifier system, self-focusing is another issue that should also be considered. It occurs at extremely high power levels due to the index profile created by the intense electric field. This effect causes focusing of a

beam onto itself. Threshold of this effect is in the order of 4-5 MW in terms of peak power. Beyond this threshold, beam breaks up into several beams with smaller power. These beams can be random or may have similar structure. No method is known to increase self-focusing limit, but it can be suppressed with decreasing the intensity of beam by increasing the effective area of fiber.

Fiber fusing is another issue that can affect the high power fiber system. It is a catastrophic damage affecting the core of the fiber and it can occur even at low power levels due to defect points inside the fiber. At this point, hot plasma is created and it travels towards the backward direction, destroying the core. Sometimes dust particle at the end of the fiber also creates such effects. Following figure demonstrates this catastrophic damage of a fiber core.

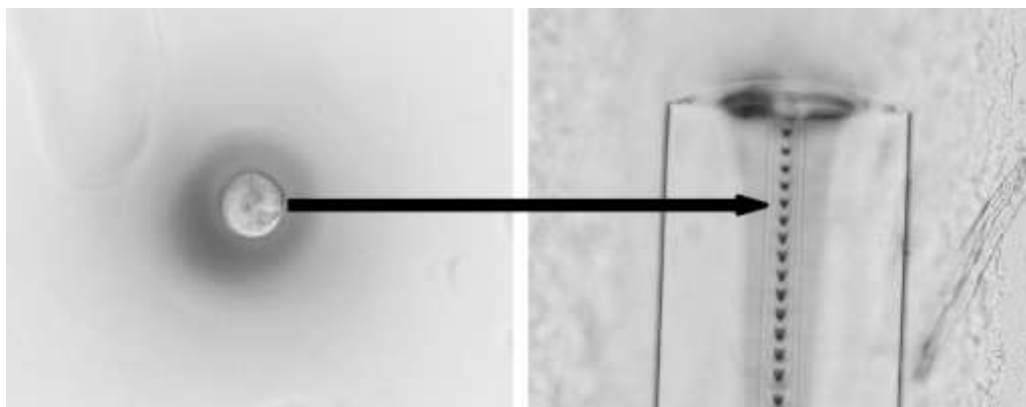


Figure 3.11: Photomicrographs of catastrophic damage to the fiber core [69].

Bulk material damage threshold and surface damage threshold are also important parameters to be considered while working with high powers. Although the surface damage threshold for pure silica is high, around the order of 2-10 GW/cm^2 , for doped silica hosts it decreases down to $500 \text{ MW}/\text{cm}^2$ and the bulk material damage threshold is expected not to be less than this value [69]. It means, the ends of fiber are more sensitive to be damaged. Figure 3.12 shows cracking at the end face of fiber. In order to prevent this situation custom end-cap can be used for increasing this threshold level [see reference 70 for custom end-caps].

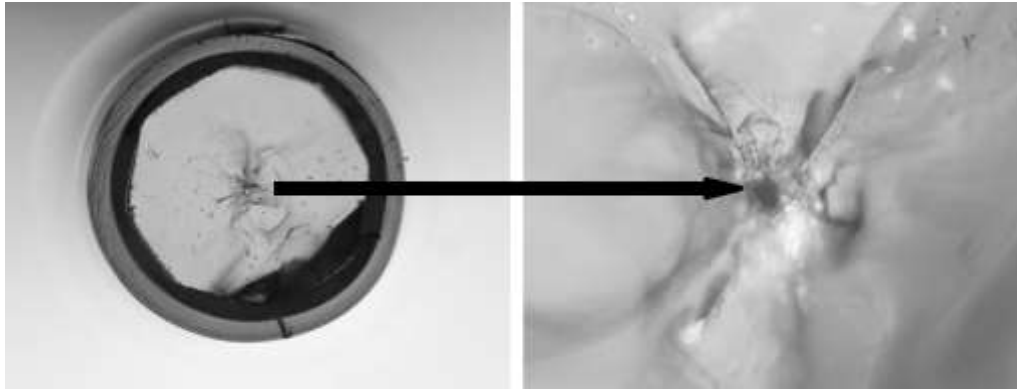


Figure 3.12: Photomicrographs of damage to a fiber end face [69].

Another important limitation comes from the thermal damage threshold of the coating. In double clad configuration, glass cladding acts as a waveguide for multimode pump beam and outer coating with low refractive index helps to keep pump power inside of the fiber. However, at high power levels, since thermal conductivity of coating material (usually acrylic polymer) is poor, high optical densities at the polymer-glass interface can cause damage which results in absorption or scattering of the pump light. Figure 3.13 shows the damage at the glass-polymer interface.

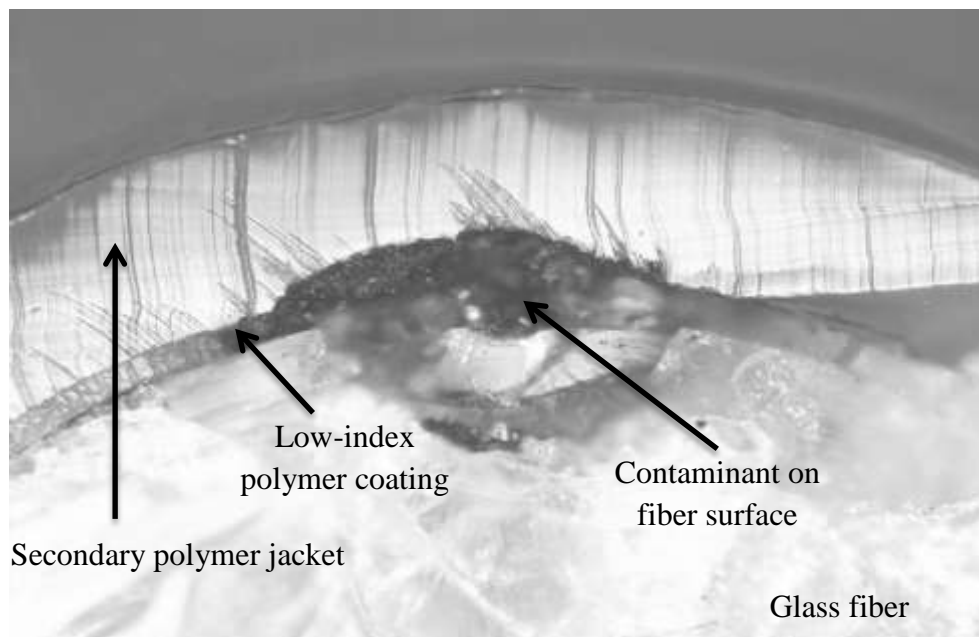


Figure 3.13: Photomicrograph of optically induced damage at the glass-polymer interface [69].

Since thermal damage limits the output power, temperature should be managed carefully in high power systems. Lifetime studies on standard coatings suggest that it is advisable to keep the temperature of the jacket below around 80 °C [69].

Lastly, photo-darkening can count as a limitation to reach high power outputs. Due to irradiation at a certain wavelength inside of the medium, reversible absorption centers are created in time. Therefore, transmission losses for signal inside the medium increase with time and performance of system may severely drop. Although the formation of absorption centers becomes easier with the presence of large diameter atoms like rare earth atoms, it can be reduced by decreasing the doping concentration. Moreover, it can be cured by annealing the fiber at 300 °C since photo-darkening is a reversible process.

CHAPTER 4

EXPERIMENTAL DEVELOPMENT OF FIBER LASER SOURCE FOR LADAR/LIDAR SYSTEMS

In this chapter, all experimental studies will be discussed during the development of a fiber laser source for LADAR/LIDAR systems. Developed source configuration for this study is based on MOPA (master oscillator power amplifier) which is a laser system consisting of a seed laser and a laser amplifier to increase the output power. For this purpose, two different seed source and suitable power amplifiers were constructed. First part will cover the seed sources while the second part will explain the amplification process.

4.1- Seed sources

Seed source is the first step that characterizes important parameters of LADAR/LIDAR system like resolution, range, etc. that covered in the first chapter. With respect to these parameters, application area and purpose of LADAR/LIDAR system can be established. In the literature, related to such systems, there is an important limitation in LADAR applications that the sources usually operate at few kHz repetition rate and this causes unacceptably long scanning times for the formation of high-resolution image. When designing a LADAR system it may be advantageous to have a system that can work at both high and low repetition rates. For this purpose, the development of a high repetition rate (few MHz, 1000 times higher than typical systems) and picosecond pulse duration fiber laser system that can be used as a LADAR source is explained. This design provides the capability to construct high-resolution images at video rates in LADAR applications utilizing all the advantages of fiber laser technology. In addition, a kHz level, nanosecond pulse duration source that can be used as a typical LADAR system is proposed for long range applications, since high repetition rates decrease the range of LADAR systems. The combination of these two systems offers both long range application and high resolution imaging.

Seed source parameters are chosen with respect to the requirements explained above. For this purpose, two different seed sources are proposed which are based on an actively mode locked laser and a fiber coupled distributed feedback semiconductor laser with suitable modulation. The next parts will explain these two seed sources respectively.

4.1.1- Actively mode locked laser

For development of LADAR/LIDAR source, first candidate is an actively mode locked fiber laser cavity. With using suitable rare earth doped fiber and modulator, it has a big potential to create high beam quality signal with desired wavelength, repetition rate and pulse duration. In this study, due to the eye safe requirements of LADAR/LIDAR applications, erbium doped system was preferred. Under these circumstances, first developed laser configuration is shown in the following figure.

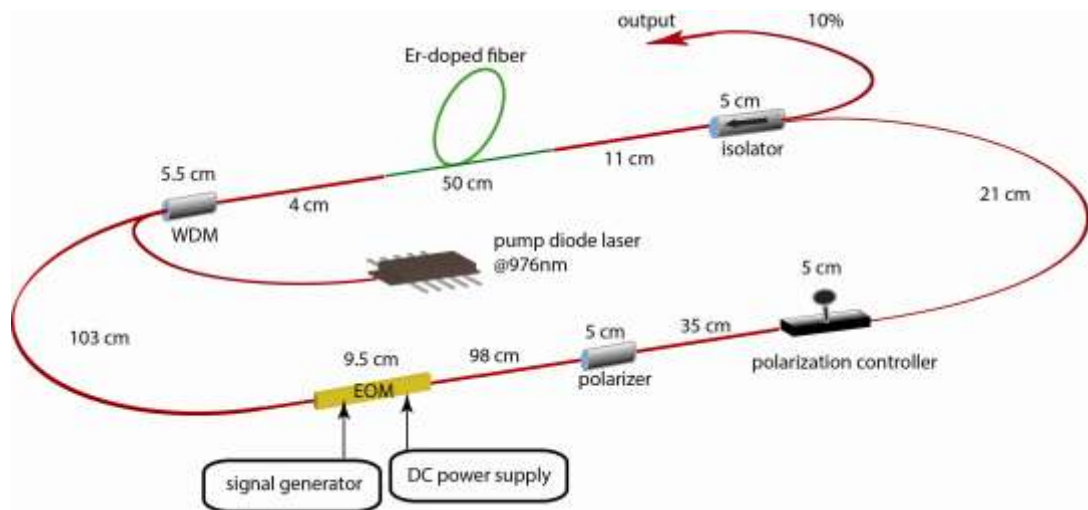


Figure 4.1: First constructed actively mode locked laser scheme for this study.

As shown in the figure, electro-optic modulator (EOM) was used as a modulator inside the cavity and the cavity length was not precisely adjusted at a specific value for this first time to control the repetition rate. This cavity was

constructed to understand the behavior of active mode-locking practically and to get experience about actively mode locked fiber lasers.

In this cavity, around 50 cm of single mode, single clad erbium doped gain fiber was pumped through the core with 980 nm single mode fiber coupled pump diode by using WDM (wavelength division multiplexer) that is suitable for combining pump and signal wavelength (980 nm- 1.5 μm). Isolator was used both for output based on reflection of signal around 10%, and for guiding the light in one direction inside the cavity. Polarization controller and polarizer were not necessary elements for this type of laser cavity, but since the modulator fiber pigtails were PM (polarization maintaining), these components provided an opportunity to control polarization for maximum energy coupling through a modulator. Then electro-optic modulator was used as an active element to obtain mode locking. As explained in the second chapter, to get into mode lock regime, cavity length was measured as around 348 cm and rf signal was arranged for corresponding cavity frequency (~ 57 MHz). In order to get maximum modulation depth, DC port of the modulator was supplied with V_{π} value of the modulator which was around 2.57 V. Following graphs are demonstrated pulse train (measured with sampling scope), RF spectrum (measured with RF spectrum analyzer) and optical spectrum (measured with optical spectrum analyzer) of 10% output from this actively mode locked fiber laser, respectively.

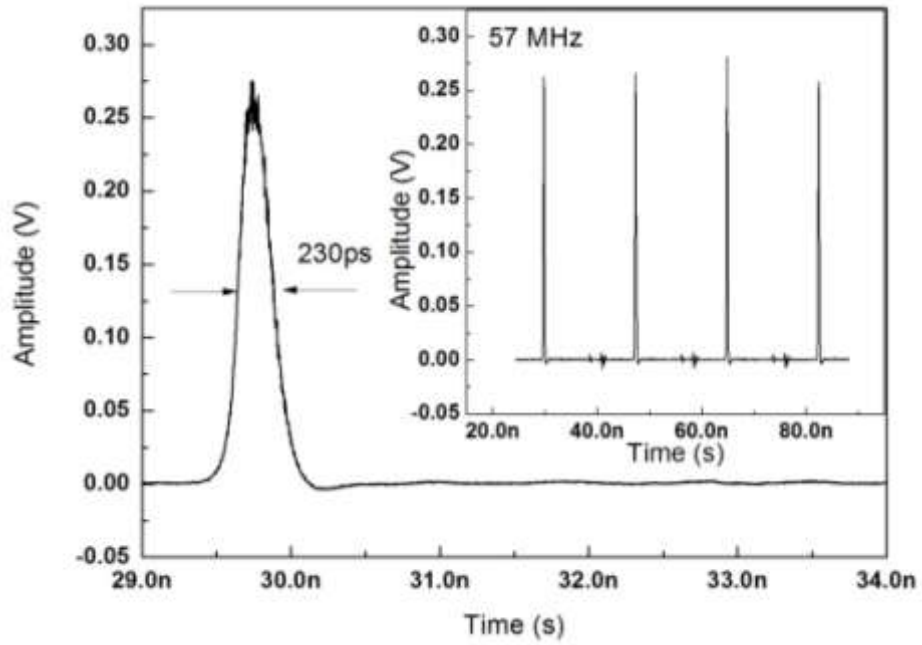


Figure 4.2: Pulse train of constructed actively mode locked fiber laser.

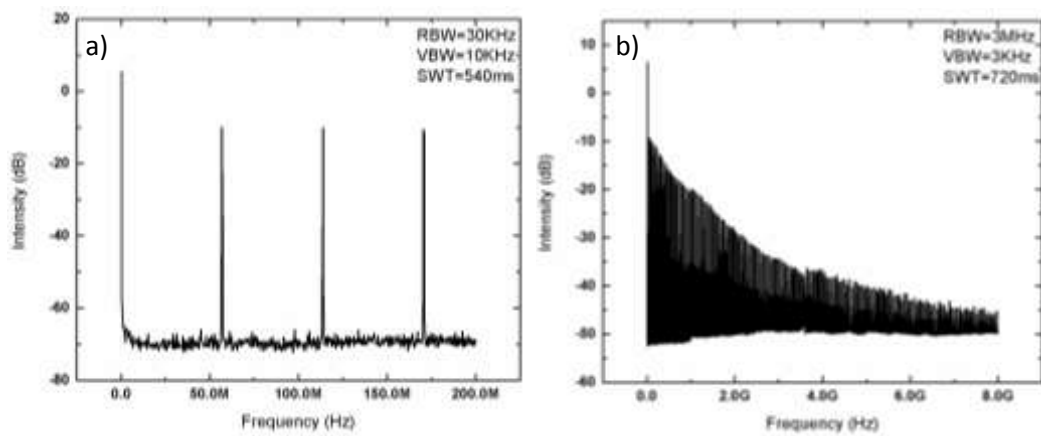


Figure 4.3: RF spectrum of constructed cavity; a) 200MHz span, b) 8GHz span

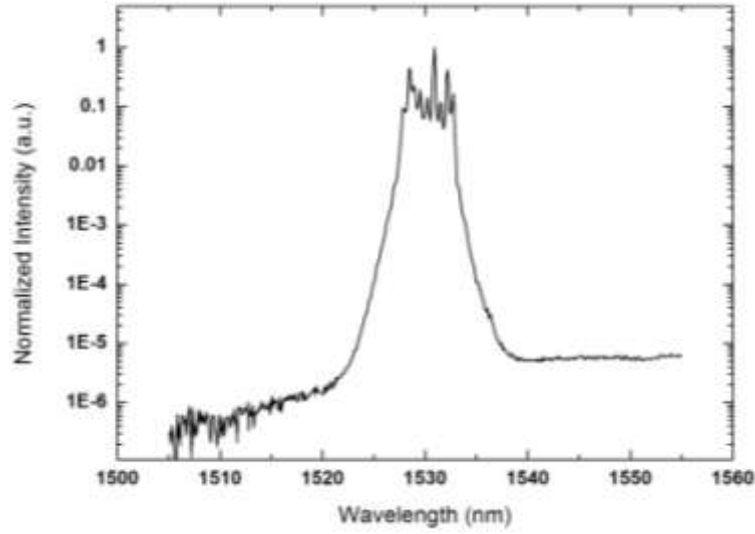


Figure 4.4: Optical spectrum of constructed cavity.

As shown in graphs, actively mode locked laser cavity creates stable pulses at 57 MHz with 230 ps pulse duration in the wavelength region around 1530 nm. Although this cavity creates desired pulse duration at high repetition rate, usual receiver in LADAR systems use avalanche photo-detector where its bandwidth and the electronics needed to analyze pulses restrict minimum pulse duration in LADAR application. Since the pulse duration theoretically depends on inverse of the modulation frequency of the cavity, increasing pulse duration 3-4 times decreases repetition rate down to few MHz allows a high enough scanning time. In order to check also experimentally the relation between pulse duration and modulation frequency and decide the cavity length for longer pulse duration, all studies were done in this first cavity. By changing the modulation frequency with multiple integer of corresponding cavity length, output pulse duration was examined. In equation 2.25, pulse duration is given as;

$$\tau_a = \sqrt[4]{\frac{D_g/M_s}{(g(T)/\Omega_g^2)/\frac{M\omega_M^2}{2}}} \quad (4.1)$$

Since the cavity is the same for all different modulation frequency, whole parameters other than modulation frequency can be written as a constant;

$$\tau_a = C\left(\frac{1}{\omega_M}\right) \quad (4.2)$$

By taking the logarithm of both sides, this expression becomes;

$$\log \tau_a = \log C - 0.5 \log \omega_M \quad (4.3)$$

which is easy to compare with the experimental result by plotting τ_a vs. ω_M and checking the slope. Following figure demonstrates the experimental fitting of this expression.

T_a Pulse duration (ps)	ω_M Modulation frequency (MHz)
230	57.849
158	115.698
121	173.547
100	231.396

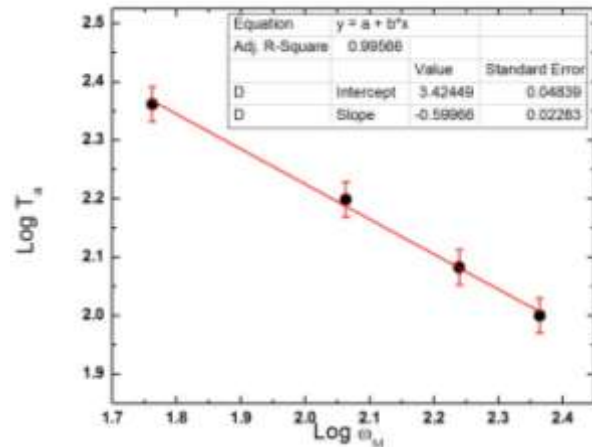


Figure 4.5: Experimental results which show the relation between τ_a vs. ω_M .

According to these experimental results, corresponding cavity length for around 1 ns pulse duration was calculated and a revised actively mode locked laser cavity was constructed with the following scheme.

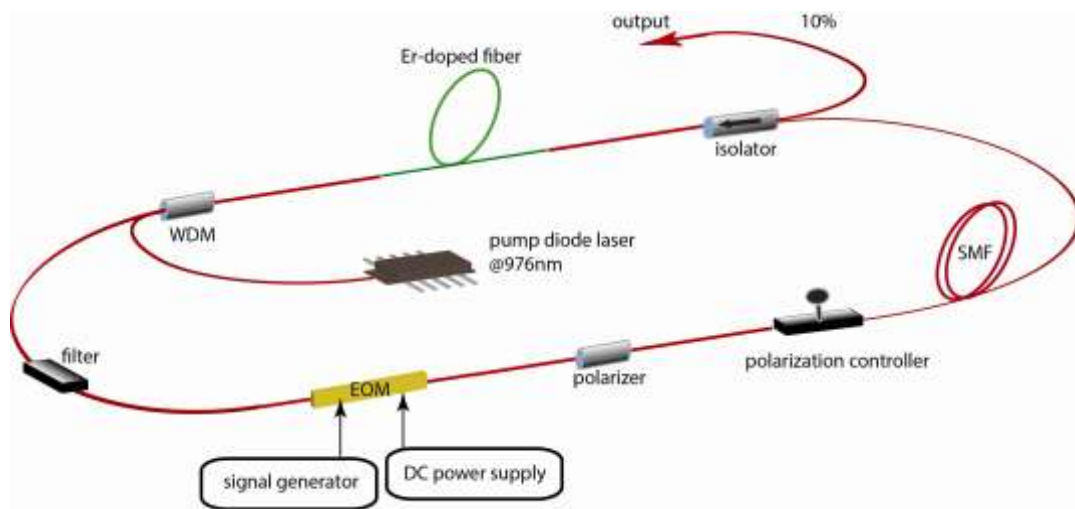


Figure 4.6: Revised actively mode locked laser cavity.

In this configuration, different than previous one, narrow bandwidth filter was used to control both central wavelength of the laser output and also the bandwidth of the spectrum. Filter central wavelength was around 1550 nm and full width half maximum (FWHM) value was around 0.15 nm. Such kind of narrow spectrum provides an opportunity to use narrow filter also in receiver part to decrease environment noise. Some length of single mode fiber (SMF) also was added to decrease the cavity frequency. Following figures show the pulse train, RF spectrum and optical spectrum graphs of this revised cavity, respectively.

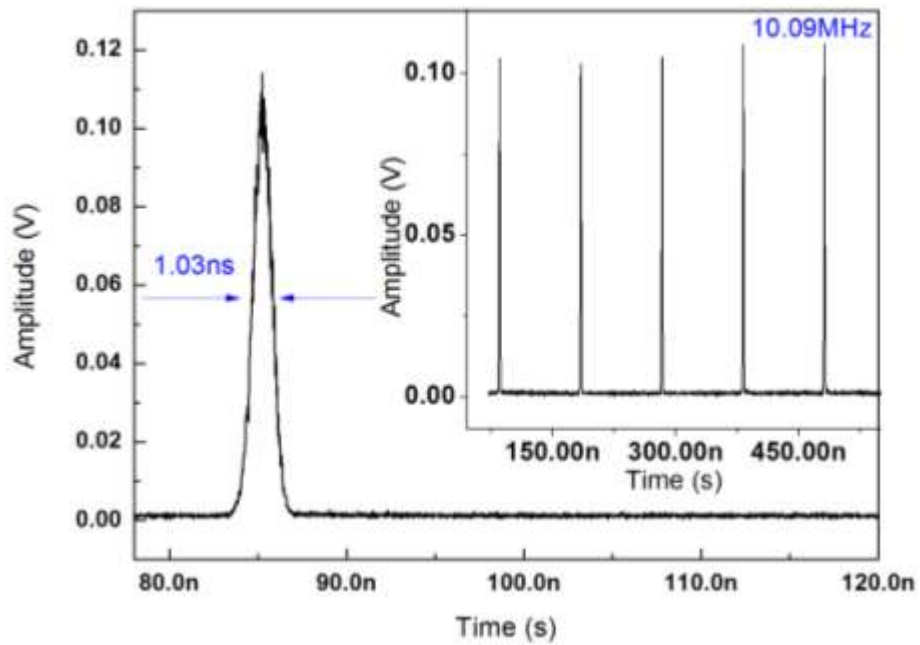


Figure 4.7: Pulse train of revised actively mode locked cavity.

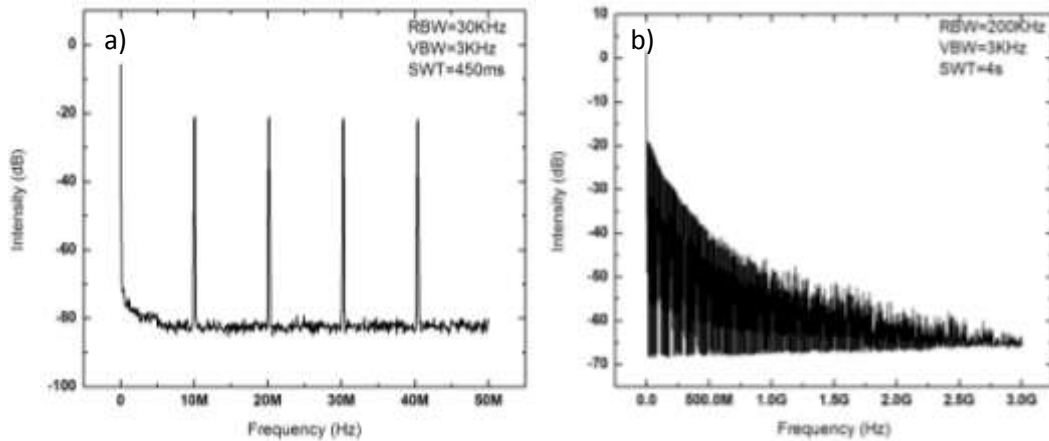


Figure 4.8: RF spectrum of revised cavity; a) 50 MHz span, b) 3 GHz span

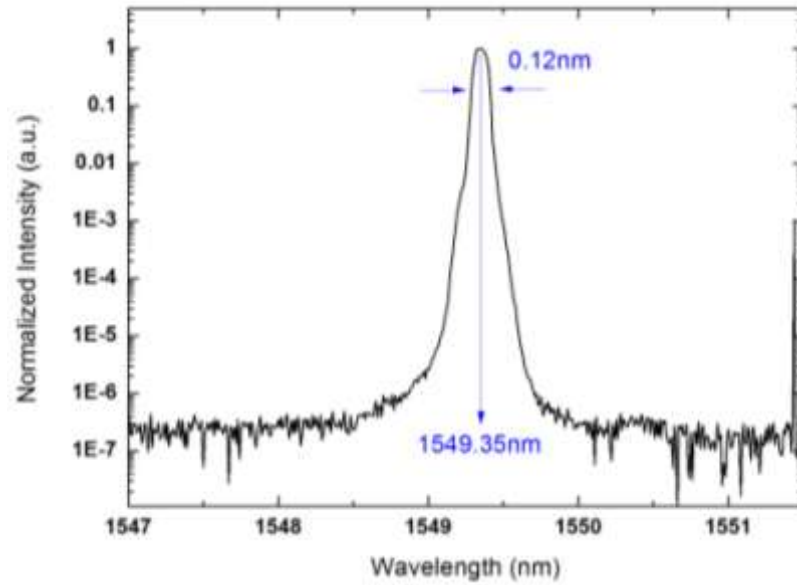


Figure 4.9: Optical spectrum of revised cavity.

Graphs demonstrate stable pulses from isolator 10% port of revised actively mode locked cavity with 1 ns pulse duration and 10 MHz repetition rate at 1550 nm as desired. Spectrum bandwidth is small as much as 0.12 nm. Output power was measured as 4 mW which is more than enough to amplify. Besides these measurements, noise suppression also tried to be measured by increasing resolution as much as Hz level and decreasing span of RF analyzer. It was measured as around 60 dB. Next figure shows this result.

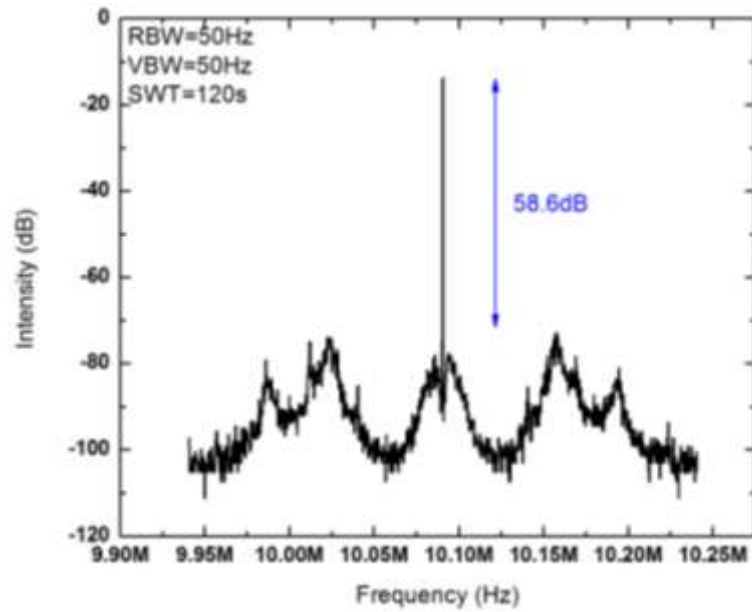


Figure 4.10: RF spectrum near 10 MHz with high resolution and low span.

All these measurements shows that actively mode locked fiber laser can provide all requirements to be a significant candidate for seed source of LADAR system. Next figure shows recent photo of cavity which has reported spectrum and time profiles reported above.

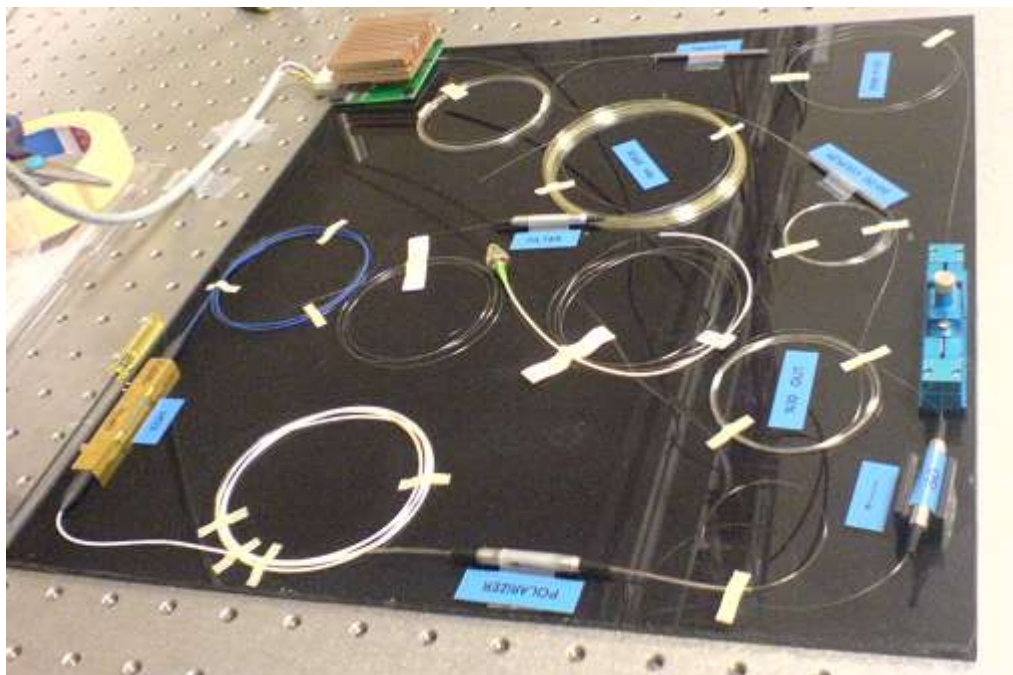


Figure 4.11: Recent photo of actively mode locked fiber laser built for this study.

4.1.2- Fiber coupled modulated distributed feedback semiconductor laser

Another alternative seed source for LADAR/LIDAR system is proposed as custom fiber coupled distributed feedback semiconductor (DFB) laser at proper wavelength with suitable modulation in terms of pulse duration and repetition rate. Such lasers are based on periodical structure (usually diffraction grating) inside the active medium of cavity which causes distributed reflectance to feed and form laser output. Although there are multiple resonator modes inside of the cavity, just one of them is favored in terms of losses. Therefore, single frequency operation is easily achieved. By changing the grating inside, also wavelength can be arranged as desired value. One drawback related to such lasers is low output power which is not so important for this study, since the output signal will be passed through amplifier system.

In this study, two single mode fiber coupled distributed feedback semiconductor lasers were used at 1551 nm and 1555 nm respectively with two different modulation modes. Since they have a modulation legs (diode legs connected to internal impedance that provide changes on current through the diode if there is an applied rf voltage) and diode response is fast enough, it was possible to modulate these diodes with not only nanosecond pulse duration but also in picosecond regime. Wavelength selection was done by considering the maximum efficiency of erbium doped amplifier system which is around 1550 nm and taking to account the availability of diodes on the market. Driven electronics were provided from a company (Highland Technology, www.highlandtechnology.com) for picosecond pulses and from Meteksan Savunma (www.meteksan.com-Ankara Teknoloji Geliştirme Bölgesi F Blok Binası Beytepe Köyü yolu, No:85/A Bilkent, Ankara / Türkiye) for nanosecond pulses.

Firstly, impulse generator (driving electronics for picosecond pulses) was used to create picosecond pulses similar to actively mode locked laser. This device was chosen, since usual pulse generators cannot produce such short pulses in the picosecond regime with high voltage amplitude [see specifications of this device in Appendix A]. The working principle of creation of optical pulses by using impulse generator is based on the conversion of high voltage to current on the impedance inside of the diode. Although the output power of diodes are around 100 mW in continuous regime for maximum operating current, due to the low duty cycle (ratio

of pulse duration to the repetition rate), this value dramatically decreases for picosecond pulses at MHz level repetition rate. Also, impulse generator output voltage is dependent on the repetition rate, so in order to get maximum optical output power from diode, first impulse generator output voltage was measured with respect to repetition rate, then it was applied to the diode and output optical power from diode was observed. Next two graphs show these results respectively.

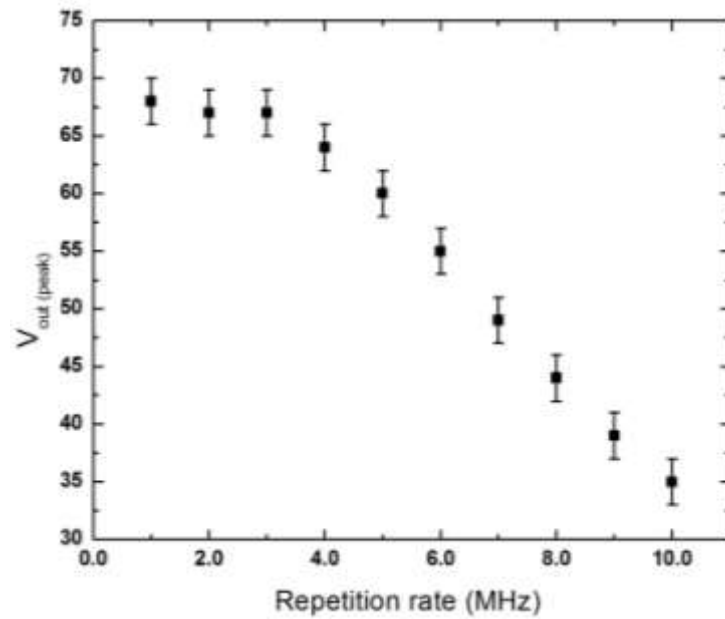


Figure 4.12: Impulse generator output voltage with respect to repetition frequency.

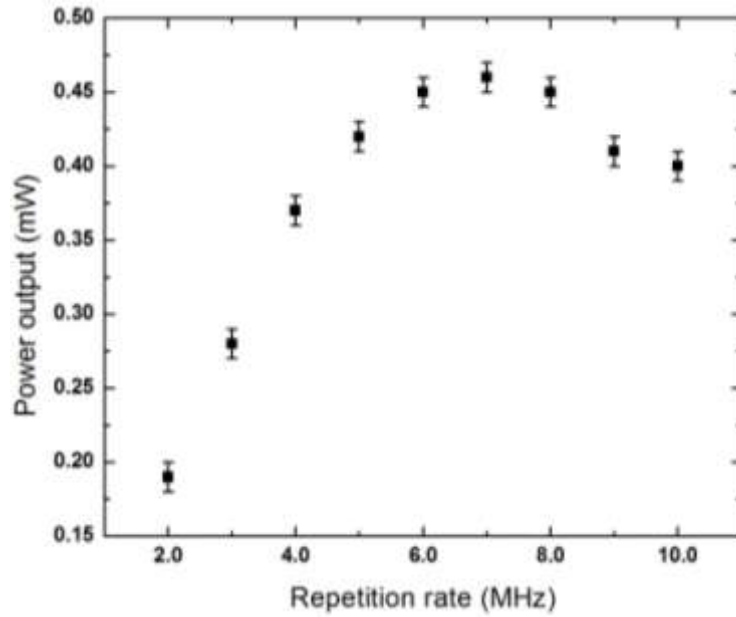


Figure 4.13: Output power of DFB laser with respect to repetition frequency.

Since two DFB lasers are identical except their wavelengths, output power graph is same for both of them. As seen in Figure 4.13, maximum output power was obtained for 7 MHz repetition frequency as 0.46 mW. Therefore this rate was accepted as a seed source frequency. Next figures demonstrate time domain graphs for both electronic output of impulse generator and optical output of DFB lasers at 7 MHz, respectively.

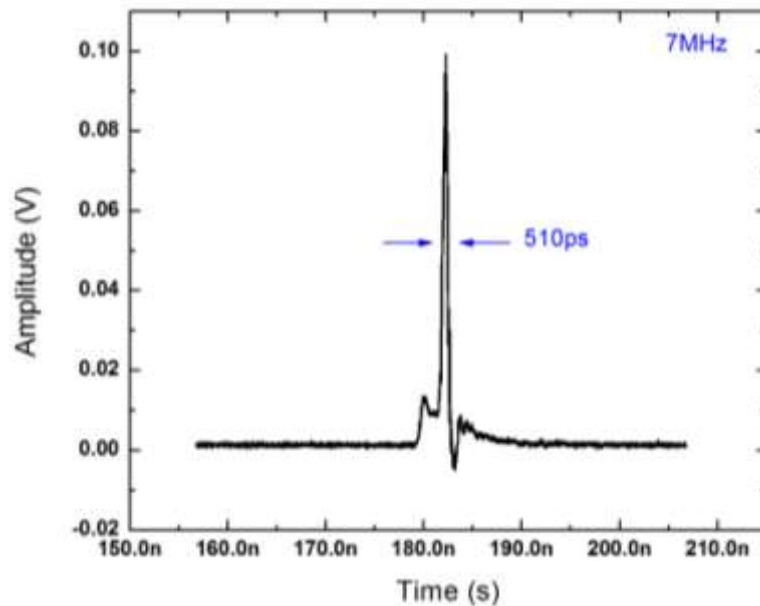


Figure 4.14: Impulse generator pulse duration at 7 MHz.

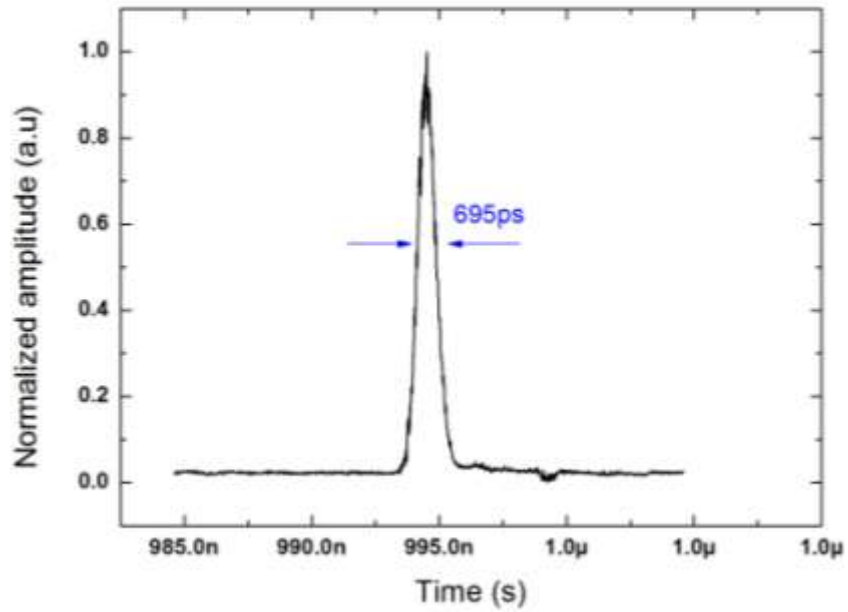


Figure 4.15: DFB laser pulse duration at 7 MHz.

Both diodes behaved similarly under this impulse generator. They created around 700 ps pulses at 7 MHz. Diodes' spectra are also given in the following figures.

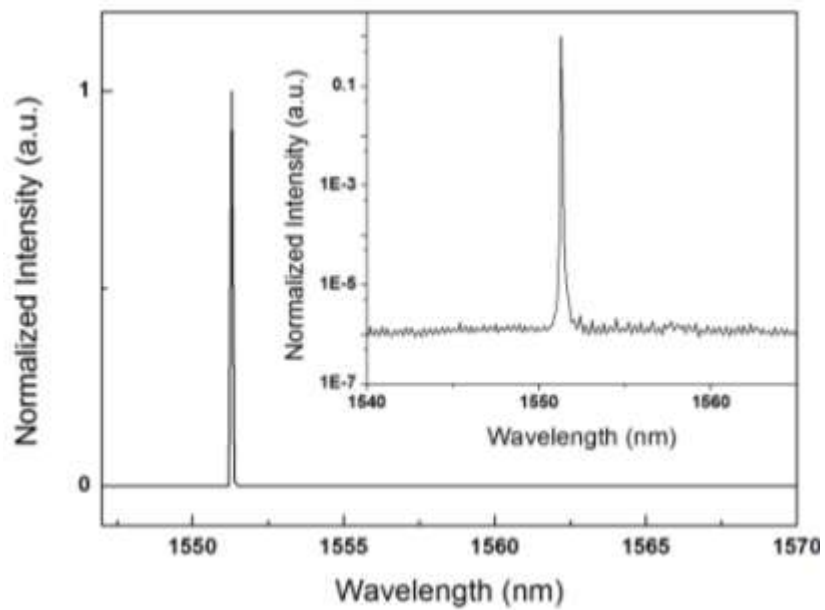


Figure 4.16: Optical spectrum for DFB laser with 1551 nm central wavelength (inset; logarithmic scale).

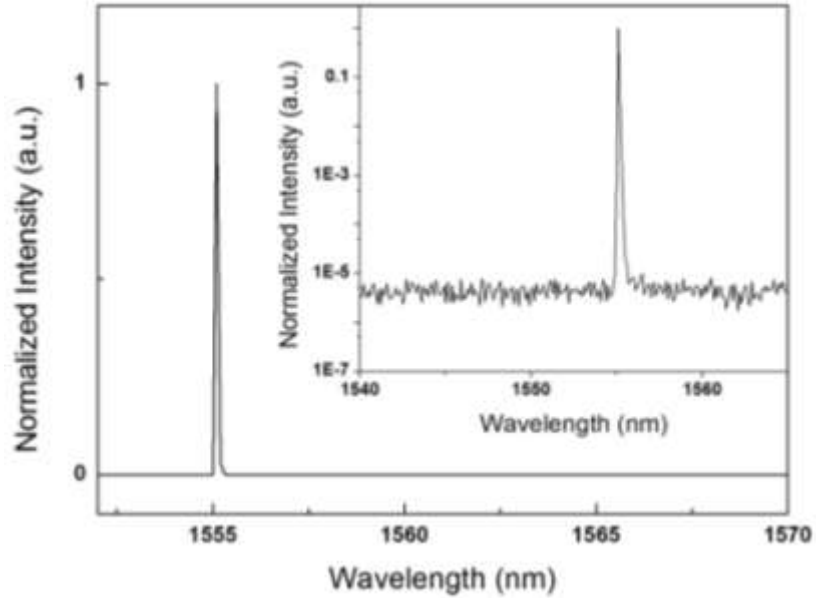


Figure 4.17: Optical spectrum for DFB laser with 1555 nm central wavelength (inset; logarithmic scale).

The line widths of these laser diodes are as small as 1 MHz ($\sim 0.008\text{nm}$) (it seems 0.1nm due to the resolution limit of the optical spectrum analyzer). All measurements and examination up to this point show that DFB lasers chosen with correct wavelength and modulation can respond to all needs for LADAR seed source similar to actively mode locked laser. It is possible to get similar efficiency from both seed source in picosecond regime.

DFB lasers were also tried with a modulation at kHz level repetition rate and around 10 ns pulse duration by using the electronic circuit developed in Meteksan Savunma for increasing the range of the LADAR system. Since nanosecond regime at kHz level rate means again low duty cycle, diodes output power were tried to optimize to get enough power for amplification process. At 500 kHz repetition rate with 10 ns pulse duration, diodes gave around 0.15 mW output power. It can be possible to increase this power level with the increasing of repetition rate but this causes decreasing of the range of LADAR system. Although even 500 kHz is high a little bit compared to the available LADAR system parameters, it is possible to decrease this during amplification process by using pulse picking with suitable modulator. Next figure shows the pulse train of DFB lasers with 10 ns duration at 500 kHz repetition rate.

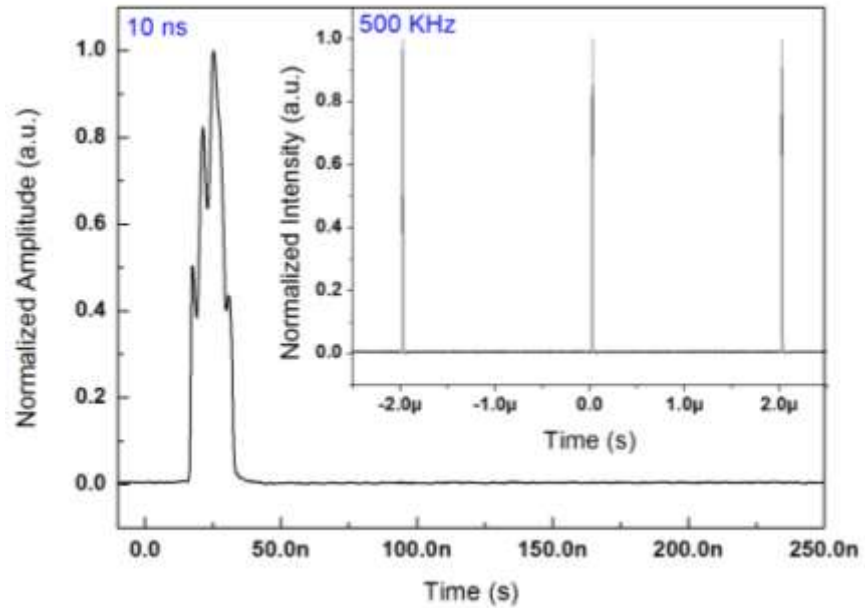


Figure 4.18: DFB lasers pulse train with nanosecond modulation.

Experimental results in nanosecond regime for DFB lasers are also satisfactory. However the pulses taken from actively mode locked laser or modulated DFB laser is not enough in terms of average output power for LADAR source. The amplification process is necessary for successful operation. Before introducing amplifier studies, the next part summarizes seed sources discussing advantages and disadvantages of both actively mode locked laser and DFB lasers.

4.1.3- Discussion

For development of a LADAR source, both actively mode locked lasers and custom DFB lasers seem to be good and sufficient candidate as seed sources. Both of them can create picosecond pulses at desired repetition rate and wavelength with narrow line width through a single mode fiber. Although actively mode locked laser has an advantage in terms of output power, DFB lasers serve flexible repetition rate with changeable pulse duration during operation by using an electronic signal. Therefore it is possible to switch picosecond regime to nanosecond regime or vice versa which creates big potential for application area of LADAR systems. By developing a very long cavity, switching pulse duration and repetition rate in small discrete numbers the same flexibility can also be possible for actively mode locked lasers. However in order to set kHz level cavity, length should be in km range which means a very delicate cavity is required that is not sensitive to changing

environmental conditions such as temperature. This situation also makes it difficult to obtain stable mode lock regime.

In conclusion, although both actively mode lock laser and fiber coupled DFB lasers seem to be suitable seed source, DFB lasers go one step forward in practical point of view with flexible signal parameters for different LADAR applications.

4.2- Amplifier system

First part of this chapter covered suitable fiber based seed sources for LADAR system. This part will explain the amplification process for both actively mode locked laser and fiber coupled modulated DFB lasers to reach enough power for LADAR application. First actively mode locked system amplification will be presented, and then modulated DFB lasers with picosecond regime and nanosecond regime will be discussed.

4.2.1- Actively mode locked laser amplification

After constructing seed source, last important step to conclude LADAR source is the amplification process. Since the application of LADAR requires enough signal when it returns back from the target, output power of LADAR source should be high enough to compensate all losses during reflection and traveling on air. By scaling from available custom LADAR system parameters, kW level peak powers and μJ level pulse energy seem enough to detect target inside the range of system (a few hundred meters for picosecond system and a few kilometers for nanosecond system) with high resolution. Since the output of actively mode locked laser developed for this study is as small as 4 mW average power, system needs a couple of amplifier stages based on single mode, single clad erbium doped fiber for pre-amplification and also double clad erbium ytterbium co-doped fiber for power amplification. First pre-amplification was considered to increase output of laser to a hundred of mW levels. In order to obtain deep understanding related to amplification process, gain simulation was developed for preamplifiers in C++ programming language by using the rate equations for three level scheme and erbium parameters with the help of post-doctoral fellow Ihor Pavlov who works at UFOLAB in Bilkent University (see appendix B for code). For solving rate equation in the simulation, the gain medium was split into small segments and inside of these segments all parameters like signal power, pump power, inversion population etc. were assumed

as constant. In every segment, input pump power, output pump power, input signal power, output signal power, amount of spontaneous emission and density of population in all levels were calculated by using the rate equations given in chapter 3 with parameters shown in the following table.

Table 2: Parameters used in preamplifier simulation.

<u>Parameters</u>	<u>Value</u>	<u>Unit</u>
Speed of light (c)	2.9979E8	m/s
Doping concentration (N)	4.8E19	cm ⁻³
Refractive index of core (n)	1.5	-
Numerical aperture (N.A.)	0.20	-
Segment length (L)	0.5 (variable)	cm
Core diameter (D)	4E-4	cm
Planck's constant (h)	6.626E-34	J*s
Pump light frequency (ν_{pump})	3.059E14	s ⁻¹
Signal light frequency (ν_{signal})	1.934E14	s ⁻¹
Pump absorption cross section (σ_{pump})	2.1E-21	cm ²
Signal absorption cross section (σ_{signal})	2.5E-21	cm ²
Upper state lifetime of level 2 (τ_{21})	10	ms
Upper state lifetime of level 3 (τ_{32})	1	μ s
Stimulated emission cross section ($\sigma_{\text{stim.signal}}$)	3.2E-21	cm ²
Core area (S_{core})	1.25E-7	cm ²

Since all erbium ions in excited state could not experience stimulated emission due to unpredictable losses inside the fiber in real situation, signal efficiency coefficient was added while calculating stimulated emission towards right and left in the code. This parameter was optimized with respect to the experimental results as 0.7. After this calibration, simulation was used to obtain optimum condition for input signal during this amplification process. First important

parameter that should be decided was pumping direction. Next figure shows ASE (amplified spontaneous emission) creation in both directions during 500 mW pump power through 1.2m erbium doped fiber while there is no seed.

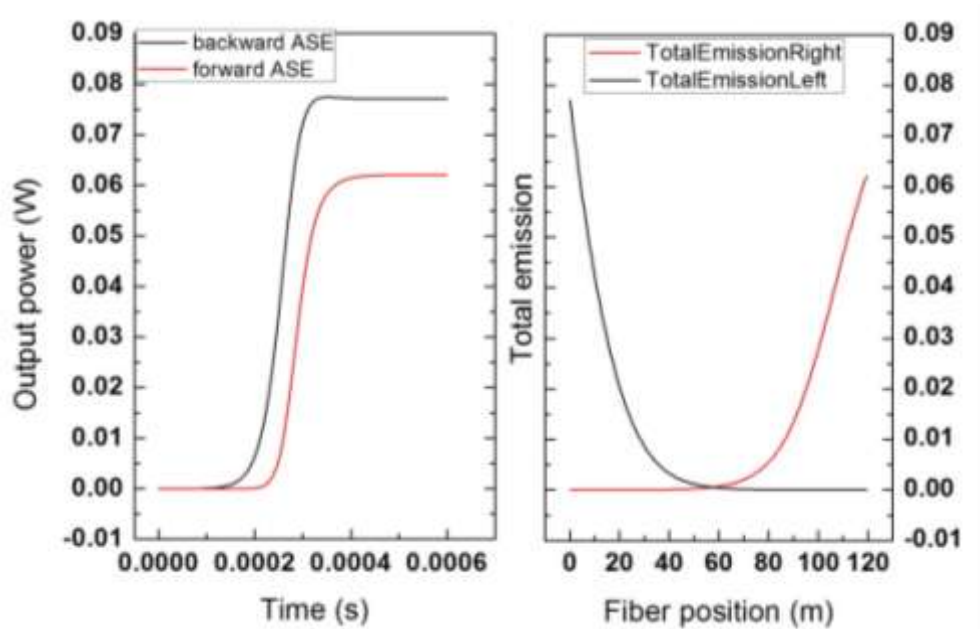


Figure 4.19: Simulation result for ASE creation in both direction in time (left) and along fiber (right).

As shown in the graph, the tendency of preamplifier stage is to create higher output power in backward direction. Since pumping edge of the fiber has high population inversion and low spontaneously emitted signal, this signal is not enough to saturate the amplifier in pump direction, but other edge of the fiber has low population inversion, so spontaneously emitted signal is enough to saturate the gain fiber through opposite side of pumping direction and it increases along fiber. The same situation also occurs when small seed signal is sent to the gain fiber for amplification. Therefore all preamplifier stages were constructed with backward pumping in this study.

After deciding the pump direction, simulation was used to decide for which length of gain fiber and how much pump power, the output of actively mode locked laser can be increased up to 70-80 mW range which seems enough to send power amplifier stage. Following graph shows the simulation result for 1.2 m erbium doped fiber with 300 mW pump power and 4 mW seed signal.

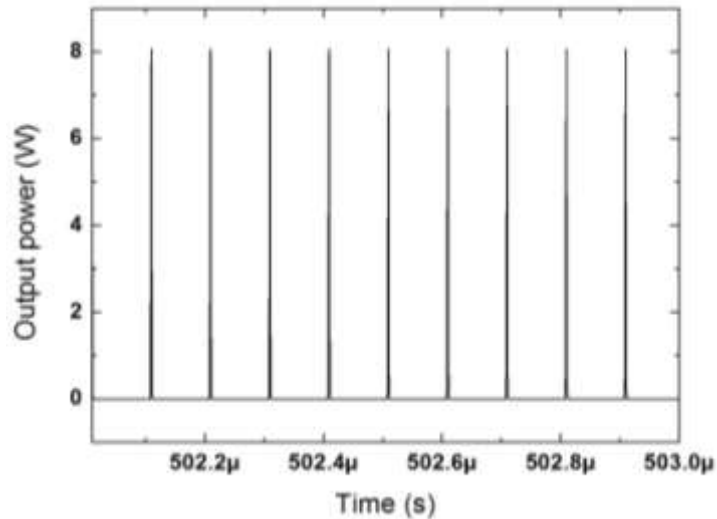


Figure 4.20: Simulation results for 1.2 m erbium fiber with 300 mW pump power and 4 mW seed signal from actively mode locked laser.

Graph shows the output power in terms of peak power for 10 MHz repetition rate and 1 ns pulse duration of actively mode locked laser output. Calculated average power gives around 80 mW output power at the end of 1.2 m erbium doped fiber with 300 mW pump power for 4 mW input seed. Under the light of this result, following preamplifier setup was constructed.

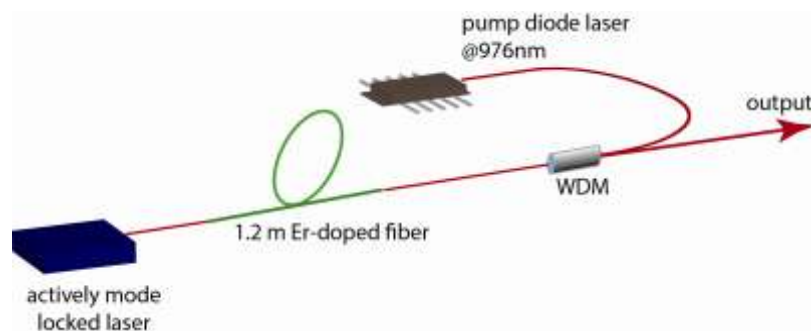


Figure 4.21: Preamplifier scheme.

As demonstrated in the figure, actively mode locked laser output was sent to the 1.2 m single clad single mode erbium doped fiber. Gain fiber was pumped in backward direction with single mode fiber coupled pump diode at 980 nm by using WDM. For 300 mW pump power, around 75 mW output power was obtained with the following spectrum profile.

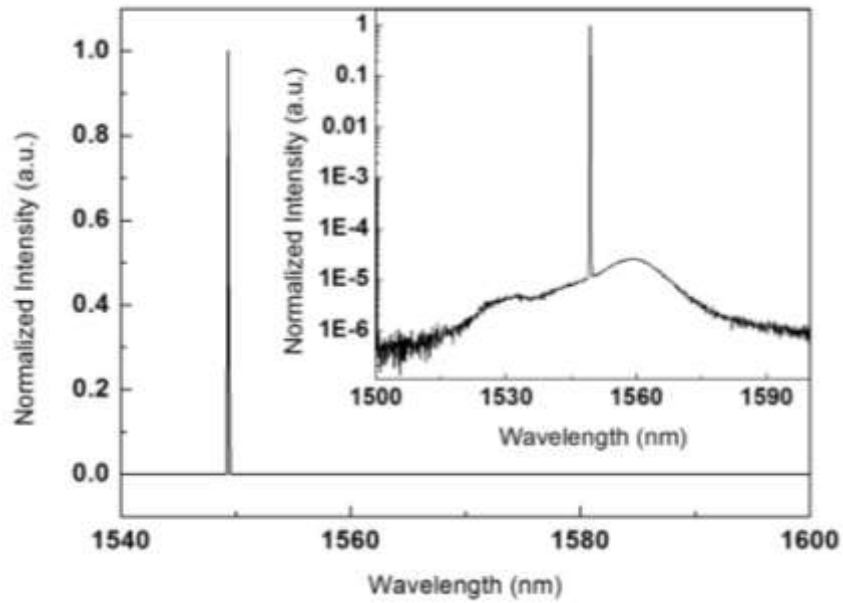


Figure 4.22: Output spectrum of preamplifier for actively mode locked laser (inset; logarithmic scale).

Although in the spectrum, there is an ASE creation, the suppression is around 45 dB, so the ratio of ASE is as small as 0.4%. After this stage, output of preamplifier was sent to power amplifier and amplification process was completed. Whole amplifier system is shown in the following figure.

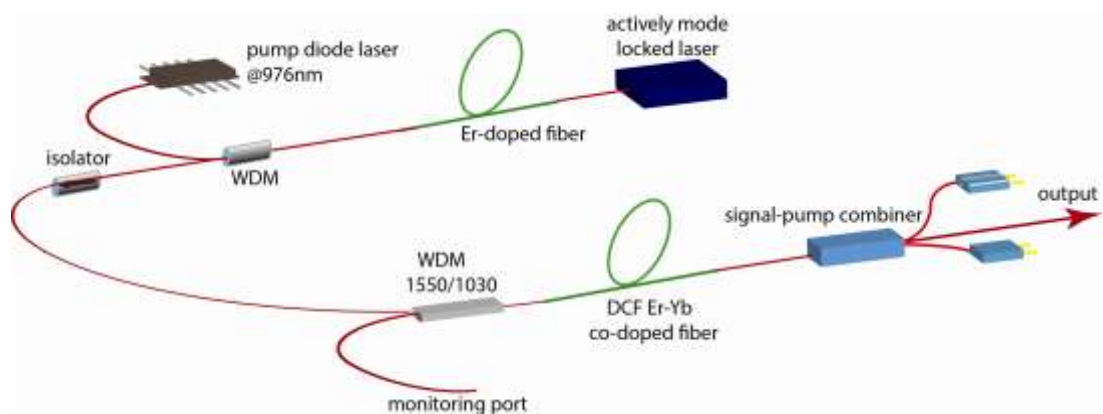


Figure 4.23: Amplifier system scheme for actively mode locked laser.

For power amplifier, again backward pumping was used with the help of two 25 W multimode pump diodes with signal-pump combiner. Since the power amplification is limited for single clad erbium doped fibers due to limited pump coupling and limited doping level explained in the third chapter, erbium ytterbium co-doped double clad fiber was used in power amplifier stage. After preamplifier, one isolator was used to prevent backward signal from power amplifier and protect the preamplifier. 1550/1030 nm WDM was used to monitor whether there is an ASE at 1 μm due to ytterbium ions or not. The gain fiber length was around 6 m with 12 μm core diameter [see Ref. 71 for detailed information related to same amplifier system in cw regime as well as femtosecond regime]. Output power of last stage with respect to pump power is shown in the following figure.

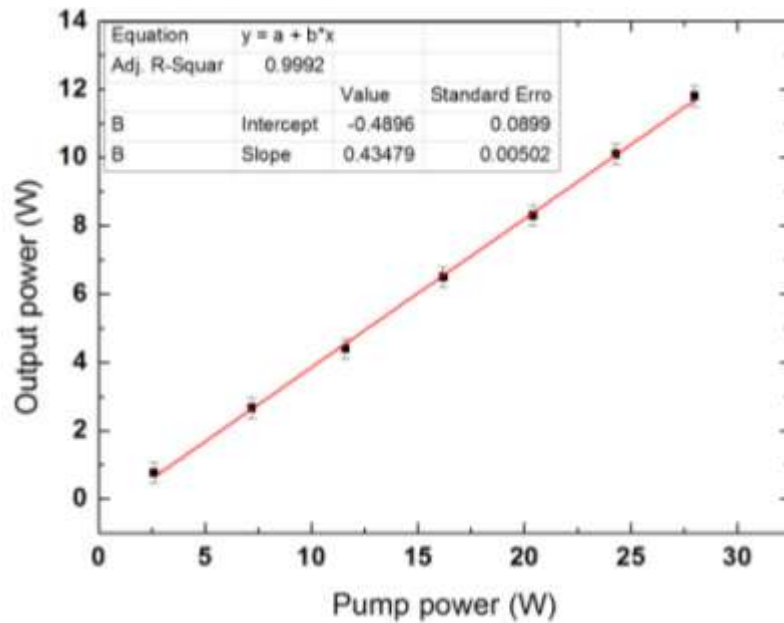


Figure 4.24: Pump power vs. output power from actively mode locked laser amplifier system.

As shown in the graph, output power was increased up to 12 W average power with 43% slope efficiency (pump power/output power) that is near the maximum efficiency for such kind of gain fiber. Around 12 W average power, output spectrum and pulse train were also measured and reported in the following figures.

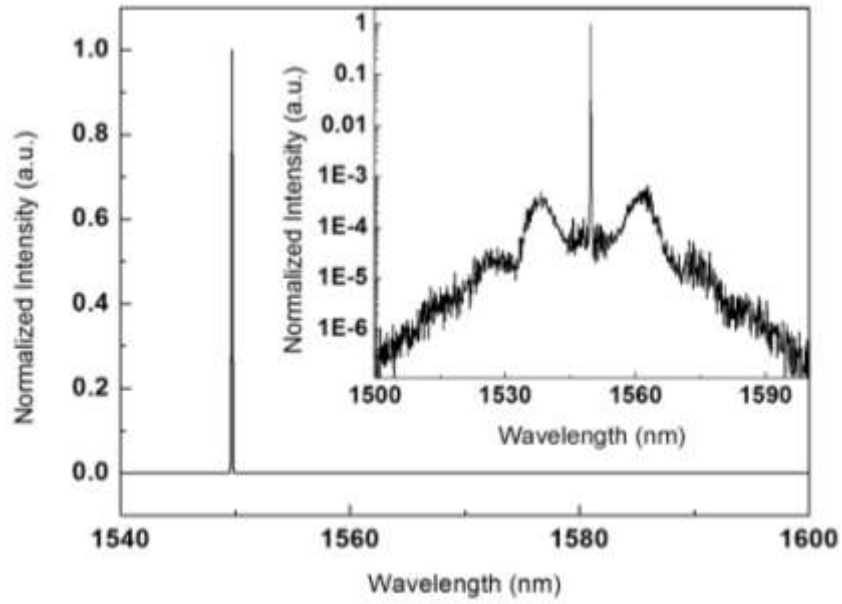


Figure 4.25: Output spectrum of actively mode locked laser amplification system at 12 W (inset; logarithmic scale).

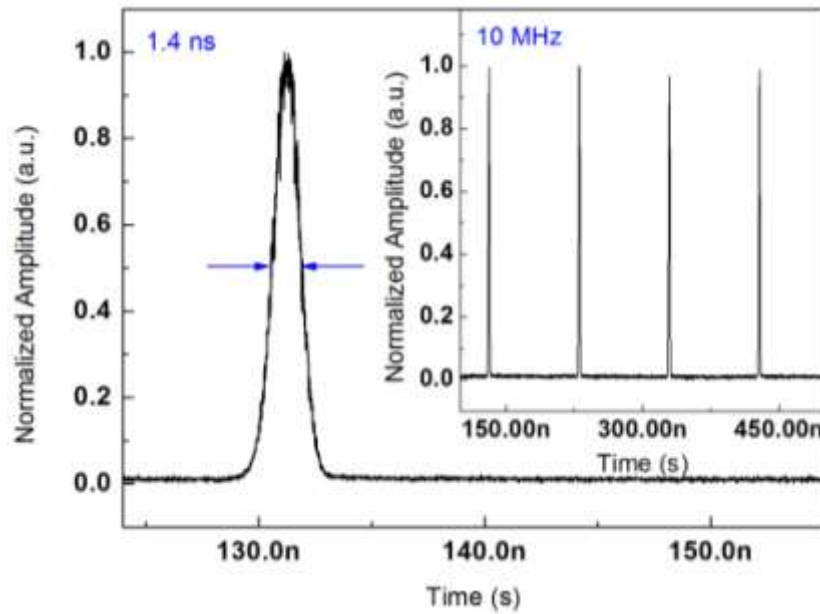


Figure 4.26: Pulse train of actively mode locked laser amplification system at 12 W.

Although nonlinear effects (especially FWM due to phase matching) become effective as broadening on both spectrum and time domain, around 92% of power was under the signal. And also there was no ASE observed at 1 μm neither forward

direction nor backward direction. It means that this system can create pure signal around 1.2 kW peak power at 10 MHz with around 1ns pulse duration through a single mode fiber. Since the proposal of this study is to demonstrate the potential of fiber laser systems as LADAR source, it can be said that all experimental results up to this point shows the amplification of actively mode locked laser can satisfy all requirements for high resolution imaging LADAR application at video rate. Although the range of this source is a little bit low with around 30 m due to 10 MHz repetition frequency, by using different signal processing technique, this limit can be increased. Also decreasing repetition rate by keeping the pulse duration constant can be possible in fiber system configuration with pulse picking method. Since modulated diode scheme gives more freedom related to repetition rate and pulse duration by controlling the electronic signal, range increasing studies were done with modulated DFB lasers which is discussed in the next part.

4.2.2- Fiber coupled modulated DFB laser amplification

Experimental result related to actively mode locked laser amplification is a promising source system for LADAR application. It serves all advantages of fiber laser configuration, including compact size, low cost, stable signal with high beam quality in eye-safe region and with adjustable power level. In order to improve this design by adding flexibility related to pulse duration and repetition rate in large range, fiber coupled modulated DFB laser was proposed as a seed source of the amplification system. First, a picosecond signal was tried to be amplified like in actively mode locked laser case but with lower repetition rate. In order to provide high output power with a few MHz repetition rates, pulse picking method with suitable acousto-optic modulator (AOM) was proposed and studies were started with DFB laser at 1551 nm central wavelength. Since the parameters of DFB laser with impulse generator modulation as explained in previous parts were very close to actively mode locked laser parameters, same preamplifier and power amplifier was planned to be used. After amplification of signal around 1 W with this system, it was thought that pulse picking could be done with suitable modulator since there was enough power to compensate the losses that came both from pulse picking and modulator insertion loss. Following figure shows the amplifier scheme constructed for DFB laser amplification include pulse picking process.

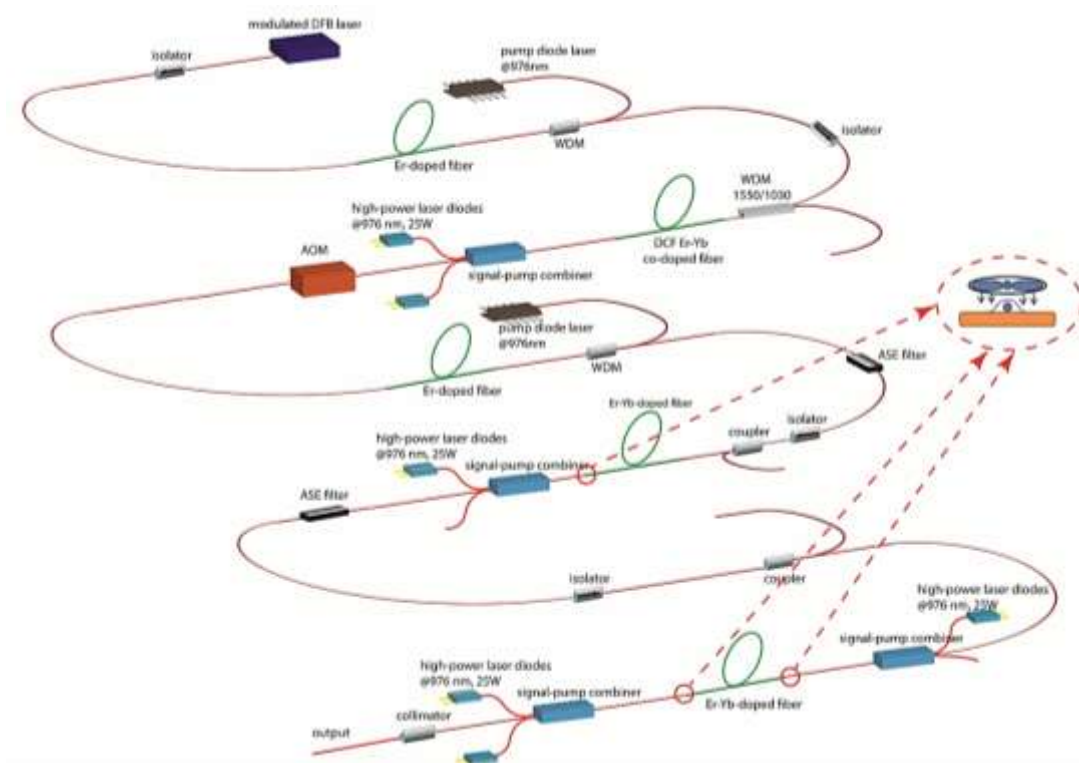


Figure 4.27: Amplifier scheme for modulated DFB laser included pulse picking process (inset; cooling system for splice point).

As shown in the figure modulated diode output (0.46 mW at 7 MHz rep.rate with 700 ps pulse duration) was sent through previous amplifier set-up for actively mode locked laser. After power level was increased around 1 W, 7 MHz repetition frequency was decreased to 1 MHz by using AOM. While doing this process driven electronic for diode and AOM driver was synchronized with each other and delay was adjusted to catch one pulse for every 7 pulses. Since there was 7 times decreasing power during pulse picking process and also modulator had around 6 dB insertion loss, after modulator 55mW average optical power was obtained at 1 MHz. Following graphs demonstrate spectral domain and time domain after AOM with 55 mW power.

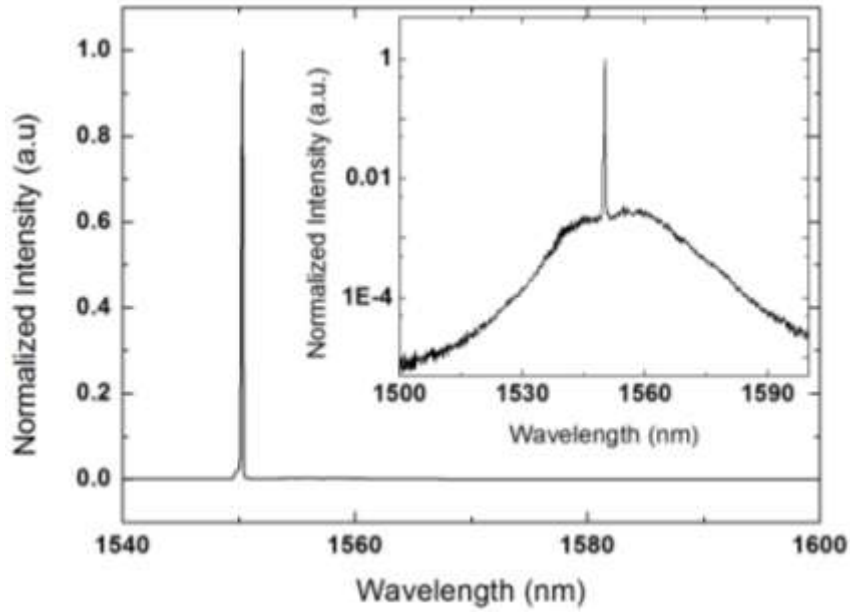


Figure 4.28: Spectrum after AOM (inset; logarithmic scale).

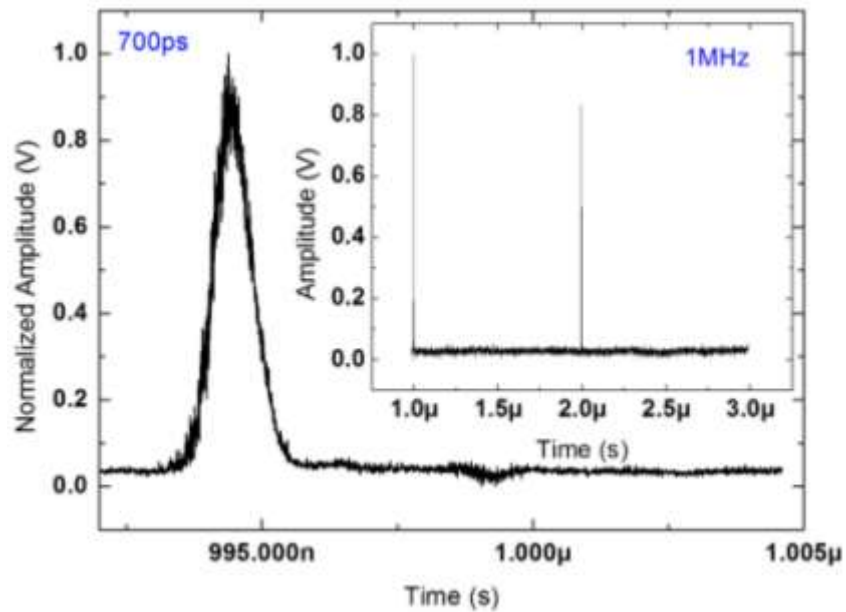


Figure 4.29: Pulse train after AOM.

Although ASE creation and spectral broadening was observed through the edge of signal spectrum at the output from AOM, pulse train showed that almost all power was under pulse. After decreasing the frequency to 1 MHz, signal was sent through a 3-stage amplifier system including a preamplifier, middle stage and power amplifier which allowed increasing the output slowly to prevent ASE creation. ASE

filters with 6 nm bandwidth at 1551 nm central wavelength were used between these stages to make spectral filtering. Amplification after AOM started with preamplifier which had the same configuration with previous one where signal was amplified to a few hundred mW level average power again, and then middle stage was used to increase this power to watt ranges. Since the repetition rate was 10 times less and pulse duration was shorter than actively mode locked laser case, experimental results showed that without middle stage, output of preamplifier could not saturate the power amplifier. Therefore, signal was amplified up to watt level in middle stage, and then sent through a power amplifier. However, there was one drawback of this system that was long fiber length which caused nonlinear effects after middle stage and power amplifier output. Preamplifier output suffered less from nonlinearity due to lower intensity. Moreover, with the help of ASE filter at the end of preamplifier stage, broad area on the spectrum after AOM was decreased down to 6%. Next figure demonstrates the output spectrum of preamplifier after ASE filter from the coupler port.

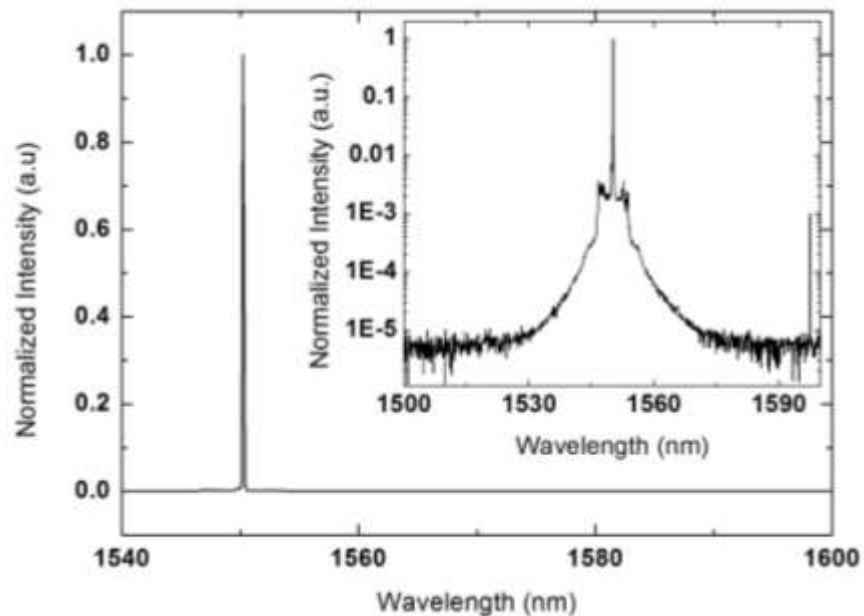


Figure 4.30: Preamplifier output after pulse picking process for picosecond amplifier system (inset; logarithmic scale).

Then this signal was sent to middle stage which consists of 3 m erbium ytterbium co-doped double clad fiber with 10 μ m core diameter. This stage was pumped with one 25 W multimode pump diode with the help of signal pump combiner. The splice point of gain fiber and combiner fiber was covered with recoating material on the copper plate and cooled down with a fan. Recoating was important to prevent pump leakage from the splice point and cooling was important since maximum power dissipation occurs at this point. At the output of this stage, one more ASE filter with high power handling capability was placed and after coupler, spectrum was measured as following.

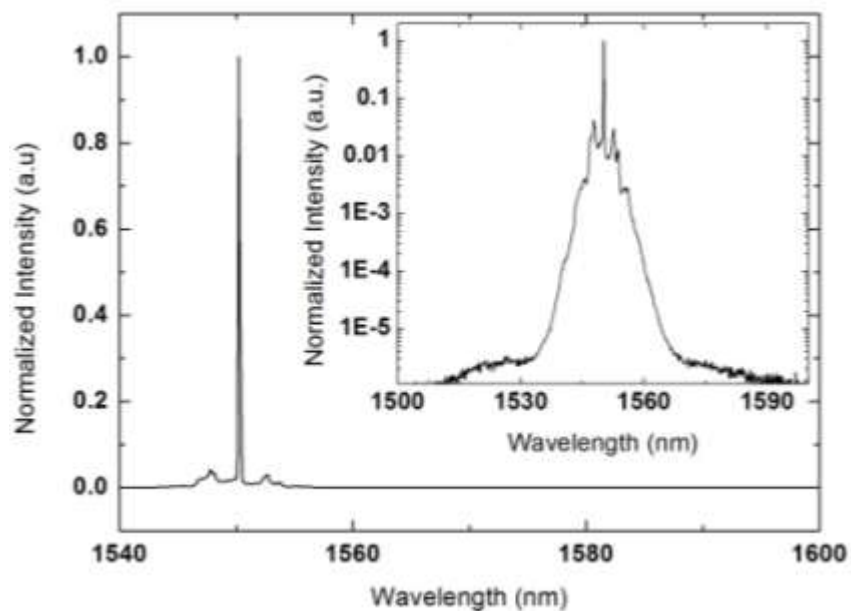


Figure 4.31: Middle stage output for picosecond amplifier system (inset; logarithmic scale).

Since middle stage increased intensity while ASE filter and coupler fiber pigtail increase the fiber length, nonlinearity began to express itself at this point. Due to FWM, spectrum started to be broadened. Then this output was sent to power amplifier stage which contains 6 m erbium ytterbium co-doped fiber with 12 μ m core diameter. This stage designed with co-pumping method to optimize output efficiency. One high power pump diode was used for forward pumping while two of them were placed for backward pumping. Following graphs shows the results of

spectrum and pulse train for 6 W average power at the output of amplifier system with 1 MHz repetition rate for 20 W pump power.

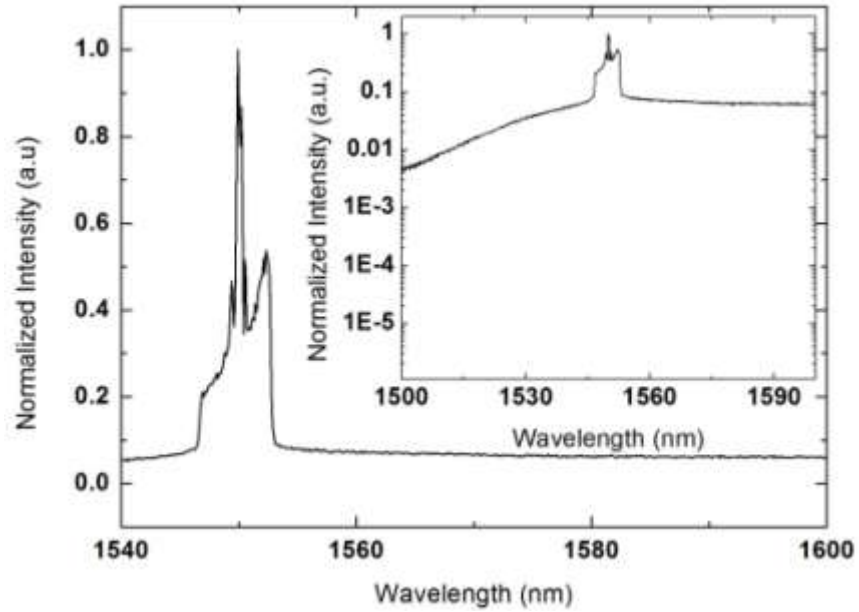


Figure 4.32: Spectrum of 6 W average power at the output of picosecond amplifier system (inset; logarithmic scale).

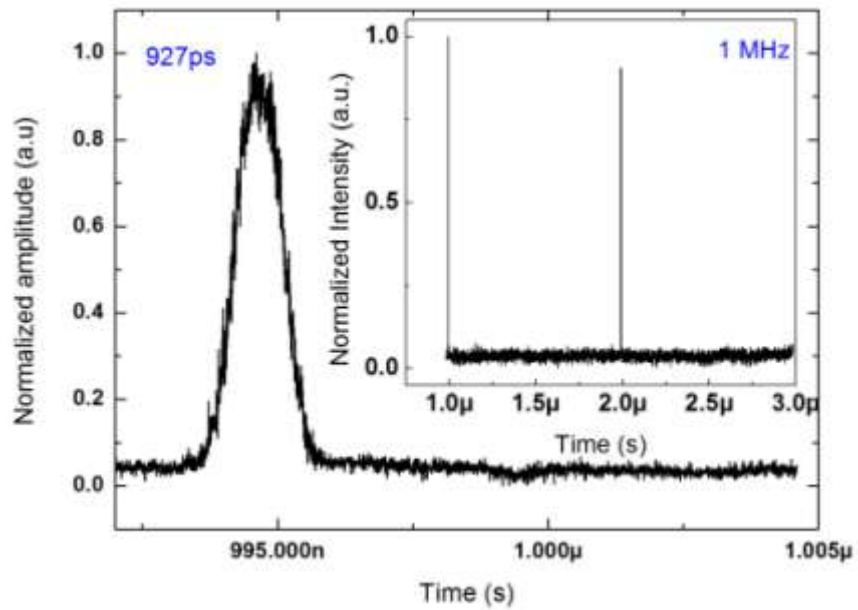


Figure 4.33: Pulse train of 6 W average power at the output of picosecond amplifier system.

Although the amplifier system can create 6 W output power with around 1 ns pulse duration at 1 MHz repetition rate, spectrum was affected from the nonlinearity due to high peak power which was calculated to be around 6 kW. Therefore pump power was not increased more to get higher output. However, even though there is a spectral broadening, most of the power is in the range of ASE filter bandwidth where the effect, coming from previous stage, can be easily seen on the output spectrum. Power inside of this bandwidth was calculated as around 90% of total power. This source can be used as source of LADAR system without any dramatic problem. It just affects the filter bandwidth on receiver part, but 6 nm (ASE filter bandwidth used in the system) is also narrow and acceptable for decreasing the environmental noise in LADAR application. If a very narrow spectrum bandwidth of the source is needed for specific purposes, then broadening caused by nonlinearity can be decreased with increasing the core diameter of gain fiber. Increasing core diameter helps to decrease the intensity and corresponding nonlinearity. Another option is to use shorter fiber length which requires highly doped gain fibers and is simpler to set-up with fewer components.

Besides picosecond amplification process, nanosecond amplifier system was also developed in parallel with DFB laser at 1555 nm central wavelength. First, the same configuration with the picosecond amplifier system was planned to be used for also the nanosecond regime, but simulation results for preamplifier showed that sending output of DFB laser modulated with nanosecond pulses at 500 kHz to same preamplifier with 1.2 m erbium doped gain fiber causes ASE creation between two pulses due to low repetition rate as shown in the following figure.

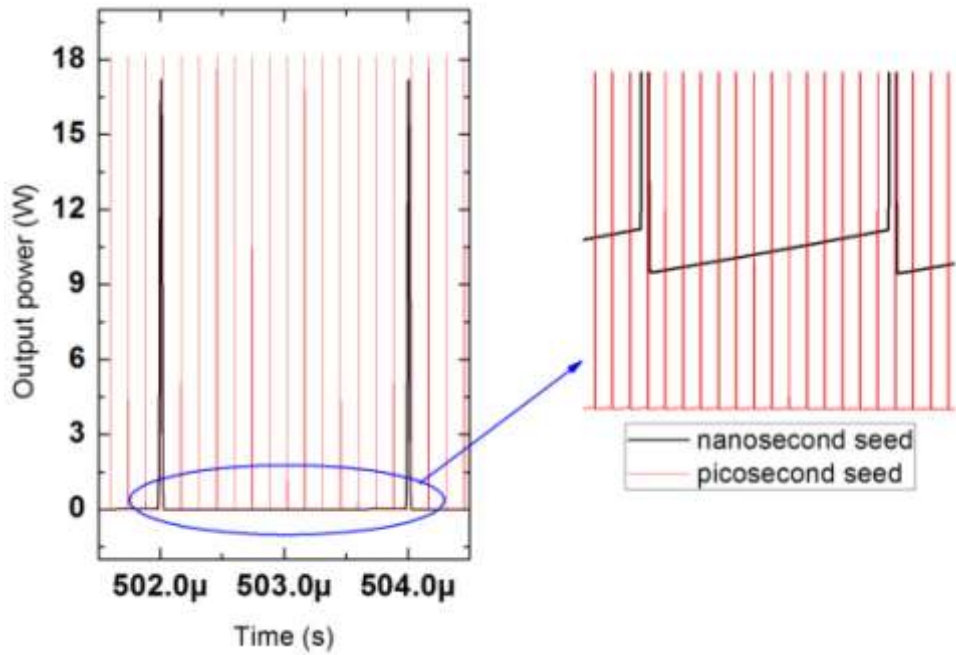


Figure 4.34: Simulation results of preamplifier for nanosecond and picosecond regime showing the ASE creation with nanosecond seed.

Although the upper state life time of erbium ions is as high as 10 ms, due to low seed signal at the output of DFB with 500 kHz, ASE creation still occurred. In order to prevent this situation, two-stage preamplifier system was constructed to decrease ASE creation as shown in the following figure.

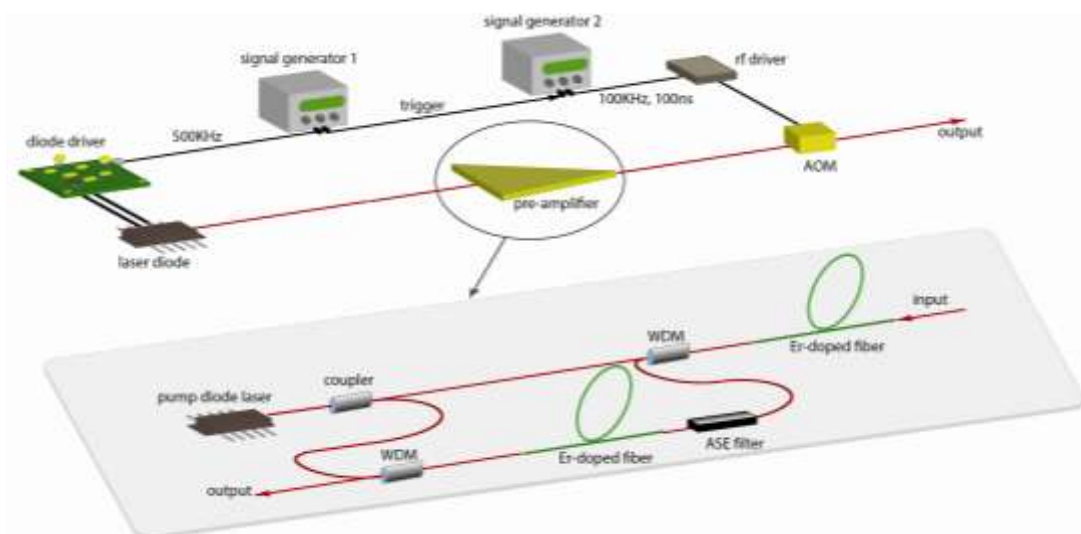


Figure 4.35: Two-stage preamplifier configuration for nanosecond pulse amplification.

Modulated DFB output signal (0.15 mW with 10 ns at 500 kHz) was sent through preamplifier stages. Since the output power of seed source and the repetition frequency was very low, first part was constructed with low pump power and around 40 cm erbium doped gain fiber was used. With this way, along the gain fiber, lower population inversion was obtained and signal power could be enough to saturate this stage and deplete all population inversion. Just in case, ASE filter was used between two stages to suppress ASE. After seed power increased a few mW, then usual preamplifier scheme was used again with 1.2 m erbium doped gain fiber to increase the signal to hundred mW level. This configuration was provided with the splitting of one single mode pump diode into two pieces with 90-10% ratio with coupler. 10% was sent to first part while 90% was sent to second part. Next figure shows the spectrum after this preamplifier stages with 100 mW average output power.

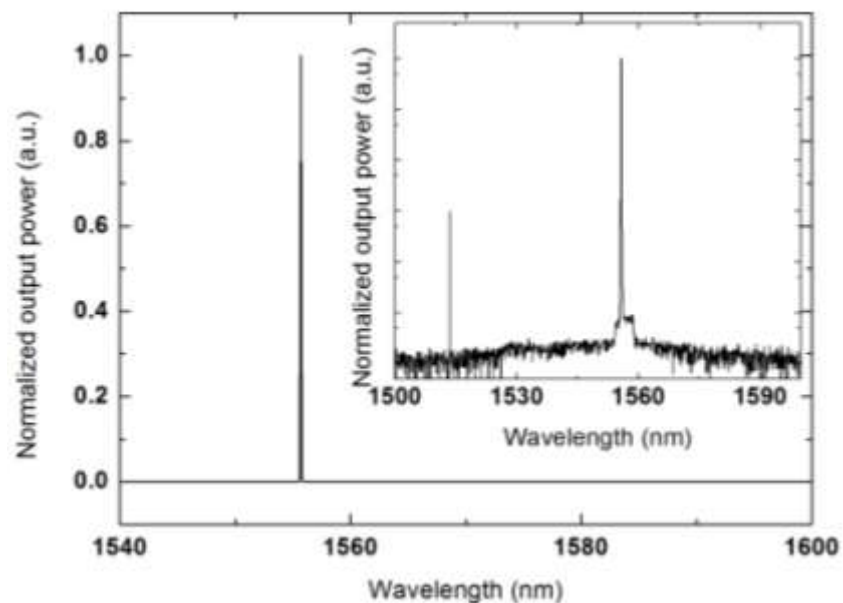


Figure 4.36: Preamplifier stages output spectrum for nanosecond seed (inset; logarithmic scale).

As shown in Figure 4.35, 100 mW output signal of preamplifier stages was sent through AOM for reducing the repetition rate to 100 kHz which is closer to usual repetition rate of available LADAR system with higher range distance. Next figures show spectrum and pulse train after AOM.

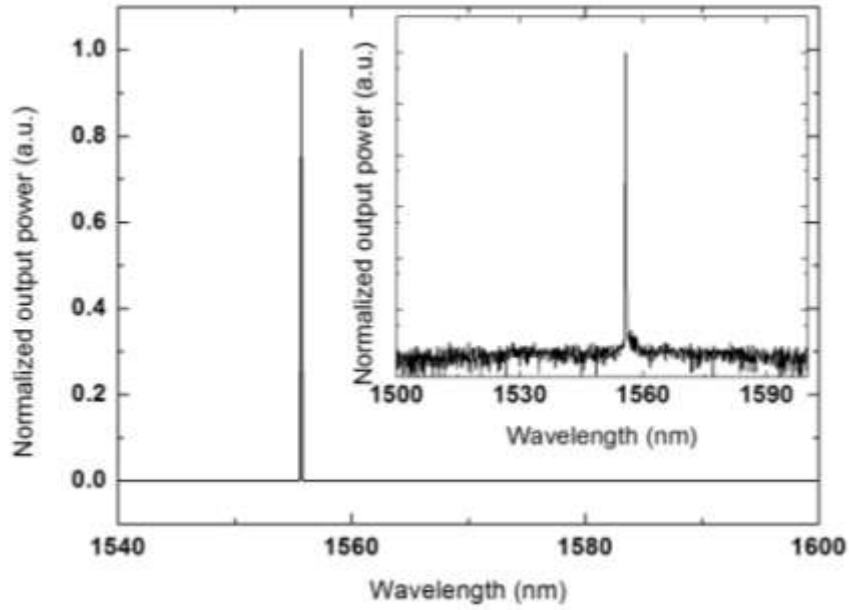


Figure 4.37: Spectrum after AOM for nanosecond seed (inset; logarithmic scale).

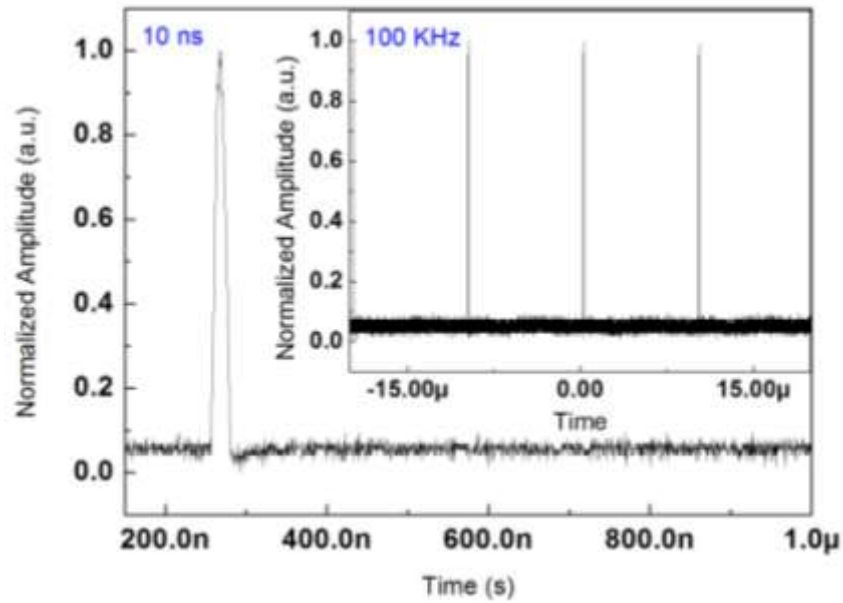


Figure 4.38: Pulse train after AOM for nanosecond seed.

Around 5 mW optical power was left after AOM due to pulse picking and insertion loss of modulator which is enough for amplification. Again 3-stage amplifier system was designed for nanosecond regime with the following scheme.

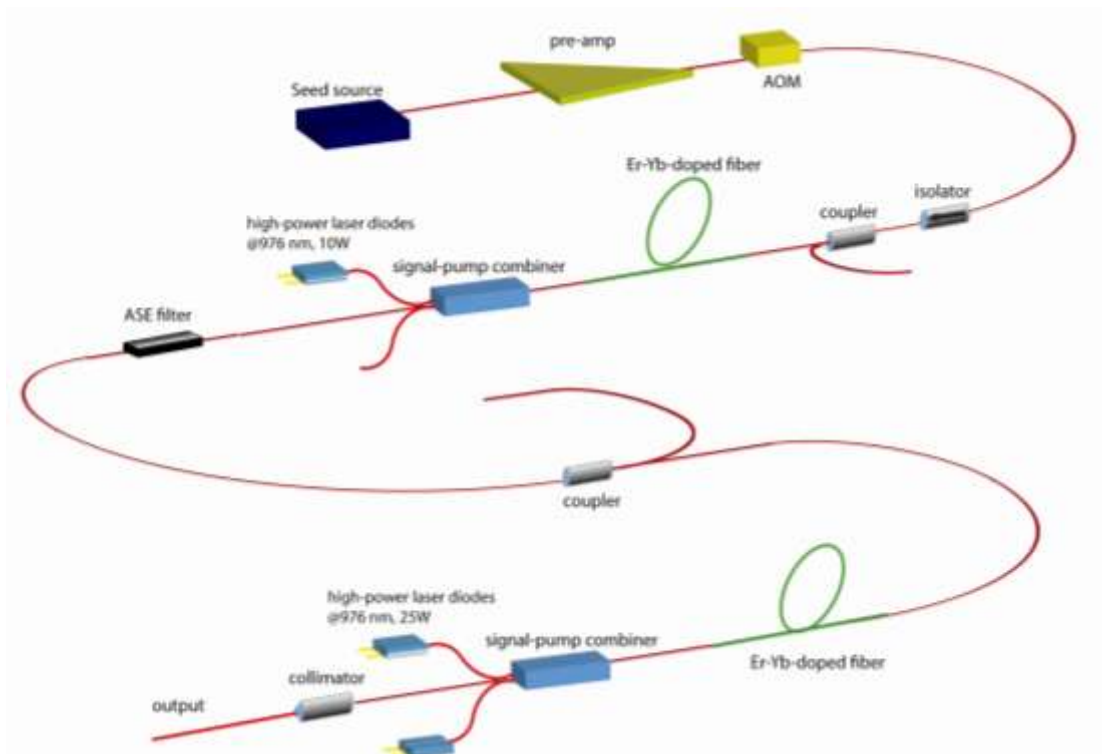


Figure 4.39: Amplifier system scheme for nanosecond seed.

Different than picosecond system, here only backward pumping was used at the last stage. Since co-pumping increases the fiber length and also experiments show that there is no significant efficiency increasing with co-pumping, backward pumping was preferred. Next figure demonstrates the spectrum and pulse train with 9.5 W average power at the output of this system for nanosecond seed signal during around 27 W pump power.

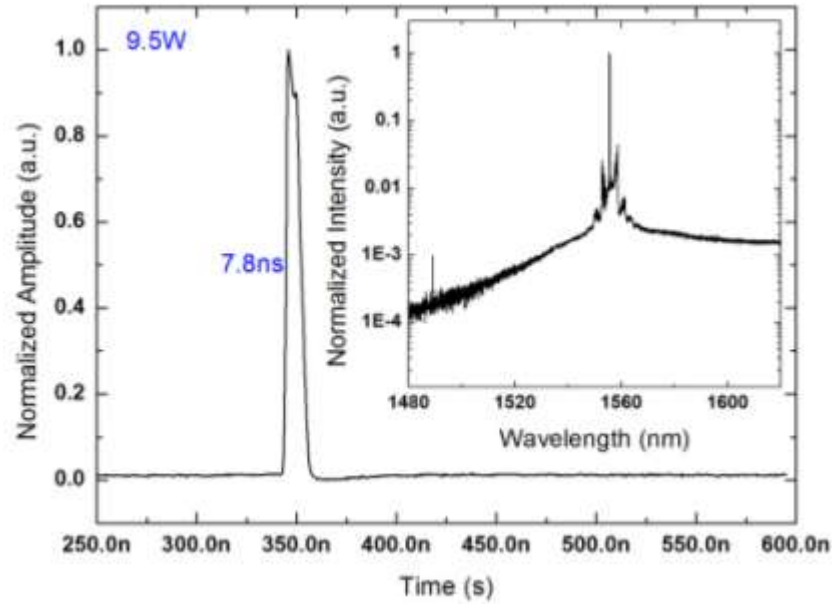


Figure 4.40: Output pulse with 9.5 W average power at the output of nanosecond seed amplifier system (inset; spectrum for same condition in logarithmic scale).

For nanosecond signal amplification with developed set-up, around 35% slope efficiency was obtained. Decreasing the efficiency compared to actively mode locked laser amplification can be assumed as normal due to higher nonlinear effects. Although there is a spectral broadening again, system can create 9.5 W average power with around 8 ns pulse duration at 100 kHz repetition rate which means around 10 kW peak power. In order to be sure about this peak power, in other words power level under the pulse, next experimental set-up was constructed.

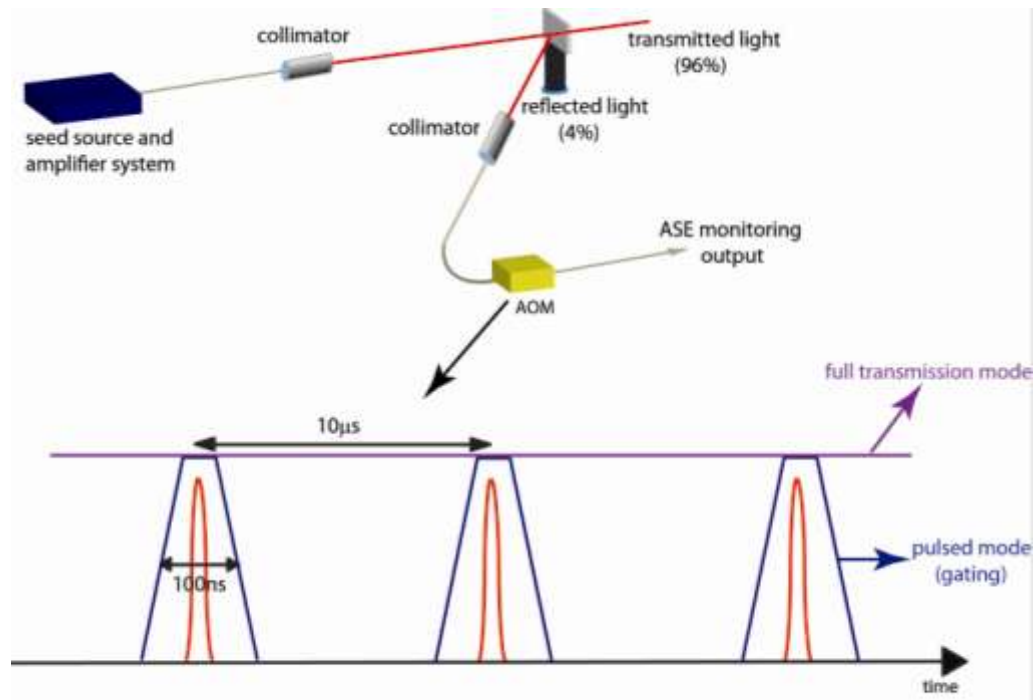


Figure 4.41: Power under the pulse measurement set-up.

In this set-up amplifier system output was sent through a beam sampler from collimator which reflects 4% of the light while transmits 96% of it. This component was used to decrease the power level to save second collimator and also modulator from high power damaging. Reflected light was coupled into second collimator with fiber pigtail which was connected to the one end of AOM. Then AOM was operated with full transmission mode to pass all power and pulse picking mode to pass only pulses from 100 ns gates around the pulses. By measuring the difference at the power level from the output of AOM, the power under pulse and between pulses can be differentiated. Measurement results which were done for 9.5 W output power showed that 95% of the output power of amplifier system was under the pulse. So it can be said that this amplifier configuration works well for nanosecond regime at low repetition frequency.

With this study, it was proved that fiber laser system can satisfy the requirements of LADAR system source with the application desired 3 km range (comes from 100 kHz repetition rate) with 150 cm resolution (comes from the pulse duration) in eye-safe region. Since the output was subtracted from single mode fiber coupled collimator, the beam quality (M^2 value) can be accepted near 1 which

increases spatial resolution. With the kW range peak power, it can compensate the loss during reflection from the target and traveling in air.

By using the advantage of flexibility for laser modulation parameters controlled with electronic signal, this amplifier system can also be converted to a system for picosecond operation. Next figure shows during same pump parameters, the output of the same system for picosecond pulse comes from the impulse generator modulation.

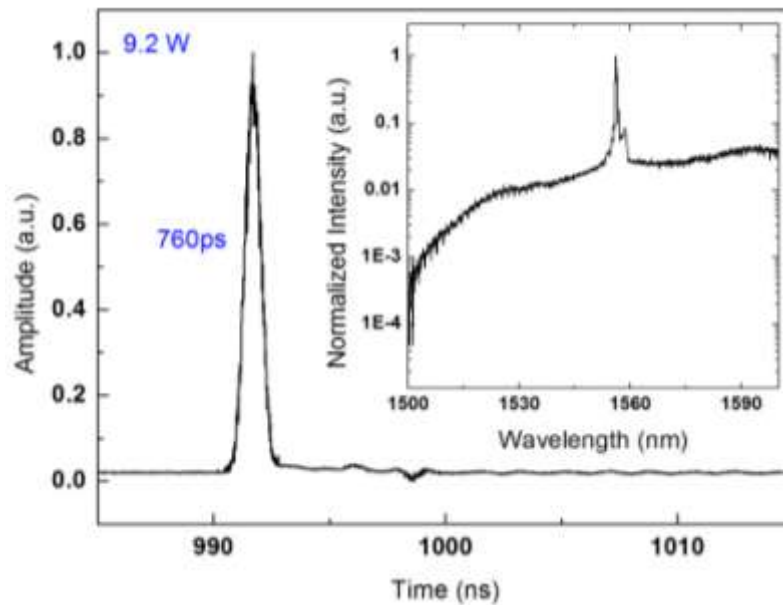


Figure 4.42: Amplifier system output in time domain at 9.2 W for picosecond seed (inset; spectrum for same condition in logarithmic scale).

Although nonlinear effect was also observed in picosecond system output as spectral broadening, a big portion of power was assumed as under the pulses due to similar peak intensity with nanosecond regime. Since there was no available AOM with fast rise and fall time to open a gate with a few ns period, previous measurement could not be performed for picosecond system. Just energy under filter bandwidth region was calculated from the spectrum domain as around 70%. It means that this source can be used for obtaining high resolution (less than 15 cm) imaging with video rate from 300 m range and 6 nm filtering in receiver part can be enough to get sufficient returning signal from target while decreasing the

background noise of LADAR system. As proposed in the beginning of this study, the development of a fiber amplifier system with combination of picosecond and nanosecond regime modulation with DFB seed laser can serve both high resolution imaging with fast scanning rate from near field and long range distance capability. Since the whole system is all-fiber integrated, this source is compact, portable and free from alignment. Next figure shows the recent photo of amplifier stage for last configuration during operation.

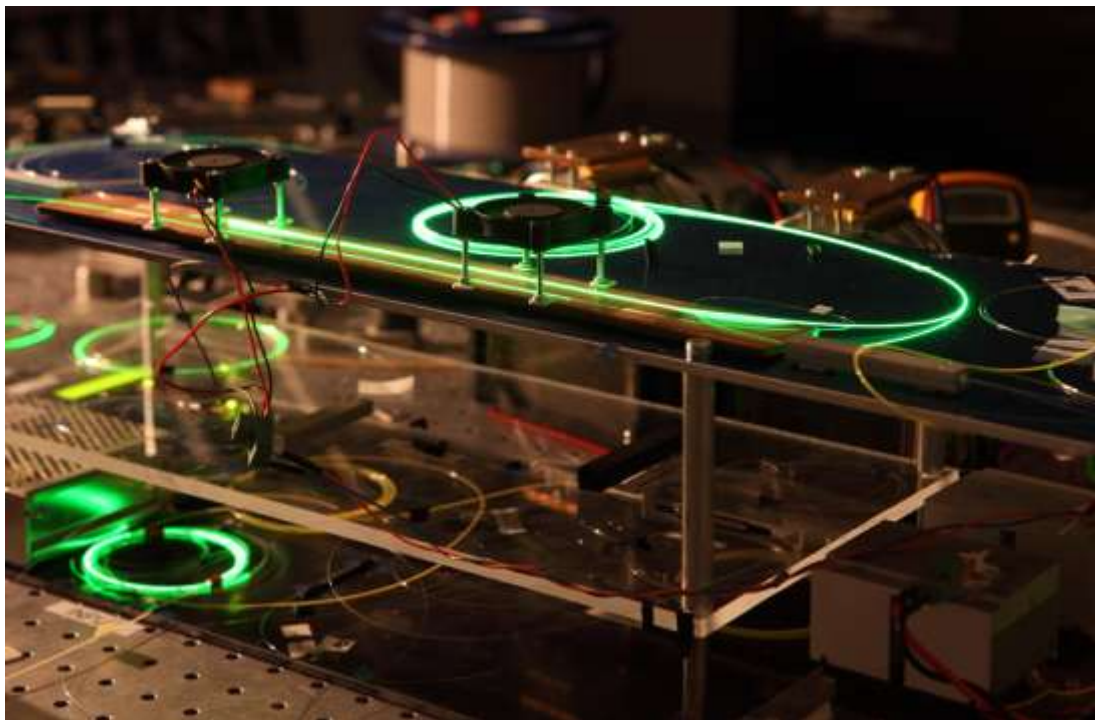


Figure 4.43: Recent photo of amplifier system during operation.

CHAPTER 5

CONCLUSION

In this study, a fiber laser system was developed for LADAR applications used in 3D imaging schemes. Typically, all available LADAR system uses low repetition rates in the laser source for high distance ranges. This type of source will cause a longer time to obtain high a resolution 3D image. Moreover, these sources are usually based on free-space solid state lasers. Such systems are inefficient in terms of high power consumption and also they are impractical for transportation due to their larger size. Therefore, there is a gap in LADAR technology in terms of the use of higher repetition rates to get higher resolution images in a short time with compact size and an efficient laser source. By using fiber laser technology and all of its advantages, a compact erbium doped fiber based pulsed laser system was developed for LADAR application which can acquire higher resolution images in a short time inside the eye-safe region. This all fiber integrated system was based on MOPA configuration with a seed source and an amplifier part. Both an actively mode locked fiber laser and direct modulation of commercial DFB lasers by using driven electronics were investigated in the construction of the seed source. The system that was built showed that active mode locking can provide stable picosecond pulses with a few MHz repetition rate at around 1550 nm central wavelength. Due to its active control on modulation frequency, pulse duration can be adjusted. For 10 MHz repetition rate, around 1 ns pulses were obtained from the output of laser cavity with 4 mW average power. All spectra were reported that can be assumed as a proof of its stable operation. In parallel, commercial fiber coupled DFB laser was modulated in both picosecond and nanosecond pulse duration at MHz and kHz repetition rates respectively. In order to get sufficient average power at the output of the DFB laser, nanosecond regime parameters were chosen as 500 kHz with 10 ns pulses, while picosecond regime parameters were chosen as 7 MHz with 700 ps. About 0.15 mW average optical power was obtained from the output.

After development of the seed, the amplifier was developed to amplify both actively mode locked laser and fiber coupled modulated DFB laser. Two-stage

amplifier system was used to amplify the actively mode locked laser output where the first stage consisted of single mode single clad erbium doped fiber and second stage consisted of erbium-ytterbium co-doped double clad fiber. Both amplifier stages were designed in backward pumping configuration to get higher efficiency that was also supported with simulation results for preamplifier case. By using this amplifier set-up, actively mode locked laser output was amplified up to an average power of 12 W at 10 MHz with 1 ns pulse duration which corresponds to 1.2 kW peak power through single mode fiber from all fiber integrated system.

Then modulated diode output was also amplified. In this case, pulse picking method was used to decrease repetition frequency to increase the range capability of LADAR system. Repetition rates of nanosecond and picosecond pulses were decreased to 100 kHz and 1 MHz respectively. For nanosecond case, simulation was performed for preamplifier part and the result showed that there is an ASE creation between pulses due to low repetition rate and low signal input power. Therefore in this set-up, single clad, erbium doped fiber based, two-stage preamplifier system was used to suppress ASE creation at the output of DFB diode. Then three-stage amplifier configuration was used to amplify the signal further. First stage was based on single clad erbium doped fiber while second and third stages were used double clad erbium-ytterbium co-doped fiber. 9.5 W average power was obtained with around 8 ns pulses at 100 kHz repetition rate through single mode fiber which corresponds to 10 kW peak power. Same set-up was used for picosecond amplification and 9.2 W average power was obtained with around 700 ps pulses at 1 MHz repetition rate which corresponds to around 10 kW peak power again. With the combination of nanosecond and picosecond modulation in the same system, the developed amplifier served the capability of both high resolution imaging at video rate and high distance range detection. To the best of our knowledge, it is first such system in an all fiber integrated configuration with strictly single mode output operating in the eye-safe region. For future improvements regarding this system, the amplifier system can be further optimized to suppress nonlinear effects. This situation will give an opportunity to use very narrow filtering in receiver part to decrease background noise and increase the performance of LADAR system. By using larger core diameter of gain fiber with higher doping concentration, it can be possible to suppress nonlinearity while increasing the output power.

Similar outputs with comparable pulse energy and average power can be obtained generally from commercial solid state lasers with large dimensions. They are as big as an optical table or double mattress whereas fiber laser system may even fit into a pizza box. Such developed fiber system with compact size and free of misalignment configuration is expected to be useful not only for LADAR application, but also other applications such as eye surgery operation, 3D silicon processing or any other material processing.

REFERENCES

- [1] Synge, E. H., *A method of investigating the higher atmosphere*, Philosophical Magazine, 52, p. 1014-1020, 1930.
- [2] Bureau, R., *Meteorologie*, 3, p.292, 1946.
- [3] Maiman, T. H., *Stimulated optical radiation in ruby*, Nature, 187, p. 493-494, 1960.
- [4] McClung, F. J. and Hellwarth, R. W., *Giant optical pulsations from ruby*, Journal of applied physics, 33, p. 828-829, 1962.
- [5] Smullin, F. and Fiocco, G., *Optical echoes from the moon*, Nature, 194, p.1267, 1962.
- [6] Smullin, F. and Fiocco, G., *Detection of scattering layers in the upper atmosphere by optical radar*, Nature, 199, p. 1275-1276, 1963.
- [7] Argall, P.S. and Sica, R.J., *Lidar*, Encyclopedia of Imaging Science and Technology, Willey, 2002.
- [8] Menzies, R. T. and Killinger, D. K., *IR Lasers Tune In to the Environment*, IEEE Circuits and Devices Magazine, vol. 10, no.2, pp.24- 29, 1994.
- [9] *Safety of Laser Products - Part 1: Equipment classification, Requirements, and User's Guide*, IEC, Editor, IEC60825-1, 2001.
- [10] Harris, M., Hand, M., and Wright, A., *Lidar for Turbine Control*, National Renewable Energy Laboratory, 2005.
- [11] Karlsson, C.J., Olsson, F.A.A., Letalick, D., and Harris, M., *All-fiber Multifunction Continuous-wave Coherent Laser Radar at 1.5 μ m for Range, Speed, Vibration, and Wind Measurements*, Applied Optics, 39(21): p. 3716-3726, 2000.
- [12] Sica, R. J., Sargoytchev, S., Argall, P. S., Borra, E. F., Girard, L., Sparrow, C. T., and Flatt, S., *Lidar measurements taken with a large-aperture liquid mirror. I. Rayleigh-scatter system*, Appl. Opt., 34, 6925-6936, 1995.
- [13] Carswell, A. I., in Killinger, D. K. and Mooradian, A., *Optical and Laser Remote Sensing*, Springer-Verlag, Berlin, pp. 318–326, 1983.
- [14] Koreshetz, J. E., *Fiber lasers for lidar*, Optical fiber communication conference, California, 2005.

- [15] Richardson, D. J., Nilsson, J., and Clarkson, W. A., *High power fiber lasers: current status and future perspectives [Invited]*, J. Opt. Soc. Am. B **27**, B63-B92, 2010.
- [16] Rao, M. K. and Goh, C. C., *A Low-Cost Near-IR Laser Radar*, Photon. Tech. Lett., vol. 2, no 9, pp. 683-685, 1990.
- [17] Cariou, J. P., and Boquet, M., *Leosphere Pulsed Lidar Principles*, Leosphere, Orsay (FR).
- [18] Baird, J. L., *British Patent 285, 738*, 1928.
- [19] Van Heel, A. C. S., *A new method of transporting optical images without aberrations*, Nature 173, 39, 1954.
- [20] O'Brian, B., *U. S. Patent 2, 825, 260*, 1958.
- [21] Snitzer, E., *Optical maser action of Nd³⁺ in barium crown glass*, Phys. Rev. Lett. **7**(12), 444-446, 1961.
- [22] Koester, C. J. and Snitzer, E., *Amplification in a fiber laser*, Appl. Opt. **3**(10), 1182-1186, 1964.
- [23] Kao, K. C., Hockham, G. A., *Dielectric-fibre surface waveguides for optical frequencies.*, Proc. IEE. **113** (7), 1151-1158, 1966.
- [24] Rensselaer Polytechnic University, <http://www.ecse.rpi.edu/~schubert/Light-Emitting-Diodes-dot-org/chap22/chap22.htm>, last visited on August 2012.
- [25] Maurer, R., Keck, D., and Schultz, P., *Optical Waveguide Fibers*, U.S. Patent 3,711,262, 1970.
- [26] Mears, R. J., Reekie, L., Poole, S. B., and Payne, D. N., *Neodymium doped single-mode fibre lasers*, Electron. Lett. **21**(17), 738-740, 1985.
- [27] Reekie, L., Mears, R. J., Poole, S. B., and Payne, D. N., *Tunable single-mode fiber lasers*, J. Lightwave Technol., **4**(7), 956-960, 1986.
- [28] Mears, R. J., Reekie, L., Jauncey, I. M., and Payne, D. N., *High-gain rare-earth doped fiber amplifier at 1.54 μm*, in Technical Digest, Optical Fiber Communication Conf. 1987, p. 167, Optical Society of America, Washington, D.C., 1987.
- [29] Snitzer, E., Po, H., Hakimi, F., Tumminelli, R., McCollum, B. C., *Double clad offset core Nd fiber laser*, Optical Fiber Sensors Topical Meeting, New Orleans, Louisiana/USA, paper PD 5, 1988.
- [30] DiDomenico, M., *Small-signal analysis of internal (coupling type) modulation of lasers*, J. Appl. Phys. **35**, 2870-2876, 1964.

- [31] Hargrove, L.E., Fork, R.L., Pollack, M.A., *Locking of He-Ne laser modes induced by synchronous intracavity modulation*, Appl. Phys. Lett. 5, 4-5, 1964.
- [32] Yariv, A., *Internal modulation in multimode laser oscillators*, J. Appl. Phys. 36, 388-391, 1965.
- [33] Haus, H. A., *A Theory of Forced Mode Locking*, IEEE Journal of Quantum Electronics QE-11, pp. 323 – 330, 1975.
- [34] Kaertner, F. X., *Mode locked laser theory*, 2006.
- [35] New, G.H.C., *Pulse evolution in mode-locked quasicontinuous lasers*, IEEE J. Quantum Electron. 10, 115-124, 1974.
- [36] RP Photonics, www.rp-photonics.com/passive_mode_locking.html, last visited on June 2012.
- [37] Haus, H. A., *Mode locking of lasers*, IEEE J. Selec. Top. Quan. Electron. 6, 1173, 2000.
- [38] RP Photonics, www.rp-photonics.com/active_mode_locking.html, last visited on June 2012.
- [39] Xu, L., Lui, L. F. K. et al., *10GHz actively mode locked erbium doped fiber ring laser using an electro-absorption modulator and linear optical amplifier*, Opt. Fib. Comm. Conf., California, 2006.
- [40] RP Photonics, www.rp-photonics.com/acousto_optic_modulators.html, last visited on July 2012.
- [41] Jen Optik, www.jenoptik.com/cms/jenoptik.nsf/res/.pdf, last visited on July 2012.
- [42] Agrawal, G. P., *Applications of Nonlinear Fiber Optics*, Academic Press, New, York, 2001.
- [43] RP Photonics, www.rp-photonics.com/rare_earth_doped_fibers.html, last visited on July 2012.
- [44] The University of North Carolina, http://www.unc.edu/~dtmoore/3_4level.html, last visited on August 2012.
- [45] Lizuka, K., *Lab instruction notes for "Erbium Doped Fiber Amplifiers"*, University of Toronto, 1998.
- [46] Miniscalco, W. J., *Erbium-doped glasses for fiber amplifiers at 1500 nm*, J. Lightwave Tech. 9, 234, 1991.
- [47] Qian, L., *Experiment on erbium-doped fiber amplifiers*, Advanced Labs for Special Topics in Photonics, 1998.

- [48] Laming, R. I., Farring, M. C., Morkel, P. R., Reekie, L., and Payne, D. N., *Efficient pump wavelengths of erbium-doped fiber optical amplifier*, Electron. Lett. **25**(1), 12–14, 1989.
- [49] Invocom, www.invocom.et.put.poznan.pl, last visited on August 2012.
- [50] Snitzer, E., Po, H., Hakimi, F., Ruminelli, T., and McCollum, B. C., *Erbium fiber laser amplifier at 1.55 μ m with pump at 1.49 μ m and Yb sensitized Er oscillator*, Proc. Optical Fiber Communications Conf. Technical Digest 1988, Optical Society of America, Washington, D.C., 1988.
- [51] Galvanauskas, A., *High power fiber laser*, Optics and Photonics News, July, 2004.
- [52] SPIE, <http://spie.org/x17329.xml>, last visited on August 2012.
- [53] Tünnermann, A., Schreiber, T. and Limpert, J., *Fiber lasers and amplifiers: an ultrafast performance evolution*, Applied Optics, (49), 25, 2010.
- [54] RP Photonics, www.rp-photonics.com/double_clad_fibers.html, last visited on July 2012.
- [55] Lumholt, O., Rasmussen, T., and Biarklev, A., *Modelling of extremely high concentration erbium-doped silica waveguides*, Electron Lett, 29 495, 1993.
- [56] Richardson, D. J., Nilsson, J., Clarkson, W. A., *High power fiber lasers: current status and futures perspectives*, J. Opt. Soc. Am. B, **27**, No 11, B63-B92, 2010.
- [57] Koplów, J. P., Kliner, D. A. V., and Goldberg, L., *Single-mode operation of coiled multimode fiber amplifier*, Optics Letters, 25, pp. 442, 2000.
- [58] Renaud, C.C., Selvas-Aguilar, R.J., Nilsson, J., Turner, P.W., and Grudinin, A.B., *Compact high-energy Q-switched cladding-pumped fiber laser with a tuning range over 40nm*, IEEE Photonics Technology Letters, 11(8), pp.976-978, 1999.
- [59] Offerhaus, H.L., Broderick, N.G., Richardson, D.J., Sammut, R., Caplen, J., and Dong, L., *High energy single-transverse mode Q-switched fiber laser based on a multimode large-mode area erbium-doped fiber*, Optics Letters, 23 (21), pp.1683-1685, 1998.
- [60] Jeong, Y. Y, et al., *Erbium:Ytterbium co-doped large core fiber laser with 297-W continuous-wave output power*, IEEE J. Sel. Top. Quant. 13, 573, 2007.
- [61] Yusim, A., Barsalou, J., Gapontsev, D., Platonov, N. S., Shkurikhin, O.B., Gapontsev, V. P., Barannikov, Y. A., and Shcherbina, F. V., *100 watt single-mode CW linearly polarized all-fiber format 1.56- μ m laser with suppression of parasitic lasing effects*, Proc. SPIE **5709**, 69–77, 2005.

- [62] Kuhn, V., Kracht, D., Neumann, J. and Wessels, P., *67W of output power from an Yb free Erbium doped fiber amplifier cladding pumped at 976nm*, IEEE PHOTONICS TECHNOLOGY LETTERS, VOL. 23, NO. 7, 2011.
- [63] Jasapara, J. C., et al., *Diffraction limited fundamental mode operation of core-pumped very-large-mode-area Er fiber amplifiers*, IEEE J. Sel. Top. Quant. 15, 3, 2009.
- [64] Fermann, M. E., Galvanauskas, A., Hofer, M., *Ultrafast pulse sources based on multi-mode optical fibers*, Appl. Phys. B 70, S13, 2000, and references therein.
- [65] Morin, F., Druon, F., Hanna, M. and Georges, P., *Microjoule femtosecond fiber laser at 1.6 μm for corneal surgery applications*, Opt. Lett. 34, 1991-1993, 2009.
- [66] Agrawal, G. P., *Nonlinear Fiber Optics*, Academic Press, 2007.
- [67] Tong, Z., Wei, H., and Jian, S., *Theoretical investigation and optimization of bi-directionally pumped broadband fiber raman amplifiers*, Optics Communications, 217, (1-2), p. 401-413, 2003.
- [68] Fini, J. M. et al., *Distributed suppression of stimulated Raman scattering in an Yb-doped filter-fiber amplifier*, Opt. Lett. 31 (17), 2550, 2006.
- [69] Carter, A., et al., *Damage mechanisms in components for fibre lasers and amplifiers*, Proc. Of SPIE, 5647, 2005.
- [70] Ozoptics, http://www.ozoptics.com/ALLNEW_PDF/DTS0037.pdf, last visited on august 2012.
- [71] Pavlov, I., Ilbey, E., Dulgergil, E. and Ilday, F. Ö., *High-power high-repetition rate single-mode Er-Yb doped fiber laser system*, Opt. Exp., 20 (9), 2012.

APPENDIX A

IMPULSE GENERATOR SPECIFICATIONS

FUNCTION	Single-channel fast electrical impulse generator
TRIGGER	Electrical input threshold user adjustable from -4.0 to +5.0 volts Selectable 50Ω / Hi-Z termination Rising edge triggers impulse (internal switch allows polarity inversion)
ANALOG O/E OUTPUT	Optical trigger equipped models feature internal O/E converter +1 volt/mW optical input into 50Ω load (50Ω source impedance)
PROPAGATION DELAY	10 ns ±500 ps from electrical trigger
IMPULSE OUTPUT PRECURSOR	< +7.8 volts
IMPULSE OUTPUT AMPLITUDE	+65 volts ±2 volts peak into 50Ω
OUTPUT RINGDOWN	< ±7.8 volts
BANDWIDTH	Impulse Generator: DC to 1 MHz repetition rate Analog O/E converter: DC to 180 MHz repetition rate
RISETIME	Impulse Generator: < 350 ps (10% to 90%) Analog O/E converter: < 750 ps
FALLTIME	< 350 ps (10% to 90%)
PULSE WIDTH	< 350 ps FWHM
JITTER	< 3 ps RMS
OPERATING TEMPERATURE	0 to 60°C; extended MIL/COTS ranges available

CALIBRATION INTERVAL	One year
POWER	+15 volts at 400 mA, nominal J15 Universal Wall-Plug Adapter recommended
CONNECTORS	Gold plated SMB electrical trigger, output and O/E monitor output jacks (optically equipped models) Threshold level test points ST or FC fiberoptic input connector (optically equipped models) 2.1 mm x 5.5 mm barrel power connector
INDICATORS	LEDS: Front panel green Power, blue Trigger

APPENDIX B

C++ CODE FOR PREAMPLIFIER SIMULATION

```
//-----
#ifndef Unit1H
#define Unit1H
//-----
#include <Classes.hpp>
#include <Controls.hpp>
#include <StdCtrls.hpp>
#include <Forms.hpp>
#include <Dialogs.hpp>
#include <Menus.hpp>
//-----
class TForm1 : public TForm
{
__published: // IDE-managed Components
    TButton *Button1;
    TMainMenu *MainMenu1;
    TMenuItem *File1;
    TMenuItem *Savefile1;
    TMenuItem *Tempfile1;
    TSaveDialog *SaveDialog1;
    TSaveDialog *SaveDialog2;
    TLabel *Label1;
    TEdit *Edit1;
    TLabel *Label2;
    TLabel *Label3;
    TEdit *Edit2;
    TLabel *Label4;
    TEdit *Edit3;
    TLabel *Label5;
    TLabel *Label6;
    TLabel *Label7;
    TEdit *Edit4;
    TLabel *Label8;
    void __fastcall Button1Click(TObject *Sender);
    void __fastcall Savefile1Click(TObject *Sender);
    void __fastcall Tempfile1Click(TObject *Sender);
private: // User declarations
public: // User declarations
    __fastcall TForm1(TComponent* Owner);
};
//-----
extern PACKAGE TForm1 *Form1;
//-----
class SegmentOfTheFiber
{
public:

    static const float Length; //The length of the gain fiber
    static float Diameter; //The diameter of -----
    static float DopingConcentration; //The doping concentration
    static float NumericalAperture; //The NA of fiber core
    static float RefractiveIndex; //Refractive index of fiber core

    static float HPlank; //
    static float c; //speed of the light
    static float NuPump; // Pump frequensy
    static float NuEmission; // signal frequensy
};
```

```

static float PumpAbsorbtionCrossSection; //Absorption crossection for pump
static float SignalAbsorptionCrossSection; //signal absorption cross section
static float SpontaneousProbability21; //spontaneous probability from 2 to 1
static float RelacsationProbability32; //Probability of relacsation from N3 to N2
static float StimulatedCrossSection; //stimulated cross section for signal
static float Square; //the area of core
static double TotalN; //The total number of ions in segment

double N1; //The number of ions in the ground state
double N2; //The number of ions in the upper working state
double N3; //The number of ions in the upper pump state
double InversionPopulation; //the value of inversion population (N2/N1)

float InputPumpPower; //the input pump power for given segment (in right
direction)
float OutputPumpPower; //unabsorbed pump power after this segment
float SpontaneousEmissiomLeft; //Power of spontaneous emission which
generated from the segment in left direction
float SpontaneousEmissionRight; //Power of spontaneous emission which
generated from the segment in right direction
float StimulatedEmissionLeft; //Power of stimulated emission which generated in
segment to left direction
float StimulatedEmissionRight; //Power of stimulated emission which generated
in segment to right direction
float AbsorbedSignalRight; //Absorbed power of the right signal in segment
float AbsorbetSignalLeft; //Absorbed power of the left signal in segment
float TotalInputEmissionRight; //
float TotalInputEmissionLeft; // power of input and output emission of the signal
to right and left direction
float TotalOutputEmissionRight; //
float TotalOutputEmissionLeft; //
double DeltaN3; //The number of ions which come to exited state due
to pump
double DeltaN2DuePump; //The number of ions which are coming to N2
due to relaxation from N3
double DeltaN2Spontaneous; //The number of ions which come from the
exidet state due to spontaneous transitions
double DeltaN2StimulatedRight; //The number of ions which come from the
exidet state due to stimulated transitions to right
double DeltaN2StimulatedLeft; //The number of ions which come from the exidet
state due to stimulated transitions to left
double DeltaN2SignalAbsorptionLeft; //The number of ions which come to exited
state due to reabsorption of the left signal
double DeltaN2SignalAbsorptionRight; //The number of ions which come to exited
state due to reabsorption of the righth signal

SegmentOfTheFiber ()
{
N2=0;
N3=0;
N1=TotalN;
InputPumpPower=0;
OutputPumpPower=0;
SpontaneousEmissiomLeft=0;
SpontaneousEmissionRight=0;
StimulatedEmissionLeft=0;
StimulatedEmissionRight=0;
TotalInputEmissionRight=0;
TotalInputEmissionLeft=0;
TotalOutputEmissionRight=0;
TotalOutputEmissionLeft=0;
AbsorbedSignalRight=0;
AbsorbetSignalLeft=0;
DeltaN3=0;

```

```

DeltaN2SignalAbsorptionLeft=0;
DeltaN2SignalAbsorptionRight=0;
DeltaN2Spontaneous=0;
DeltaN2StimulatedRight=0;
DeltaN2StimulatedLeft=0;
InversionPopulation=0;
DeltaN2DuePump=0;
}

void deltaTimeCalculation (float * DeltaT)
//the function calculates the quantity of the time for one cycle DeltaTime
{
float DeltaTime=0.01*RefractiveIndex*Length/c;
*DeltaT=DeltaTime;
}

void calculation (float * TotalInversionPopulation)
//The function calculates all processes in the segment during DeltaTime (main function for
calculation)
{
float DeltaTime=0.01*RefractiveIndex*Length/c;
float Square=3.1415*Diameter*Diameter/4;
//Area of the core of the fiber
float
CoeffSpon=(1.0001/4.0001)*(NumericalAperture*NumericalAperture/(RefractiveIndex*Refrac
tiveIndex)); //ratio for spontaneous emission that can directed through the right or
left due to NA
float InputPumpIntensity=InputPumpPower/Square;

DeltaN3=(InputPumpIntensity/(HPlank*NuPump))*PumpAbsorbtionCrossSection*N1*DeltaTi
me-(InputPumpIntensity/(HPlank*NuPump))*PumpAbsorbtionCrossSection*N3*DeltaTime-
N3*RelacsationProbability32*DeltaTime; //The N3 changes

DeltaN2DuePump=N3*RelacsationProbability32*DeltaTime;
//The number of ions which are coming to N2 from N3 due to nonradiative relaxation

DeltaN2StimulatedRight=TotalInputEmissionRight*(N2/(HPlank*NuEmission*Square))*Stim
ulatedCrossSection*DeltaTime; //

DeltaN2StimulatedLeft=TotalInputEmissionLeft*(N2/(HPlank*NuEmission*Square))*Stimulat
edCrossSection*DeltaTime;

DeltaN2SignalAbsorptionLeft=(TotalInputEmissionLeft/(HPlank*NuEmission*Square))*Signal
AbsorptionCrossSection*N1*DeltaTime;

DeltaN2SignalAbsorptionRight=(TotalInputEmissionRight/(HPlank*NuEmission*Square))*Sig
nalAbsorptionCrossSection*N1*DeltaTime;
DeltaN2Spontaneous=N2*SpontaneousProbability21*DeltaTime;
//The N2 change due to the spontaneous emission

SpontaneousEmissionRight =
(CoeffSpon)*N2*SpontaneousProbability21*HPlank*NuEmission;
SpontaneousEmissionLeft
=(CoeffSpon)*N2*SpontaneousProbability21*HPlank*NuEmission; //The
power of spontaneous emissioin to the left and right direction

StimulatedEmissionRight=0.7*DeltaN2StimulatedRight*HPlank*NuEmission/DeltaTime;

StimulatedEmissionLeft=0.7*DeltaN2StimulatedLeft*HPlank*NuEmission/DeltaTime;
//The power of stimulated emission to the left and right direction

AbsorbedSignalRight=DeltaN2SignalAbsorptionRight*HPlank*NuEmission/DeltaTime;

```

```

AbsorbetSignalLeft=DeltaN2SignalAbsorptionLeft*HPlank*NuEmission/DeltaTime;
//the signal power which is absorbed in the segment in left and right direction

        OutputPumpPower=InputPumpPower-
(DeltaN3+N3*RelacsationProbability32*DeltaTime)*HPlank*NuPump/DeltaTime;        //the
unabsorbed pump power after segment

TotalOutputEmissionRight=TotalInputEmissionRight+SpontaneousEmissionRight+Stimulate
dEmissionRight-AbsorbedSignalRight;

TotalOutputEmissionLeft=TotalInputEmissionLeft+SpontaneousEmissionLeft+StimulatedE
missionLeft-AbsorbetSignalLeft;        //total stimulated and spontaneous emission power in
left and right direction

        N3=N3+DeltaN3;
//Total amount of ions in the N3 state after cicle

N2=N2+DeltaN2DuePump+DeltaN2SignalAbsorptionLeft+DeltaN2SignalAbsorptionRight-
DeltaN2Spontaneous-DeltaN2StimulatedRight-DeltaN2StimulatedLeft; //

        N1=TotalN-N2-N3;
        InversionPopulation=(N2)/(N1+N2);

        *TotalInversionPopulation=*TotalInversionPopulation+InversionPopulation;
    }
};
float SegmentOfTheFiber::c=2.9979E8;        //speed of the light    m/s
float SegmentOfTheFiber::DopingConcentration=4.8E+19;        //particles per cm^3
float SegmentOfTheFiber::RefractiveIndex=1.5;
float SegmentOfTheFiber::NumericalAperture=0.20;
const float SegmentOfTheFiber::Length=0.5;        //cm
float SegmentOfTheFiber::Diameter=4E-4;        //cm
float SegmentOfTheFiber::HPlank=6.626E-34;        //J*s
float SegmentOfTheFiber::NuPump=c/980E-9;
float SegmentOfTheFiber::NuEmission=c/1550E-9;
float SegmentOfTheFiber::PumpAbsorbtionCrossSection=2.1E-21;        //cm^2
float SegmentOfTheFiber::SignalAbsorptionCrossSection=2.5E-21;        //cm^2
float SegmentOfTheFiber::SpontaneousProbability21=1/(1E-2);        // 1/s
float SegmentOfTheFiber::RelacsationProbability32=1/(1E-6);        //1/s
float SegmentOfTheFiber::StimulatedCrossSection=3.2E-21;        //cm^2
float SegmentOfTheFiber::Square=Diameter*Diameter*3.1415/4;        // cm^2
double SegmentOfTheFiber::TotalN=Square*Length*DopingConcentration;

//-----
#endif
//-----

#include <vcl.h>
#pragma hdrstop

#include <fstream.h>

#include "Unit1.h"
#include <math.h>
//-----
#pragma package(smart_init)
#pragma resource "*.dfm"
TForm1 *Form1;

const int TheNumberOfSegments=240;        //number of segments of the fiber
SegmentOfTheFiber Segment [TheNumberOfSegments];        //the array of segments of the
fiber

```

```

AnsiString TimeFileName;           //The output data in time domain file name
AnsiString SpatialFileName;        //The temp file for diagnostic
void segment_initialization (SegmentOfTheFiber * Segment, int TheNumberOfSegments, float
PumpPower, float InputSignalLeft, float InputSignalRight); //the function initialize all
segments parameter for calculation
int cycles_number_calculation (float DeltaTime, float TimePeriod); //calculation of
number of cycles
//-----
__fastcall TForm1::TForm1(TComponent* Owner)
: TForm(Owner)
{
}
//-----

void __fastcall TForm1::Button1Click(TObject *Sender)
{
    TDateTime T1, T2; //The variables for calculating the time of execution
    T1=Time (); //
    AnsiString dT; //
    //*****

    float IsTimeForOut=StrToFloat(Form1->Edit1->Text); //The time after which the data
for every segment along the fiber will move out
    bool SpaceFileFlag=true; //The flag indicate is data along the fiber
moved out or no

    float CalculationPeriod=0; //total period of time for calculation
    int NumberOfCyclesForTime=0; //the number of cycles for calculation
    float TotalInversionPopulation=0;
    float InputSignalLeft=0.0; //input signal to the left
    float InputSignalRight=0.00; //
    ofstream flow1(TimeFileName.c_str());
    flow1.precision(10);
    ofstream flow2(SpatialFileName.c_str());
    flow2<<"FiberPosition"<<" " <<"InputPumpPower"<<" " <<"OutputPumpPower"<<"
"<<"TotalEmissionRight"<<" " <<"TotalEmissionLeft"<<" " <<"N1"<<" " <<"N2"<<"\n";
    double TimeCounterForOutput=0; //This variable counts total time of process and
puts it to the output file
    float PumpPower=0.5; //Watt
    float DeltaTime=0; //quantity of the time in program (the light time
propagation through segment) second
    float RepetitionRate=7E6; //Hz rep. rate for pulsed operation
    float PulsePosition=0; //The position for the first pulse in the train
    float PulseTrainPeriod=1/RepetitionRate; //Period between two pulses
    float PeakPower=0.09; //(Watt) Peak instantaneous power for Gaussian
pulse
    float PulseWidth=700E-12; //(s) pulse width
    float StartingTimeForOutput=StrToFloat (Form1->Edit2->Text); //
    float EndingTimeForOutput=StrToFloat (Form1->Edit3->Text); //
    int PointsRateForOut=StrToInt(Form1->Edit4->Text); //

    Segment [1].deltaTimeCalculation (&DeltaTime);
    CalculationPeriod=6E-4;
    NumberOfCyclesForTime=cycles_number_calculation (DeltaTime, CalculationPeriod);

    for (long int i=0; i<NumberOfCyclesForTime; i++) //cycle for time
    {
        InputSignalLeft=PeakPower*exp(-((TimeCounterForOutput-
PulsePosition)*(TimeCounterForOutput-PulsePosition))/(PulseWidth*PulseWidth));
        segment_initialization (Segment, TheNumberOfSegments, PumpPower,
InputSignalLeft, InputSignalRight);
        TotalInversionPopulation=0;
        for (int j=0; j<TheNumberOfSegments; j++)
        {
            Segment [j].calculation (& TotalInversionPopulation);
            if (TimeCounterForOutput>IsTimeForOut && SpaceFileFlag)

```

```

        {
            flow2<<j*Segment[j].Length<<"          "<<Segment[j].InputPumpPower<<"
"<<Segment[j].OutputPumpPower<<"          "<<Segment[j].TotalOutputEmissionRight<<"
"<<Segment[j].TotalOutputEmissionLeft<<"    "<<Segment[j].N1<<"    "<<Segment[j].N2<<"
"<<Segment[j].InversionPopulation<<"\n";
        }
    }
    if (TimeCounterForOutput>IsTimeForOut && SpaceFileFlag) SpaceFileFlag=false;
    TotalInversionPopulation=TotalInversionPopulation/TheNumberOfSegments;
    if ((StartingTimeForOutput<TimeCounterForOutput) &&
(TimeCounterForOutput<EndingTimeForOutput))
    {
        if (fmod (i, PointsRateForOut)==0) flow1<<TimeCounterForOutput<<"
"<<Segment [0].TotalOutputEmissionLeft<<"          "<<Segment [TheNumberOfSegments-
1].TotalOutputEmissionRight<<"          "<<TotalInversionPopulation<<"          "<<Segment
[TheNumberOfSegments-1].TotalInputEmissionLeft<<"\n";
    }
    TimeCounterForOutput=TimeCounterForOutput+DeltaTime;
    if ((fabs(TimeCounterForOutput-PulsePosition))>(0.5*PulseTrainPeriod))
PulsePosition=PulsePosition+PulseTrainPeriod;
}

T2=Time ();
DateTimeToString (dT, "hh:nn:ss:zzz", T2-T1);
ShowMessage("Ok! Time of execution - "+dT);
}
//-----
void __fastcall TForm1::Savefile1Click(TObject *Sender)
{
    AnsiString FileExt="";
    if (SaveDialog1->Execute())
    {
        TimeFileName=SaveDialog1->FileName;
        for (int i=strlen(TimeFileName.c_str())-2; i<strlen(TimeFileName.c_str())+1; i++)
FileExt=FileExt+TimeFileName[i];
        if (FileExt!="dat") TimeFileName=TimeFileName+".dat";
        Sleep (100);
    }
}
//-----

void __fastcall TForm1::Tempfile1Click(TObject *Sender)
{
    AnsiString FileExt="";
    if (SaveDialog2->Execute())
    {
        SpatialFileName=SaveDialog2->FileName;
        for (int i=strlen(SpatialFileName.c_str())-2; i<strlen(SpatialFileName.c_str())+1; i++)
FileExt=FileExt+SpatialFileName[i];
        if (FileExt!="dat") SpatialFileName=SpatialFileName+".dat";
        Sleep (100);
    }
}
//-----
void segment_initialization (SegmentOfTheFiber * Segment, int TheNumberOfSegments, float
PumpPower, float InputSignalLeft, float InputSignalRight)
{
    for (int j=0; j<TheNumberOfSegments; j++) //for fiber,z dimension
    {
        if (j==0)
        {
            Segment [j].InputPumpPower=PumpPower;
            Segment [j].TotalInputEmissionLeft=Segment
[j+1].TotalOutputEmissionLeft; //initialization of first segment

```

```

        Segment [j].TotalInputEmissionRight=InputSignalRight;
    }
else
    {
        if (j==TheNumberOfSegments-1)
            {
                Segment [j].InputPumpPower=Segment [j-1].OutputPumpPower;
                Segment [j].TotalInputEmissionLeft=InputSignalLeft;
//initialization of last segment
                Segment [j].TotalInputEmissionRight=Segment [j-1].TotalOutputEmissionRight;
            }
        else
            {
                Segment [j].InputPumpPower=Segment [j-1].OutputPumpPower;
                Segment [j].TotalInputEmissionRight = Segment [j-1].TotalOutputEmissionRight; //initialization of all segments except of first and last
                Segment [j].TotalInputEmissionLeft =Segment[j+1].TotalOutputEmissionLeft;
            }
    }
}
}
//-----
-----
int cycles_number_calculation (float DeltaTime, float TimePeriod)
{
    return int(TimePeriod/DeltaTime);
}

```